

American University in Cairo

AUC Knowledge Fountain

Theses and Dissertations

Student Research

Summer 6-9-2021

Facilitating SARS-CoV-2 RNA-Dependent RNA Polymerase (RdRp) Drug Discovery by the Aid of HCV NS5B Palm Domain Binders: In Silico Approaches and Benchmarking

laila khaled

lailakhaled@aucegypt.edu

Follow this and additional works at: <https://fount.aucegypt.edu/etds>

Recommended Citation

APA Citation

khaled, I. (2021). *Facilitating SARS-CoV-2 RNA-Dependent RNA Polymerase (RdRp) Drug Discovery by the Aid of HCV NS5B Palm Domain Binders: In Silico Approaches and Benchmarking* [Master's Thesis, the American University in Cairo]. AUC Knowledge Fountain.

<https://fount.aucegypt.edu/etds/1532>

MLA Citation

khaled, laila. *Facilitating SARS-CoV-2 RNA-Dependent RNA Polymerase (RdRp) Drug Discovery by the Aid of HCV NS5B Palm Domain Binders: In Silico Approaches and Benchmarking*. 2021. American University in Cairo, Master's Thesis. *AUC Knowledge Fountain*.

<https://fount.aucegypt.edu/etds/1532>

This Master's Thesis is brought to you for free and open access by the Student Research at AUC Knowledge Fountain. It has been accepted for inclusion in Theses and Dissertations by an authorized administrator of AUC Knowledge Fountain. For more information, please contact thesisadmin@aucegypt.edu.



THE AMERICAN UNIVERSITY IN CAIRO
الجامعة الأمريكية بالقاهرة

School of Sciences and Engineering

**Facilitating SARS-CoV-2 RNA-Dependent
RNA Polymerase (RdRp) Drug Discovery by
the Aid of HCV NS5B Palm Domain Binders:
In Silico Approaches and Benchmarking**

A Thesis Submitted to

The Chemistry Master's Program

In partial fulfillment of the requirements for

The degree of Master of Science

By:

Laila Khaled Mohamed El-ghoneimy Omara Ayad

Under the supervision of:

Prof. Dr. Hassan M.E. Azzazy (Advisor)

Professor and Chairman, Chemistry Department, The American
University in Cairo (AUC), Egypt

Assoc. Prof. Dr. Tamer M. Ibrahim (Co-advisor)

Associate Professor of Pharmaceutical Chemistry, Faculty of
Pharmacy, Kafrelsheik University, Egypt

Fall 2020

ACKNOWLEDGEMENTS

First and foremost, praises and thanks to the GOD for granting me with countless blessings throughout my journey. This work would not be possible without his holy willing.

I would like to express my deep and sincere gratitude to Prof. Dr. Hassan Azzazy, my advisor and Chairman of Chemistry Department for his guidance, support and kind approval to conduct this work. There are no words that can convey how grateful I am for his encouragement, flexibility and foresight. I will always be proud to call myself his student.

I am very delighted to have worked with Assoc. Prof. Dr. Tamer Ibrahim and to have been supervised and guided by him. Indeed, I do thank him from the bottom of my heart for not sparing any time or effort while guiding me throughout my research. He gave me a true opportunity to learn new skills and taught me how to practice critical thinking and analyzing the results. He is an exceptional role model when it comes to dedication and hard work. I have learned a lot from him and I would like to acknowledge my debt for his continuous support and endless advices.

Heartfelt thanks to Dr. Hatem Tallima, my dearest previous supervisor, for not letting me until everything was planned and settled again. I was extremely lucky to pass by such a respecting personality.

I cannot express enough thanks to Prof. Dr. Mohamed Farag, the Director of the Chemistry Graduate Program, for his sincere advices and support not only for me, but also for all the graduate students. He was always keen to teach us how to write and think in an academic manner.

Special thanks to each and everyone in the Chemistry Department of the AUC. You are really embodying the true meaning of a loving family. I consider myself very fortunate to get a precious chance to join the AUC and to hopefully obtain my Master Degree from such a highly reputable university.

Last but not least, I would love to dedicate this work to my mother for supporting me spiritually throughout my life and for being a real role model for me and my sisters. I owe many thanks to my father for preparing me for my future. I am very much thankful to my sisters for their love, care, understanding, prayers and encouragement. I am extending my thanks to my friends for motivating me when things get tough. I really admit that I have been blessed by GOD to be surrounded by supportive family and amazing friends.

ABSTRACT

Facilitating SARS-CoV-2 RNA-Dependent RNA Polymerase (RdRp) Drug Discovery by the Aid of HCV NS5B Palm Domain Binders: In Silico Approaches and Benchmarking

Corona Virus 2019 Disease (COVID-19) is a rapidly emerging pandemic caused by a newly discovered beta coronavirus, called Sever Acute Respiratory Syndrome Coronavirus 2 (SARS COV-2). SARS COV-2 is an enveloped, single stranded RNA virus that depends on RNA dependent RNA polymerase (RdRp) to replicate. Therefore, SARS COV-2 RdRp is considered as a promising target to cease virus replication. SARS COV-2 polymerase shows high structural similarity to Hepatitis C Virus-1b genotype (HCV-1b) polymerase.

In our present study, we are relying on in-silico analysis to propose possible SARS COV-2 RdRp palm subdomain inhibitors to be used as a remedy for COVID-19. Additionally, providing an example of how to make use of a high quality custom-made DEKOIS 2.0 benchmark set as a procedure to elevate the virtual screening success rate against a vital target of the rapidly emerging pandemic.

Arising from the high similarity between SARS COV-2 RdRp and HCV-1b polymerase, we used the reported small-molecule palm binders to HCV-1b polymerase to generate a high-quality DEKOIS 2.0 benchmark set and conducted a benchmarking against HCV-1b polymerase. The three highly cited and publicly available docking tools AutoDock Vina, FRED and PLANTS were benchmarked. Based on the benchmarking analysis, we used the highest performing docking tool to virtually screen FDA-approved drugs (from the DrugBank database) and the BindingDB database against the palm site of SARS COV-2 polymerase.

From the benchmarking results, PLANTS showed the best performance with pROC-AUC value equals 0.97. Moreover, AutoDock Vina exhibited better-than-random performance with pROC-AUC value of 0.66 (above 0.43). Based on the virtual screening outcome, Quinupristin, which is an anti-biotic used in several bacterial infections, showed the best docking score among the screened compounds.

In conclusion, Quinupristin as well as the top docking scored compounds are recommended to be biologically investigated as COVID-19 medications.

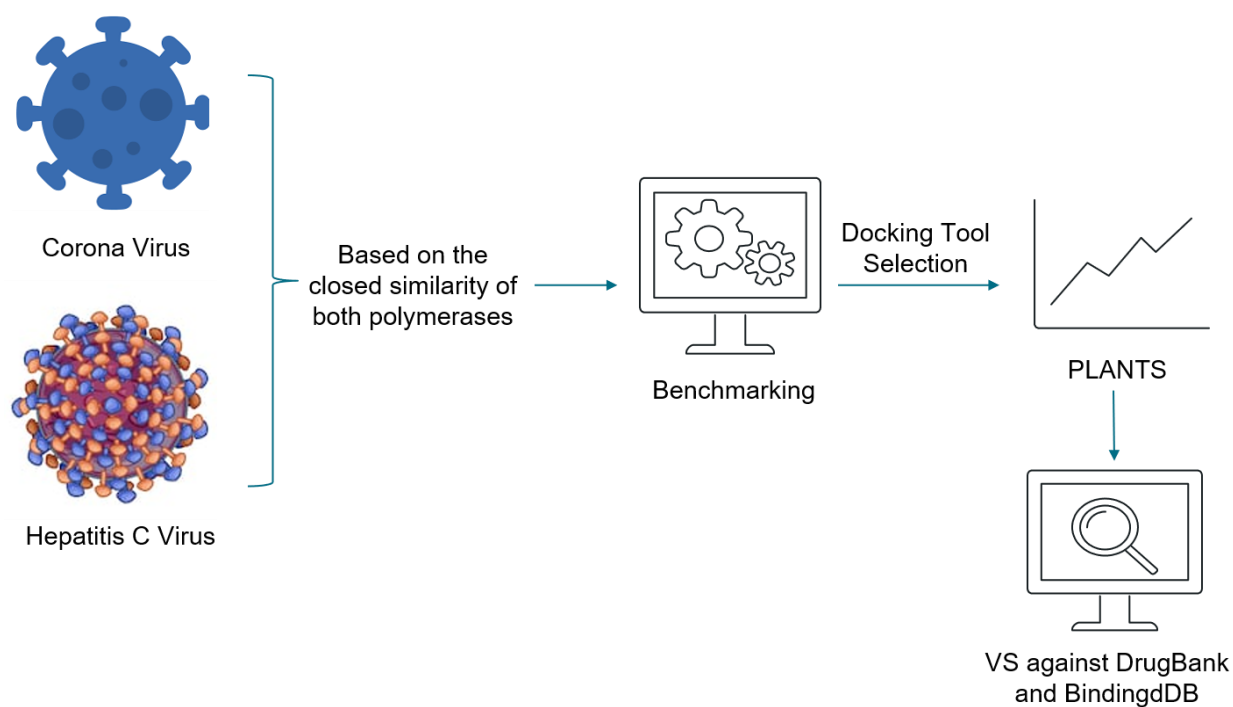


Diagram 1: Schematic overview of the workflow.

TABLE OF CONTENTS

Acknowledgements.....	i
Abstract.....	ii
Table of contents.....	iv
List of tables.....	vi
List of figures.....	vii
List of abbreviations.....	x
1. INTRODUCTION AND LITERATURE REVIEW.....	1
1.1 Coronaviruses.....	1
1.2 SARS COV-2 viral genome.....	2
1.3 SARS COV-2 RdRp (nsp12).....	5
1.4 Hepatitis C virus (HCV).....	8
1.5 HCV RdRp (ns5b).....	11
1.6 Alignment study.....	13
1.7 Structure based virtual screening (SBVS).....	14
1.8 Rational	15
1.9 Hypothesis	15
1.10 Objectives and Aims	15
2. MATERIALS AND METHODS.....	16
2.1 Preparation of protein macromolecules	16
2.2 Preparation of small molecules including: DEKOIS 2.0 benchmark set, DrugBank database and BindingDB ligands.....	17
2.3 Docking experiments.....	17
2.3.1 For benchmarking.....	17
2.3.2 For virtual screening of DrugBank and BindingDB ligands.....	18
2.4 pROC and pROC-Chemotype calculations.....	18
3. RESULTS AND DISCUSSION.....	19

3.1 Selection of HCV-ns5b actives for decoys generation.....	19
3.2 Selection of representative PDB structure(s) for HCV ns5b-1b.....	27
3.3 Benchmarking.....	33
3.4 Prospective VS based on Benchmarking.....	40
4. CONCLUSION AND FUTURE PERSPECTIVES	68
References.....	70
Appendix.....	81

LIST OF TABLES

Table 1: Non-structural COV-2 proteins and their functions.....	4
Table 2: Structural COV-2 proteins and their functions.....	4
Table 3: The active set to be used in the benchmarking	20
Table 4: HCV ns5b structures with the highest resolution values.....	28
Table 5: The available SARS COV-2 polymerase structures.....	40
Table 6: The best ranked 1% of the VS efforts for FDA-approved drugs against the SARS COV-2 RdRp Apo form (PDB ID: 7BV1).....	43
Table 7: The best ranked 1% of the VS efforts for the BindingDB database ns5b inhibitors against the SARS COV-2 RdRp Apo form (PDB ID: 7BV1).....	51
Table 1.A: AutoDock Vina, PLANTS and FRED scoring functions.....	81
Table 2.A: All HCV ns5b available structures in the protein data bank (PDB).....	82

LIST OF FIGURES

Diagram 1: Schematic overview of the workflow	iii
Figure 1: Classification of human coronaviruses.....	2
Figure 2: SARS COV-2 genome orientation.....	3
Figure 3: SARS COV-2 RdRp Apo structure complex.....	6
Figure 4: Structural comparison and superposition between COV-2 nsp12 and HCV polymerase (ns5b).....	7
Figure 5: Two views of the nsp12 surface.....	8
Figure 6: Sequence alignment of HCV RdRp amino acid sequence of the seven genotypes.....	9
Figure 7: A ribbon diagram of the X-ray structure of the HCV ns5b with an inhibitor (PDB ID: 3H98).....	12
Figure 8: Alignment of a huge data set of RdRps, including nsp12, secondary structure..	13
Figure 9: Similarity between COV-2 polymerase and RNA polymerases.....	14
Figure 10: Superposition of the top five whole protein structures of HCV ns5b-1b (PDB IDs: 3TYV, 4MZ4, 3HHK, 3SKA and 3TYQ).....	30
Figure 11: Superposition of the palm subdomains of the top five HCV ns5b-1b protein structures (PDB IDs: 3TYV, 4MZ4, 3HHK, 3SKA and 3TYQ).....	31
Figure 12: Superposition of the thumb and finger sites of the top five HCV ns5b-1b protein structures (PDB IDs: 3TYV, 4MZ4, 3HHK, 3SKA and 3TYQ).....	32
Figure 13: DEKOIS 2.0 target overview.....	34
Figure 14: DEKOIS 2.0 target overview with pROC AUC enrichment results for Glide, GOLD and AutoDock Vina.....	35

Figure 15: pROC plots of docking experiments showing the screening performance of both including and excluding key water molecules in the palm subdomain for HCV ns5b (PDB ID: 3HHK) for (A) and (B), respectively	36
Figure 16: (A) pROC-Chemotype plot of the HCV-ns5b (in the palm subdomain – PDB ID: 3HHK, including key water molecules) using PLANTS docking tool.....	38
Figure 17: Docking poses of the best two scoring compounds from the active set in the palm subdomain of HCV-ns5b-1b (PDB ID: 3HHK).....	39
Figure 18: Superposition of HCV ns5b-1b Apo structure (PDB ID: 2XHV) and the co-crystallized form (PDB ID: 3HHK).....	42
Figure 19: The binding pockets occupied by the best ranked 1% of the VS efforts against SARS COV-2 nsp12 palm site (PDB ID: 7BV1).....	49
Figure 20: The palm binding pocket occupied by a benzothiadiazine ns5b inhibitor (PDB ID: 3HHK).....	50
Figure 21: Docking pose of Quinupristin in the palm pocket of SARS COV-2 polymerase (PDB ID: 7BV1).....	58
Figure 22: Docking pose of Acetyldigitoxin in the palm pocket of SARS COV-2 polymerase (PDB ID: 7BV1).....	59
Figure 23: Docking pose of Diosmin in the palm pocket of SARS COV-2 polymerase (PDB ID: 7BV1).....	60
Figure 24: Docking pose of Hesperidin in the palm pocket of SARS COV-2 polymerase (PDB ID: 7BV1).....	61
Figure 25: Docking pose of Voxilaprevir in the palm pocket of SARS COV-2 polymerase (PDB ID: 7BV1).....	62
Figure 26: Docking pose of compound number 2 in the palm pocket of SARS COV-2 polymerase (PDB ID: 7BV1).....	63

Figure 27: Docking pose of compound number 3 in the palm pocket of SARS COV-2 polymerase (PDB ID: 7BV1).....	64
Figure 28: Docking pose of compound number 3 in the palm pocket of SARS COV-2 polymerase (PDB ID: 7BV1).....	65
Figure 29: Docking pose of compound number 3 in the palm pocket of SARS COV-2 polymerase (PDB ID: 7BV1).....	66
Figure 30: Docking pose of compound number 3 in the palm pocket of SARS COV-2 polymerase (PDB ID: 7BV1).....	67
Diagram 2: Simplified outline of the workflow.....	69

LIST OF ABBREVIATIONS

AUC	Area under the curve
COVID-19	Corona virus 2019 disease
EC	Enzyme commission numbers
EF	Enrichment factor
GPCRs	G protein-coupled receptors
HCV	Hepatitis C virus
LOA	Level of activity
MERS-COV	Middle east respiratory syndrome coronavirus
MOE	Molecular operating environment
RdRp	RNA dependent RNA polymerase
NiRAN	Nucleotidyltransferase
Ns5b	Non-structural protein 5b
Nsp	Non-structural protein
NTP	Nucleoside triphosphate
ORF	Open reading frame
ROC	Receiver operating characteristic
RMSD	Root mean square deviation
SARS COV-1	Sever acute respiratory syndrome coronavirus 1
SARS COV-2	Sever acute respiratory syndrome coronavirus 2
SBVS	Structure based virtual screening
TOD	Type of data

1. INTRODUCTION AND LITERATURE REVIEW

A pandemic coronavirus had arisen at the end of 2019 resulting in a worldwide crisis. This novel coronavirus is known as Sever Acute Respiratory Syndrome Coronavirus 2 (SARS COV-2) that causes a pulmonary disease with pneumonia like symptoms called Corona Virus 2019 Disease (COVID-19). In the 14th of November, 2020, the World Health Organization (WHO) Coronavirus Disease (COVID-19) Dashboard reported that there have been 53,164,803 confirmed cases of COVID-19, including 1,300,576 deaths, worldwide. This raises the attention to essentially develop a valid cure for this global pandemic.

1.1 Coronaviruses

Coronaviruses (COVs) are single stranded, positive sense RNA viruses that belong to *Coronaviridae* family (Figure 1) (Malik, 2020; D. Yang & Leibowitz, 2015). In terms of morphology, they are spherical, and enveloped with surface spikes that give the appearance of a solar corona (Malik, 2020). The *Coronaviridae* family is further classified to alpha, beta, gamma and delta genera (Malik, 2020; D. Yang & Leibowitz, 2015). Human coronaviruses are either alpha-coronaviruses or beta-coronaviruses (Figure 1) (Malik, 2020). SARS COV-2 is the new beta human coronavirus (Buonaguro, Tagliamonte, Tornesello, & Buonaguro, 2020; Q. Wang et al., 2020; Z. Zhao & Bourne, 2020). Previously, humans were subjected to several infections by a wide variety of COVs ranging from mild to severe infections. hCoV-OC43, HKU1, and 229E are examples of COVs that cause mild to moderate upper respiratory tract sickness (Malik, 2020). However, highly pathogenic human coronaviruses had appeared over the past two decades that were able to lead to acute respiratory distress syndrome (ARDS), which may lead to lung failure, arrhythmia, and death (Malik, 2020). These highly pathogenic COVs are; Sever Acute Respiratory Syndrome Coronavirus 1 (SARS COV-1) (Drosten et al., 2003), Middle East Respiratory Syndrome Coronavirus (MERS COV) (Zaki, Van Boheemen, Bestebroer, Osterhaus, & Fouchier, 2012) and the current Sever Acute Respiratory Syndrome Coronavirus 2 (SARS COV-2) (Malik, 2020; Rabi, Al Zoubi, Kasasbeh, Salameh, & Al-Nasser, 2020). Unlike MERS and COV-1, SARS COV-2 is known to be a fast-spreading illness that can infect many people in a community at the same time (Malik, 2020; Z. Zhao & Bourne, 2020).

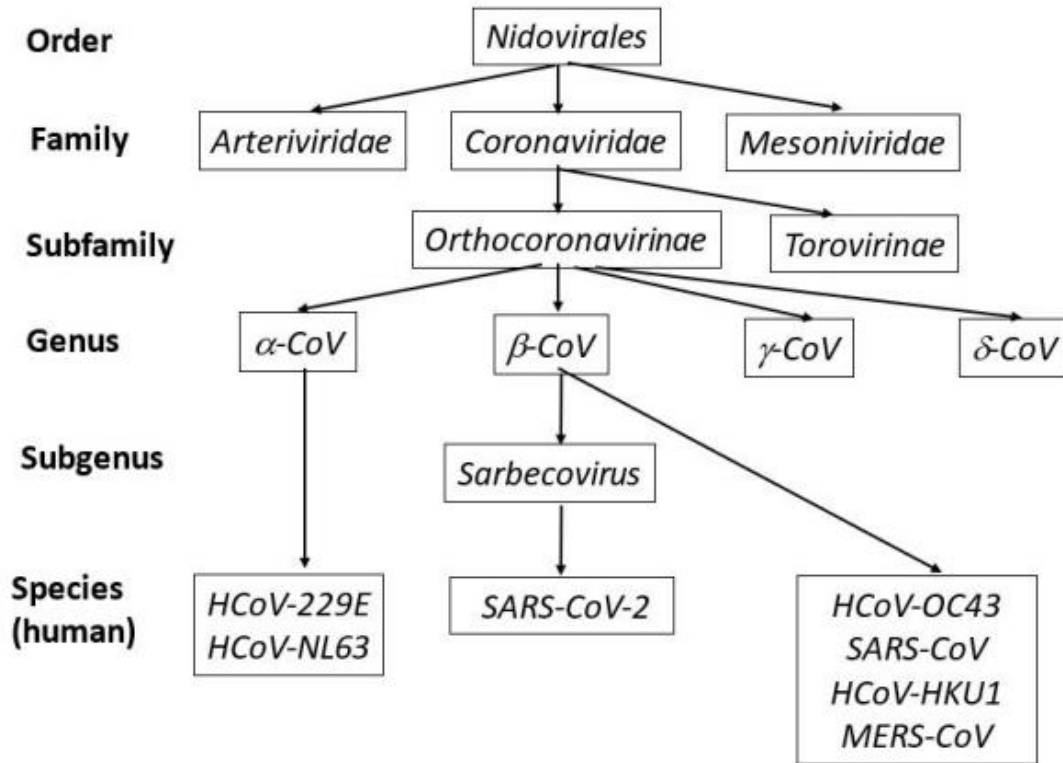


Figure 1: Classification of human coronaviruses.(Malik, 2020)

1.2 SARS COV-2 viral genome

The SARS COV-2 viral genome is around 30 kb in length encoding to 14 open reading frames (ORFs) at the N-terminal and 4 structural proteins at the C-terminal (Figure 2) (Gao et al., 2020; Jiang, Yin, & Xu, 2020; Wu et al., 2020; Yin et al., 2020). The open reading frames, ORF 1a and ORF 1b, which occupy 67% of the genome, encode two polyproteins (pp. 1a and pp. 1ab) (Jiang et al., 2020; Wu et al., 2020).

These precursor polyproteins will be cleaved into 16 non-structural proteins (nsp) (Table 1), which are necessary for viral replication as well as the host immunity replication (Gao et al., 2020; Jiang et al., 2020; Wu et al., 2020; Yin et al., 2020). Regarding the four structural proteins, spike (S), membrane (M), envelope (E) and nucleocapsid (N), Table 2 shows how crucial are they in maintaining virus integrity as well as its access into the host cell (Gordon et al., 2020; Jiang et al., 2020). Either structural or non-structural proteins, all are working in harmony to ease the viral invasion and replication inside the host cells (Gordon et al., 2020; Jiang et al., 2020; Littler, Gully,

Colson, & Rossjohn, 2020; Pillon et al., 2020). Therefore, all are considered as targets for designing new candidates aiming for the treatment of COVID-19.

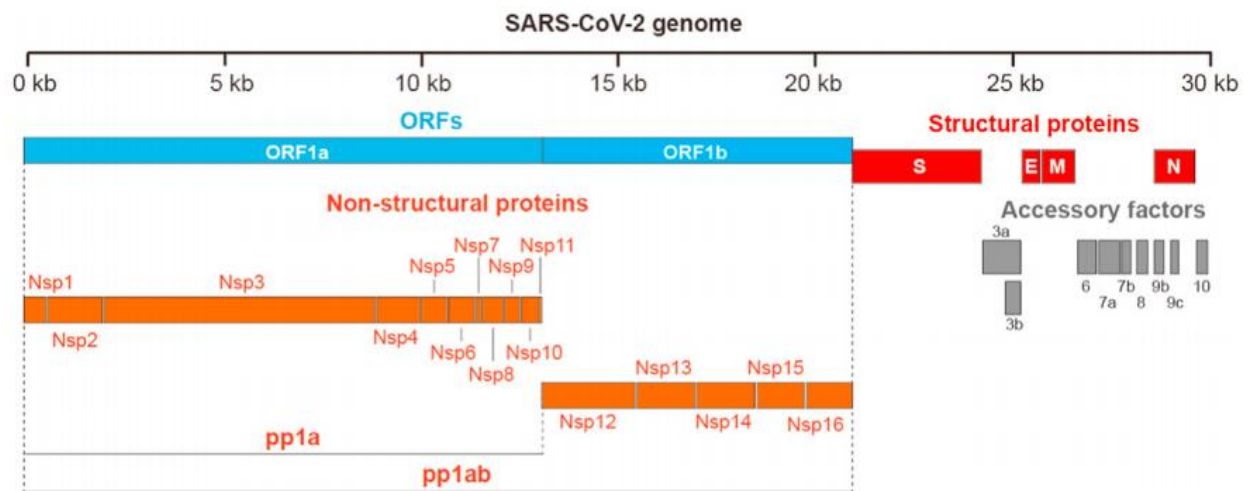


Figure 2: SARS COV-2 genome orientation.

COV-2 viral RNA is 30kb in size. The two poly proteins (1a and 1ab), at the 5' end, are precursors to 16 non-structural proteins that are vital for the virus life cycle. Besides, there are four structural proteins at the 3' end. Accessory factors are also found at the 3' end and are considered as ORFs (Jiang et al., 2020).

Table 1: Non-structural COV-2 proteins and their functions (Malik, 2020).

Protein	Functions
Nsp1	Stimulates cellular mRNA degradation leading to the blockage of host innate immune response
Nsp2	Unknown function
Nsp3	Stimulates the expression of cytokines, viral polyprotein cleavage and host innate immune response blockage
Nsp4	Potential transmembrane scaffold protein
Nsp5	Viral polyprotein cleavage
Nsp6	Potential transmembrane scaffold protein
Nsp7	Forms complex with nsp8 and cofactor for nsp12
Nsp8	Forms complex with nsp7 and cofactor for nsp12
Nsp9	RNA binder
Nsp10	Cofactor for nsp16 and nsp14
Nsp12	RNA dependent RNA polymerase
Nsp13	RNA helicase
Nsp14	3'-5'Exoribonuclease
Nsp15	Viral endoribonuclease
Nsp16	2'-O-Methyltransferase

Table 2: Structural COV-2 proteins and their functions.

Protein	Functions
Spike (S)	Mediates viral entry and fusion with the host cell via the interaction with the host cell surface receptors
Membrane (M)	Maintains the envelope shape of the virus
Envelope (E)	Aids the budding and the assembly of the virus
Nucleocapsid (N)	It is attached to the RNA and aids the viral assembly and budding

1.3 SARS COV-2 RdRp (nsp12)

SARS COV-2 RdRp, or nsp12, is the enzyme responsible for COV-2 replication by catalyzing the synthesis of RNA from RNA template (Gao et al., 2020; Subissi et al., 2014). Generally, RNA dependent RNA polymerase (RdRp) is a key enzyme in the viral biological cycle of all RNA viruses. Therefore, RdRp has a highly conserved architecture among RNA viruses especially when it comes to the catalytic residues at the active site (Gao et al., 2020; Subissi et al., 2014; Yin et al., 2020; Ziebuhr, 2005). Nsp12 is not active on its own, it needs the assistance of two accessory units nsp7 and nsp8 (Gao et al., 2020; Kirchdoerfer & Ward, 2019; Subissi et al., 2014; Yin et al., 2020). As a consequence, the structure of SARS COV-2 RdRp is composed of one nsp12 unit, one nsp7 unit and two nsp8 units (Figure 3) (Gao et al., 2020; Kirchdoerfer & Ward, 2019; Subissi et al., 2014; Yin et al., 2020). The nsp12 is composed of a canonical cupped right-handed RdRp domain (S367-F920) at the C-terminal, a nidovirus specific domain (D60-R249) at the N-terminal, which adopts a nidovirus RdRp-associated nucleotidyltransferase (NiRAN) and an interface (A250-R365) linking the previous two domains together (Figure 3) (Gao et al., 2020). Additionally, COV-2 RdRp is uniquely characterized by a β -hairpin (D29-K50) at the N-terminus (Gao et al., 2020). The RdRp domain is consisted of three conserved subdomains; finger (L366 to A581 and K621 to G679), palm (T582 to P620 and T680 to Q815) and thumb (H816 to E920), which are further contains seven invariant motifs (A to G) (Figure 3) (Gao et al., 2020). Motifs A to E are located in the palm, while F (L544 to V557) and G (D499 to L514) motifs are in the finger subdomain (Gao et al., 2020). Motif A (611-TPHLMGWDYPKCDRAM-626) and Motif C (753-FSMMILSDDAVVCFN-767) form the active site of the nsp12 by containing the classical catalytic residues that are essential for the divalent cation binding. These residues are D618 in A motif and (759-SDD-761) in C motif (Gao et al., 2020). Interestingly, based on a structural comparison study (Figure 4), these catalytic residues are invariant among most viral polymerases, such as (D220) and (317-GDD-319) in hepatitis C virus (HCV) ns5b (Gao et al., 2020).

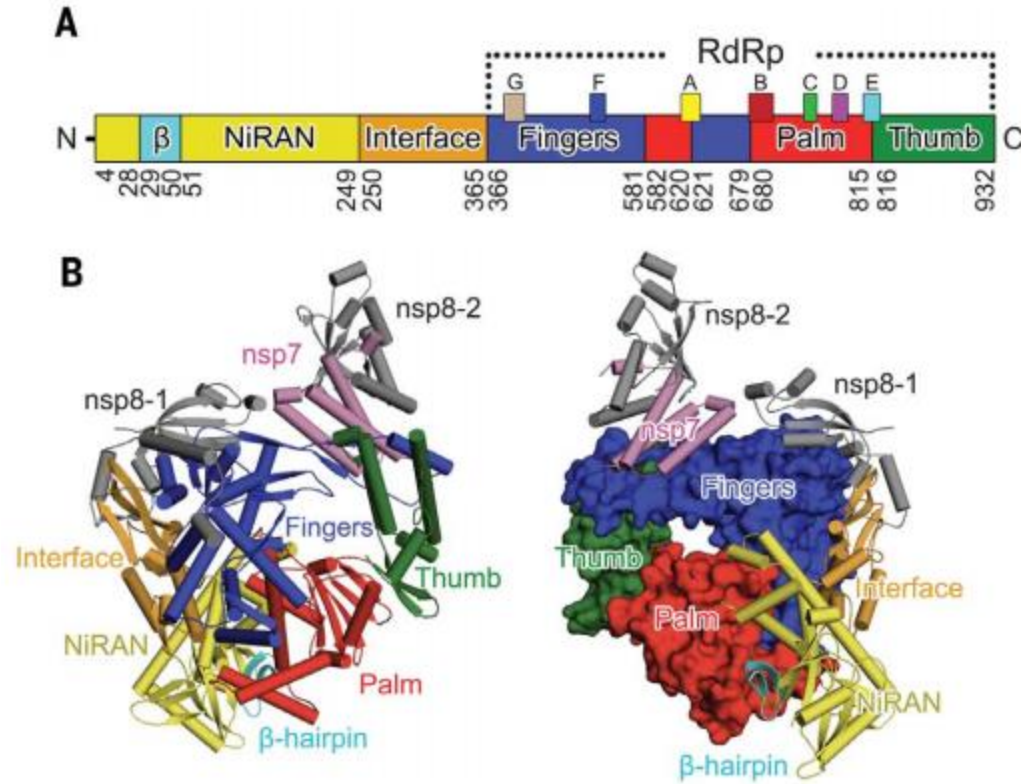


Figure 3: SARS COV-2 RdRp Apo structure complex.

(A) Schematic diagram of nsp12 domain organization. Motifs A to G, which are forming the catalytic core, are colored in yellow, red, green, violet, cyan, blue and light brown, respectively. (B) Ribbon diagram of the polypeptide chains of COVID-19 RdRp. Domains are colored similarly to (A). Nsp7 and nsp8-1 heterodimer binds to the thumb subdomain and the other nsp8-2 subunit attached to the finger subdomain (Gao et al., 2020).

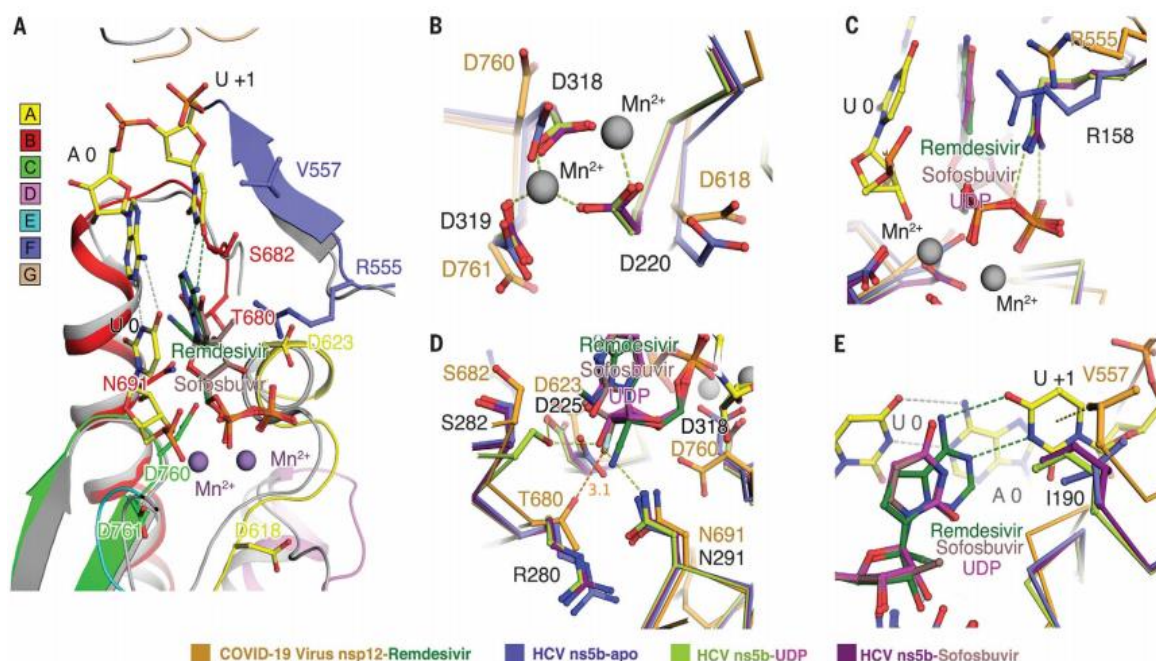


Figure 4: Structural comparison and superposition between COV-2 nsp12 and HCV polymerase (ns5b).

(A) Superposition of HCV ns5b co-crystallized with pp-sofosbuvir (PDB ID: 4WTG) with COVID-19 virus nsp12 shows the corresponding amino acid residues in each. (B to E) Comparison between HCV ns5b structures, either in the apo form or co-crystallized with UDP and pp-sofosbuvir, and COV-2 nsp12 (Gao et al., 2020).

The nsp12 has three positively charged paths; a template-primer entry, a nucleotide entry, and an exit shaft at the front face of the polymerase (Figure 5). The NTP entry is generated by hydrophobic residues (K545, R553 and R555) in motif F (Gao et al., 2020; Hillen et al., 2020; Yin et al., 2020). The active site groove in motifs A and C is made up by motifs F and G, while the primer entry is supported by E motif and the thumb subdomain (Gao et al., 2020; Hillen et al., 2020; Yin et al., 2020). In the presence of the RNA or a nucleotide inhibitor the catalytic residues D618 (A motif), D760 and D671 (C motif) of the active site will go through conformational changes to coordinate the divalent cations present in the catalytic region (Gao et al., 2020; Hillen et al., 2020; Yin et al., 2020). The divalent cations are responsible for linking the phosphate group of the incoming nucleotide or an inhibitor with the R555 residue (Gao et al., 2020; Yin et al.,

2020). The incoming nucleotide is stabilized by hydrogen bond network of N691, S682 and D623 residues (Yin et al., 2020). Their correspondents in ns5b are N291, S282 and D225 (Figure 4D) (Appleby et al., 2015; Gao et al., 2020). In addition to an interaction between +1 base of the primer and K545 and R555 of the F motif (Gao et al., 2020; Yin et al., 2020). In COV-2, additional Hb is formed with 2'OH by T680 residue (Gao et al., 2020). The residues that bind to the RNA template and those that constitute the active site are invariant among polymerases (Gao et al., 2020; Hillen et al., 2020; Jiang et al., 2020; Yin et al., 2020). Nsp7 and nsp8 are not involved in the interactions between the polymerase protein and the template-primer RNA (Yin et al., 2020). Hence, they only aid and catalyze nsp12 polymerization role.

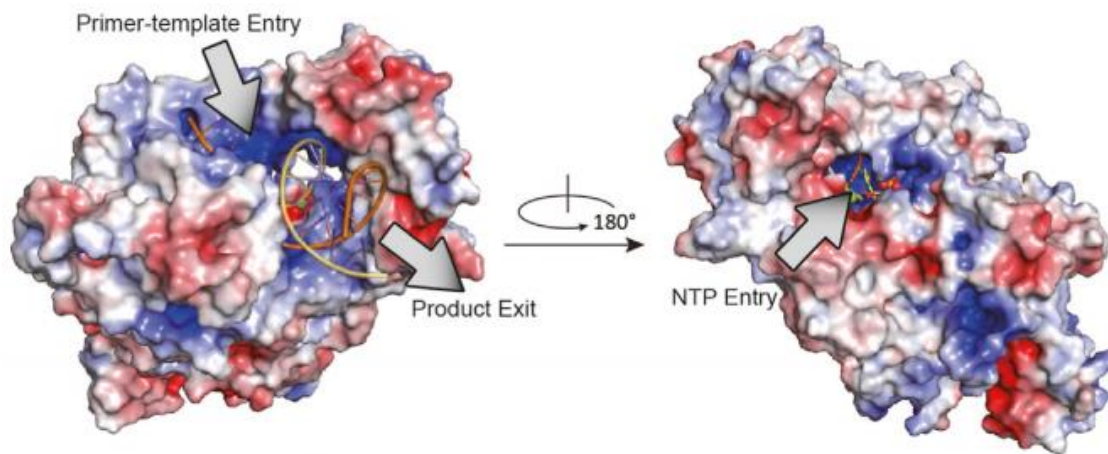


Figure 5: Two views of the nsp12 surface.

Two entry paths for the primer-template and the NTP. In addition to the exit tunnel, a path for the end product (Jiang et al., 2020).

1.4 Hepatitis C virus (HCV)

Hepatitis C virus is a single-stranded positive-sense RNA virus, which belongs to *Flaviviridae* family (Furman, Lam, & Murakami, 2009). HCV is a highly replicating virus with no proof-reading ability; therefore, its viral genome is characterized by high genetic variability that gives a rise to seven genotypes and more than 100 subtypes (Di Maio et al., 2014). Based on several sequence alignment studies (Figure 6); 31% to 33% nucleotide difference is found among the seven genotypes and 20% to 25% nucleotide difference is found among the subtypes (Di Maio

et al., 2014; Kuiken & Simmonds, 2009; Nakano, Lau, Lau, Sugiyama, & Mizokami, 2012). The difference between the genotypes is mainly on the surface of the polymerase where the amino acid mutation will not affect the functionality of the polymerase (Di Maio et al., 2014). The HCV RNA genome contains open reading frame (ORF) region that is upon translation results in a precursor polyprotein. This polyprotein is further processed to structural and non-structural proteins. Non-structural protein 5b (Ns5b) is one of the non- structural proteins that have a vital role in the replication process of the virus (Das et al., 2011; Di Maio et al., 2014; Furman et al., 2009; Sofia, Chang, Furman, Mosley, & Ross, 2012).

NS5B polymerase amino acid positions		1	10	20	30	40																																					
GT-1b		S	M	S	Y	T	W	T	G	A	L	I	T	P	C	A	A	E	E	T	K	L	P	I	N	A	L	S	N	S	L	L	R	H	H	N	L	V	Y	A	T		
GT-1a		S	Q	S
GT-2		S	S	P	C
GT-3		S	E	S	
GT-4		S	S	M	
GT-5		S	S	
GT-6		S	S	
GT-7		S	S	G	P	S	

NS5B polymerase amino acid positions		41	50	60	70	80																																						
GT-1b		T	S	R	S	A	S	L	R	Q	K	K	V	T	F	D	H	L	Q	V	L	D	D	H	Y	R	D	V	L	K	E	M	K	A	K	A	S	T	V	K	A			
GT-1a		T
GT-2		.	.	T	K
GT-3		.	.	S
GT-4		P
GT-5		.	.	S
GT-6		H
GT-7	

NS5B polymerase amino acid positions		81	90	100	110	120																																						
GT-1b		K	L	L	S	V	E	E	A	D	K	L	T	P	F	H	S	A	T	S	K	F	G	Y	G	A	K	D	V	R	N	L	S	S	K	A	V	N	H	I	L			
GT-1a		N	N
GT-2		R	.	.	.	T	M	K
GT-3		R	.	M	.	T	I
GT-4		R	.	.	.	T	T	S
GT-5		R	.	.	.	P	L	E
GT-6		R	T	D
GT-7		Q	K

NS5B polymerase amino acid positions		121	130	140	150	160																																						
GT-1b		S	V	W	K	D	L	L	E	D	I	E	T	P	I	D	T	T	I	M	A	K	N	E	V	F	C	V	R	P	E	K	G	G	R	K	P	A	R	L	I			
GT-1a	
GT-2	
GT-3		E
GT-4	
GT-5		G
GT-6	
GT-7		E

NS5B polymerase amino acid positions		161	170	180	190	200
GT-1b		V F P D L G V R V C E K M A L Y D V V S T L P Q A V M G S S Y G F Q Y S P Q Q H				
GT-1a	
GT-2		Y	.	.	.	A Q
GT-3		Y	.	R	.	A
GT-4		Y	S	H	.	A
GT-5		Y	.	.	.	A
GT-6		Y	S	.	.	S
GT-7		Y	.	R	.	S

NS5B polymerase amino acid positions		201	210	220	230	240
GT-1b		V E F L V M A W K A K K D P M G F A Y D T R G F D S T V T E N D I R V E E S I Y				
GT-1a		.	Q	.	.	A
GT-2		.	L K M	S	R	T
GT-3		R	L K M	S	Q	E
GT-4		.	L T	S	K	E V
GT-5		D	L K M	S	H	M T
GT-6		Y	L K M	S	R	D
GT-7		Y	K T	S	Q	T S E

NS5B polymerase amino acid positions		241	250	260	270	280
GT-1b		Q C C D L A F I A R D A I R S L T E R L Y I G G P L T N S K G Q N C G Y R R C R				
GT-1a		.	D	V	R	E
GT-2		R A	S P E	H T	M F	T Q
GT-3		.	N	K V	C	A D
GT-4		.	E	K V	M H	Q L
GT-5		S	Q	V	M Y	Q
GT-6		S	Q	D T	C	E S
GT-7		.	N D	T I	V	R V

NS5B polymerase amino acid positions		321	330	340	350	360
GT-1b		V V I C E S A G T Q E D E A S L R A F T E A M T R Y S A P P G D P P K P E Y D L				
GT-1a		.	V	A	.	Q R
GT-2		.	S	Q	E	A
GT-3		.	V A	D	V E	A T
GT-4		.	A	D	V E	A T
GT-5		.	A	Q	H	V T
GT-6		.	.	V	V A	Q
GT-7		.	K	V E R	R D	Q A

NS5B polymerase amino acid positions		361	370	380	390	400
GT-1b		E L I T S C S S N V S V A H D A S G K R V Y Y L T R D P T T P L A R A A W E T A				
GT-1a		.	.	G A	.	V
GT-2		.	.	L G P Q	R	.
GT-3		.	.	R	Y	.
GT-4		.	.	D K T	K	.
GT-5		.	V	R	I	.
GT-6		.	.	G T	Q	.
GT-7		H	D	R	N	.

NS5B polymerase amino acid positions		401	410	420	430	440
GT-1b		R H T P V N S W L G N I I M Y A P T L W A R M I L M T H F F S I L L A A Q E Q L E				
GT-1a		.	.	F	.	V
GT-2		.	S	.	.	I
GT-3		.	.	.	V	M
GT-4		.	.	V	.	.
GT-5		K	S	.	I	V
GT-6		.	.	.	V	.
GT-7		.	S	.	V	.

NS5B polymerase amino acid positions		441	450	460	470	480
GT-1b		R A L D C Q I Y G A C Y S I E P L D L P Q I I Q R L H G L S A F S L H S Y S P G				
GT-1a		Q	N	F E E M	.	T
GT-2		Q N	N F E E M	V	V S	H
GT-3		R P	F E E M	T	V T	V
GT-4		.	F E E M	V T	T	H
GT-5		T	A F E E M	S V	V T	S
GT-6		A	N F E E M	V T	V T	T
GT-7		D P V S F E E M	T	T V C	T	A

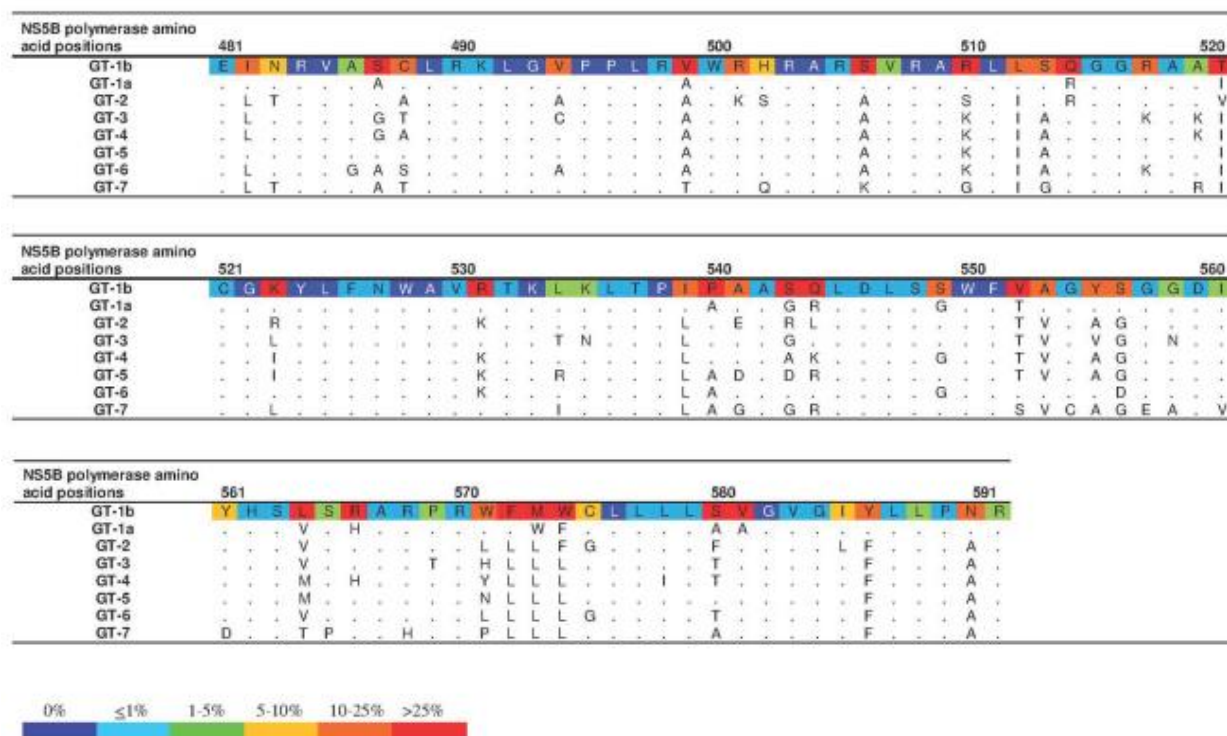


Figure 6: Sequence alignment of HCV RdRp amino acid sequence of the seven genotypes.

Genotype 1b is considered as a reference and colored in accordance with the frequency of substitution among 1,145 HCV sequences. Dots refer to identical amino acids among all the genotypes (Di Maio et al., 2014).

1.5 HCV RdRp (ns5b)

The three-dimensional structure of ns5b (Figure 7) has a right-hand architecture with finger (1 to 187 and 228 to 286), thumb (371 to 563) and palm (188 to 227 and 287 to 370) subdomains (Das et al., 2011). Regarding the variability of the polymerase subdomains, the thumb is found to be the most variable subdomain. However, the palm, that encompasses the active site, is the most well conserved subdomain. For the finger part, it contains the highly conserved F motif which plays a vital role in directing the incoming NTPs towards the active site (Das et al., 2011; Di Maio et al., 2014; Sofia et al., 2012). Similar to SARS COV-2, the palm site is made up of well conserved motifs A to E. Motif A (212-234), contains the catalytic aspartic acid D220, and motif C contains the catalytic triad 317-GDD-319 (Di Maio et al., 2014). Residues D220, D318

and D319 that are responsible for divalent cations binding, are invariant between the different HCV genotypes (Das et al., 2011; Di Maio et al., 2014; Furman et al., 2009). Besides the catalytic site, four allosteric pockets were recognized; palm I, close to the catalytic site, palm II, towards the catalytic site, thumb I and thumb II (Das et al., 2011). Palm I and palm II are known as palm pocket, as they are overlapping making the palm allosteric pocket large enough for a wide variety of inhibitors. However, the two thumb sites are distinct and separate from each other (Sofia et al., 2012). To date, no characterized binding site for inhibitors at the finger subdomain (Sofia et al., 2012).

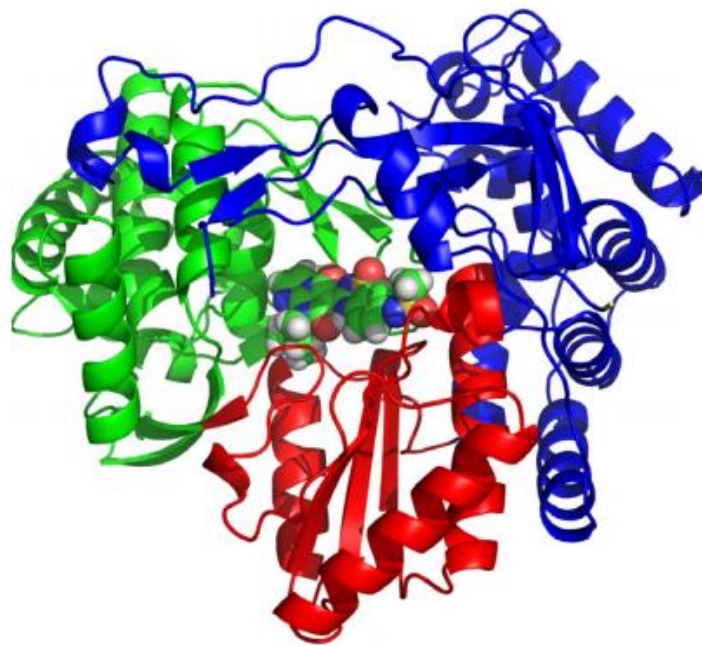


Figure 7: A ribbon diagram of the X-ray structure of the HCV ns5b with an inhibitor (PDB ID: 3H98).

The structure reveals the palm subdomain in red, the finger subdomain in blue and the thumb in green (Das et al., 2011).

1.6 Alignment study

An alignment study of a huge data set of RdRps, including nsp12, shows the extreme similarity between the secondary structure of the polymerases, from different RNA viruses, especially at the catalytic binding domains (Figure 8) (Z. Zhao & Bourne, 2020). According to the previous study, the top three similar viruses to SARS COV-2 are poliovirus type 1, HCV genotype 2a, and HCV genotype 1b (Figure 9) (Z. Zhao & Bourne, 2020). On this basis of similarity and due to the lack in poliovirus inhibitors as well as the limited availability of ns5b-2a non-nucleotide inhibitors, HCV ns5b-1b is the protein chosen to conduct the benchmarking study.

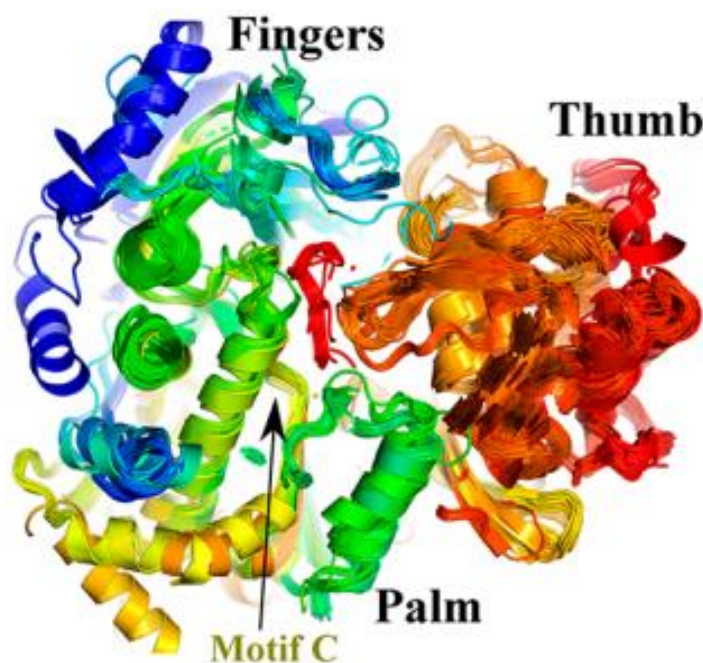


Figure 8: Alignment of a huge data set of RdRps, including nsp12, secondary structures. A high degree of similarity is shown among polymerase catalytic sites of different RNA viruses (Z. Zhao & Bourne, 2020).

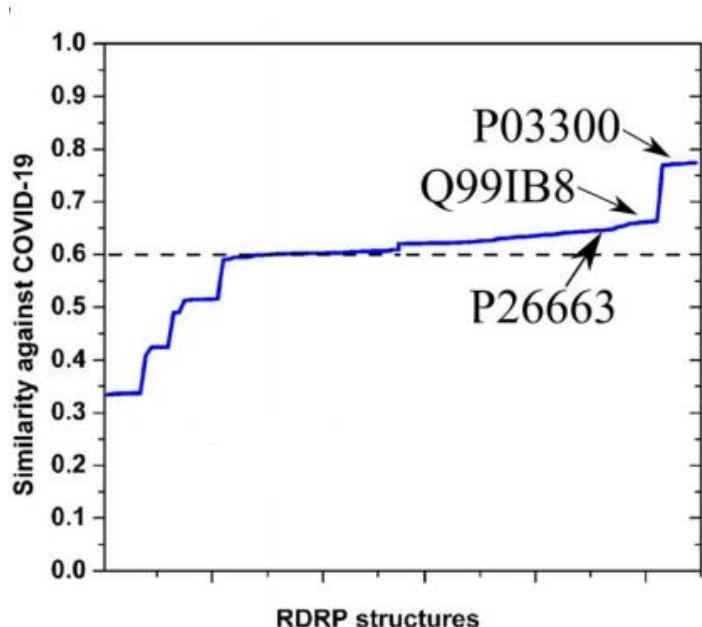


Figure 9: Similarity between COV-2 polymerase and RNA polymerases.

Hepatitis C virus genotypes 1b and 2a and poliovirus type 1 show high similarity percentage, above 0.65%. P03300 is for poliovirus type1. Q99IB8 and P26663 refer to HCV ns5b-2a and 1b, respectively (Z. Zhao & Bourne, 2020).

1.7 Structure based virtual screening (SBVS)

Structure based virtual screening (SBVS) is a computational technique that is widely used during the early stages of drug discovery. It is based on the molecular docking of a novel group of bioactive compounds against the binding site of the 3D structure of the target protein. It aims at predicting the binding poses of the new candidates and understanding the structural aspects of the targets binding sites. Compounds that show high predicted binding scores will be selected for further biological investigations (Santiago et al., 2012; Schapira, Abagyan, & Totrov, 2003; Schneider, 2010; Scior et al., 2012). To guarantee more successful VS efforts, the docking tool needs to be assessed by the aid of benchmarking molecular sets (Matthias R Bauer, Tamer M Ibrahim, Simon M Vogel, & Frank M Boeckler, 2013; Tamer M Ibrahim, Bauer, & Boeckler, 2015).

1.8 Rational

In this study, we are proposing possible candidates to be used in COVID-19 treatment, based on in-silico testing. We have created a benchmark set using ns5b palm site inhibitors to be used in benchmarking study against palm unit of ns5b (PDB ID: 3HHK). Guided by the benchmarking outcome, we used PLANTS, the best performing docking tool, in the virtual screening of compounds from DrugBank database and BindingDB database (Liu, Lin, Wen, Jorissen, & Gilson, 2007) against palm subdomain of nsp12 (PDB ID: 7BV1).

This study aims at repurposing drugs that may show effective inhibition towards SARS COV-2 RdRp palm unit. This is justified as follows; First, SARS COV-2 is a global rapidly growing pandemic with no specific cure. Secondly, the literature has provided a very limited number of potential pro-drugs that act against SARS COV-2 RdRp as nucleotide analogues. Moreover, RdRp is a vital enzyme during viral replication with a highly similar structure among RNA viruses. Therefore, it can be used to conduct a drug repurposing by homology. Thirdly, there are no actives reported to target the nsp12 palm subdomain and it is an allosteric pocket that can be directly targeted by small molecule binders. Furthermore, it contains the active site so that its localization will block the entry of the nucleotides (NTP) into the catalytic site leading to the inhibition of the initiation and the elongation steps during RNA synthesis.

1.9 Hypothesis

Based on the high similarity between the RdRp of HCV-1b and SARS COV-2, we hypothesized that ns5b-1b palm inhibitors will be effective in generating high-quality decoy set (using DEKOIS 2.0 protocol) to be used in benchmarking against ns5b to gain insight into the docking tool to be used for VS campaigns against SARS COV-2 RdRp (palm subdomain).

1.10. Objectives and Aims

The objective of the present study is to provide basis on how to repurpose FDA-approved drugs (from DrugBank database) and HCV-1b ns5b palm inhibitors against the palm pocket of SARS COV-2 RdRp by homology.

In addition, the specific aims of the current study are to:

1. Provide in-depth insights on how to choose a docking approach by utilizing the high quality DEKOIS 2.0 benchmarking.
2. Recognize the best performing docking tool among AutoDock Vina, FRED and PLANTS, to be applied in a prospective virtual screening against the palm subdomain of HCV-ns5b and SARS-CoV2 RdRp by homology.
3. Computationally recommend compounds from both databases, DrugBank and BindingDB, that are able to bind at the SARS COV-2 RdRp.

- *Novelty of this research*

In this project we provide an in-depth benchmarking study that reveals the effectiveness of PLANTS as a docking tool in the screening against the nsp12 palm site. Additionally, this study is proposing compounds that target a novel binding site on nsp12, which will potentiate other combination of drugs that are believed to provide synergistic effects. Furthermore, the results of this thesis showed promising candidates for treating COVID-19 via in silico methods.

2. MATERIALS AND METHODS

2.1 Preparation of protein macromolecules

Molecular Operating Environment (MOE), *Molecular Operating Environment (MOE 2018 and 2015)*, Chemical Computing Group Inc.: Montreal, <http://www.chemcomp.com>, was employed prior to the docking experiments to prepare the protein structures, including: (i) HCV-ns5b structures (PDB ID: 3TYQ and 3HHK), (ii) the SARS-CoV-2 RdRp (PDB ID: 7BV1). After eliminating the unessential ions, redundant chains, molecules of crystallization and unessential solvent molecules (if any), “Quickprep” Function of MOE was applied at default settings. Such parameters incorporate using “Protonate 3D” function to enhance H-bonding network and permit ASN/GLN/HIS to flip for optimum protonation and H-bonding networking. Additionally, the ligand and binding site atoms were refined through minimizing the energy to an RMS gradient of 0.1 kcal/mol/Å, while a force constant (strength = 10) was applied for the restraints of the binding site atoms. The remaining receptor atoms, which lie outside the binding pocket were kept the same. The outcome of these parameters showed no significant difference concerning the binding site /

ligand coordinates (T. M. Ibrahim, M. I. Ismail, M. R. Bauer, A. A. Bekhit, & F. M. Boeckler, 2020). We conducted the benchmarking experiment on HCV-ns5b twice, including and excluding key water molecules in the palm subdomain.

The prepared structures were saved as mol2 for both FRED and PLANTS docking programs, and as PDBQT format for AutoDock Vina docking experiments.

2.2 Preparation of small molecules including: DEKOIS 2.0 benchmark set, DrugBank database and BindingDB ligands

DEKOIS 2.0 (M. R. Bauer, T. M. Ibrahim, S. M. Vogel, & F. M. Boeckler, 2013) protocol was applied on 40 HCV-ns5b (genotype 1b) bioactives, which were extracted from BindingDB (Liu et al., 2007) and literature (Sofia et al., 2012), to produce 1200 challenging decoys (1:30 ratio). All small molecules were prepared by MOE. ‘Molecule wash’ module was employed to create reliable protonation states via strong bases protonation and strong acids deprotonation (if required). The energy of the compounds was minimized using the Amber: 10EHT force field at a gradient of 0.01 RMSD. The rest options were kept at default settings. For each compound, one conformer was saved, and one protonation state was produced at pH 7.0. The stereo configuration of all molecules (Liu et al., 2007) was reserved (T. M. Ibrahim et al., 2020). The prepared compounds were kept as SD files and used for FRED docking experiments. For docking experiments using AutoDock Vina, the SD files were transformed and split into individual PDBQT files by OpenBabel (O'Boyle et al., 2011). While for PLANTS docking, they were converted and split into mol2 format.

2.3 Docking experiments

2.3.1 For benchmarking

For docking using AutoDock Vina (version 1.1.2) (Trott & Olson, 2010), Python script (*prepare_receptor4.py*) provided by the MGLTools package (version 1.5.4) was employed to convert protein files to PDBQT format (Sanner, 1999). The search algorithm efficiency was retained at a default level. However, to consider all the possible conformations of the docked molecules, the grid box docking dimensions were $28 \text{ \AA} \times 28 \text{ \AA} \times 28 \text{ \AA}$, with a spacing of 1 \AA .

For docking using PLANTS (Korb, Stutzle, & Exner, 2009), ‘ChemPLP’ was employed as the scoring function, with the ‘screen’ mode selected. The binding site was set to include the

receptor atoms around the coordinates of the co-crystal ligand by 5 Å, in the palm subdomain of HCV ns5b (PDB ID: 3HHK).

For the OEDocking v3.2.0.2 docking (McGann, 2011, 2012), FRED docking (McGann, 2011, 2012) was set at default levels using the following commands (> fred.bat -receptor 3hhk.oeb -dbase actives-decoys.oeb.gz -out docked.sdf). Omega was used for generating different conformations of the ligands, actives and decoys, via the following command; > omega2.bat -in actives-decoys.sdf -out actives-decoys.oeb.gz. MakeReceptor GUI of OpenEye was utilized to describe the binding pocket as a search box in the vicinity of the co-crystal ligand with dimensions of 28.21 Å × 28 Å × 28.01 Å. Three water molecules were marked as a part of the protein, since they are essential for mediating certain interactions between the protein amino acid residues and the ligand.

The scoring function of each docking tool is shown in table 1.A. Non classical interactions are included empirically in the scoring functions. Additionally, to minimize any uncertainties in the calculations, grid box dimensions for the docking tools were kept at certain level of similarity and the other parameters were maintained at default level in order to provide the standard performance. Moreover, the community usually uses these tools at default levels.

2.3.2 For virtual screening of DrugBank and BindingDB ligands

Based on the superior performance of PLANTS in the benchmarking study, we selected it for virtual screening efforts against the SARS COV-2 RdRp (PDB ID: 7BV1). The protein is an apo form and no PDB structure is available yet for a co-crystallized complex in the palm subdomain. Therefore, the palm binding site was defined via docking the co-crystal ligand of HCV-NS5B (PDB ID: 3HHK) into the palm subdomain of the apo structure of SARS COV-2 RdRp (PDB ID: 7BV1). Then the docking search volume was defined based on 5 Å around of the coordinates of the docked molecule.

2.4 pROC and pROC-Chemotype calculations

The score-based docking order was utilized in calculating the pROC-AUC using “R-Snippet” component of KNIME (Berthold et al., 2007), based on the subsequent equation: (Clark & Webster-Clark, 2008)

$$pROC\ AUC = \frac{1}{n} \sum_i^n [-\log_{10}(D_i)] = \frac{1}{n} \sum_i^n \log_{10}\left(\frac{1}{D_i}\right)$$

The bioactives number is given by n , while D_i is the decoys fraction that is ordered higher than i th bioactive detected. Where i th is the number of the bioactive in the rank.

The pROC-Chemotype plots were created by the “pROC-Chemotype plot” tool accessible in <http://www.dekois.com/>. (T. M. Ibrahim, Bauer, & Boeckler, 2014; T. M. Ibrahim, Bauer, Dorr, Veyisoglu, & Boeckler, 2015)

To assess the ability of the docking tool to recognize true positives, from the active set, in the score-ordered list compared to the random collection, enrichment factor (EF) was computed based on the following equation (Wei, Baase, Weaver, Matthews, & Shoichet, 2002):

$$EF = \frac{Bioactives_{subset}}{N_{subset}} / \frac{Bioactives_{total}}{N_{total}}$$

All superpositions were conducted using MOE 2014.0901 and MOE 2018.

Chemical structures were drawn using ACD/ChemSketch Freeware (<https://www.acdlabs.com/resources/freeware/chemsketch/>)

3. RESULTS AND DISCUSSION

3.1 Selection of HCV-ns5b actives for decoys generation

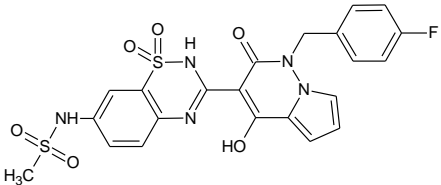
The active set to be used in the decoy generation for benchmarking study needs to include a high variety of chemotypes with potent reported activity. As was mentioned before, polymerase sites for inhibition are either the catalytic pocket or the allosteric pockets in thumb and palm subdomains. The active site is targeted by nucleotide inhibitors that bind to polymerases as alternative substrates (Sofia et al., 2012). Upon the incorporation of such inhibitors into the growing RNA chain, elongation step will be terminated. Since they are nucleotide analogues, they are very limited in terms of diversity. Modifications are only concerned with Ribose sugar substitutions and/or modifications at the base part (Sofia et al., 2012). On the contrary, non-nucleotide inhibitors are compounds with highly diverse scaffolds that inhibit polymerases through

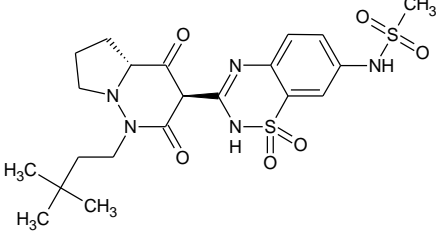
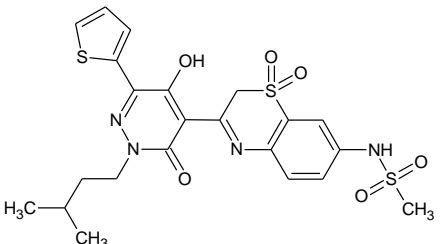
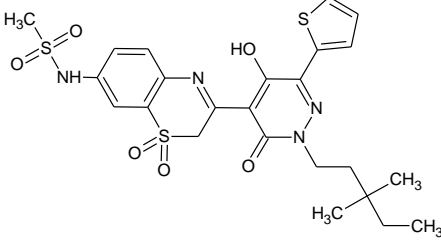
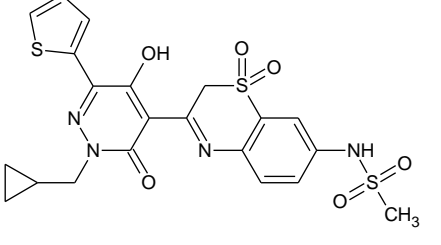
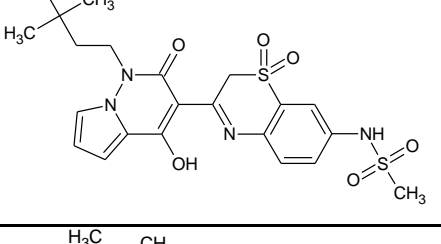
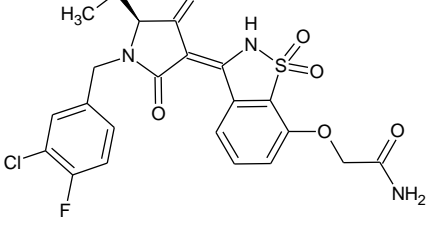
causing conformational changes, upon which polymerases will not be able to function effectively causing inhibition in the initiation step during RNA synthesis (Sofia et al., 2012). Here we selected our active set to be composed of ns5b-1b allosteric palm inhibitors based on the following justifications; the palm site is the most conservative subdomain with 15 Å in width and 20 Å in depth (Sofia et al., 2012). Consequently, a wide range of inhibitors targeting palm subdomain is available which will enrich the active set. Additionally, this subdomain encompasses the active site so targeting it will lead to blocking the nucleotide entry, hence, interfere with the RNA initiation and elongation steps (Sofia et al., 2012). Moreover, literature is mainly focusing on nucleotide analogues and lacks investigation about palm subdomain especially for the COVID-19.

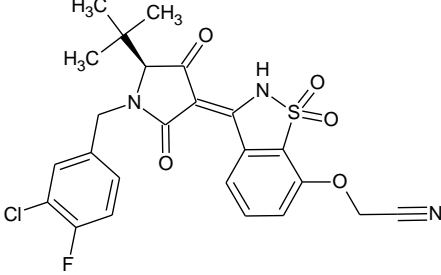
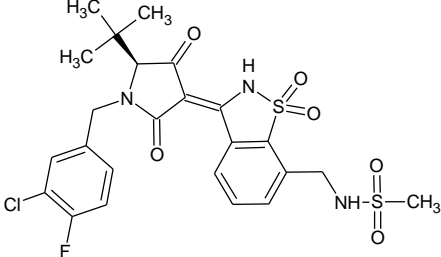
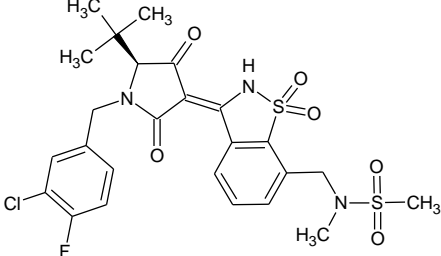
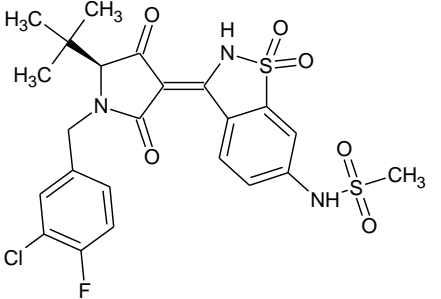
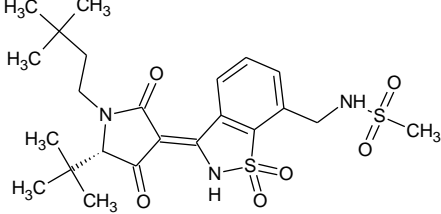
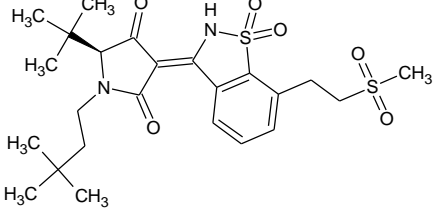
The palm allosteric pocket is actually known to be the interface between palm and thumb subdomains. In addition, palm residues from 363 to 369 are forming a deep hydrophobic pocket called primer grip. The primer grip region is formed from one wall of the palm and the opposite wall of the thumb, which is called β -hairpin loop (Sofia et al., 2012). This justifies why palm inhibitors may go through interactions with residues from the thumb site like Tyr448.

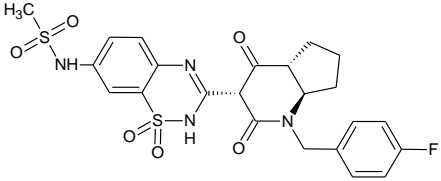
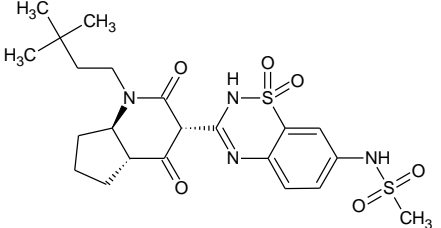
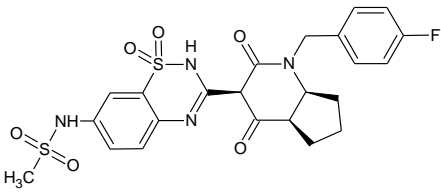
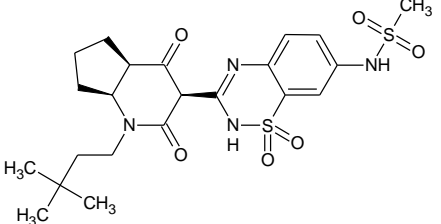
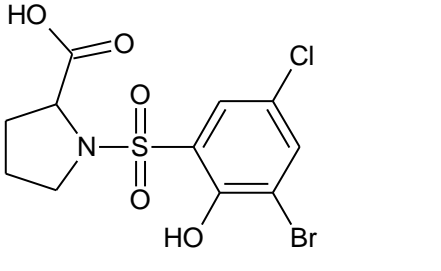
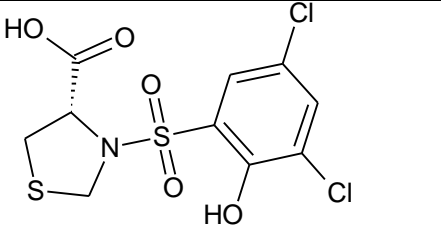
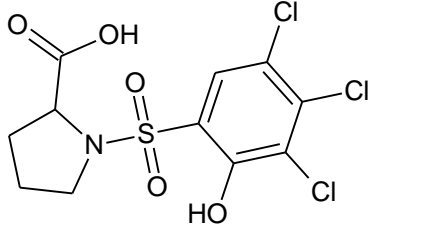
To build our active set (Table 3), we downloaded around 1.8 million molecules, from the BindingDB (Liu et al., 2007), that are found to have inhibitory effects on polymerases. Around 2900 compounds of them were acting on HCV polymerase (ns5b). 233 of them specifically inhibited 1b genotype, and 140 were targeting the palm subdomain. In addition to the compounds reported in BindingDB (Liu et al., 2007), we compiled scaffolds manually from literature to achieve the best diversity in the chemotypes. We selected around 2 to 4 molecules, with the lowest IC₅₀ values, as representatives for each scaffold. The activity is ranging from IC₅₀=5 nM to IC₅₀=470 nM. It is important to highlight that irreversible inhibitors as well as metal chelators inhibitors were excluded from the set.

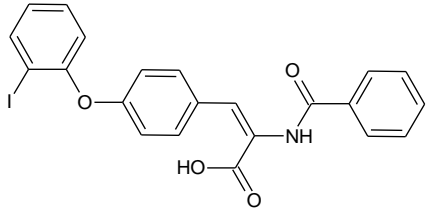
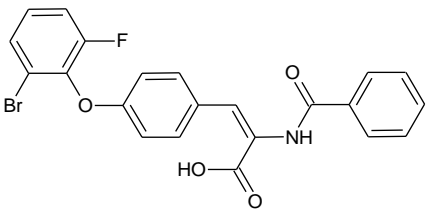
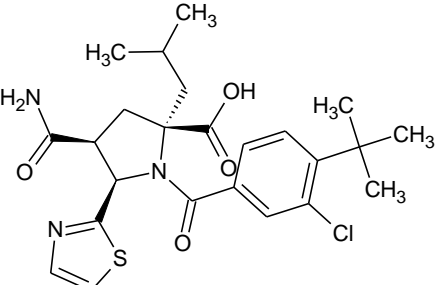
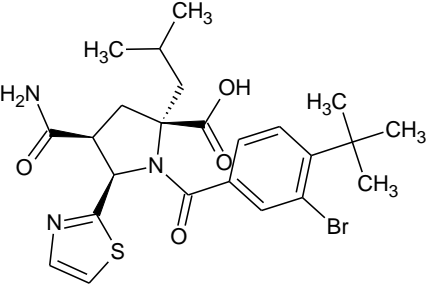
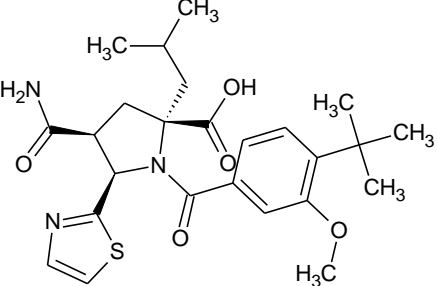
Table 3: The active set to be used in the benchmarking.

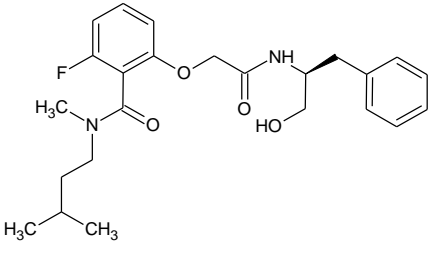
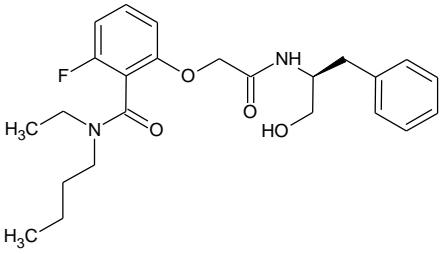
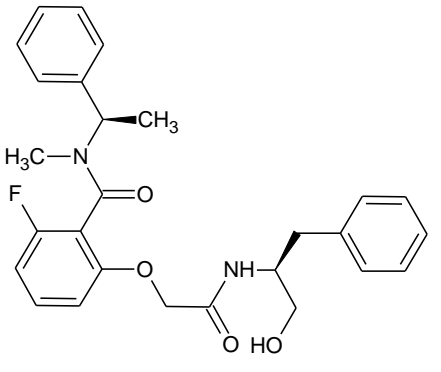
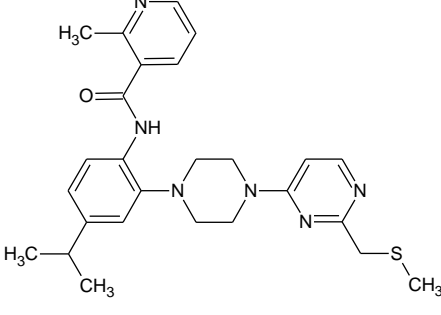
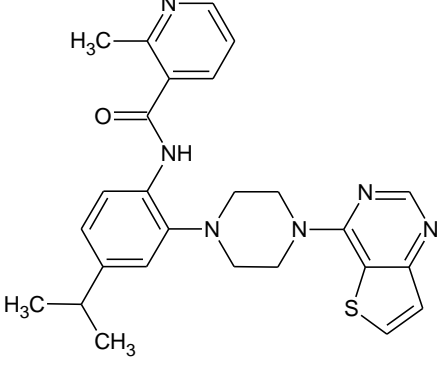
Structure	Scaffold Name	IC ₅₀ (nM)	PDB	The interacting amino acid residues	Refer ences
	Hexahydro- pyrrolo[1,2-b] pyridazin-2-one	10		Asp318 Asn291 Tyr448	(Rueb sam, Sun,

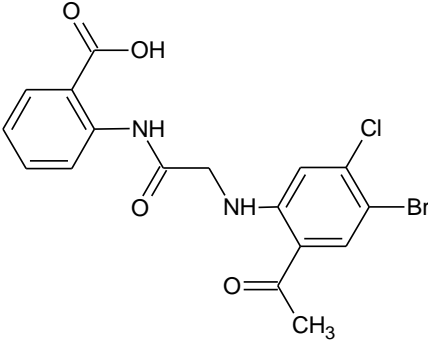
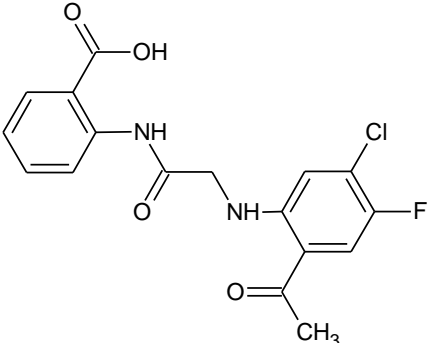
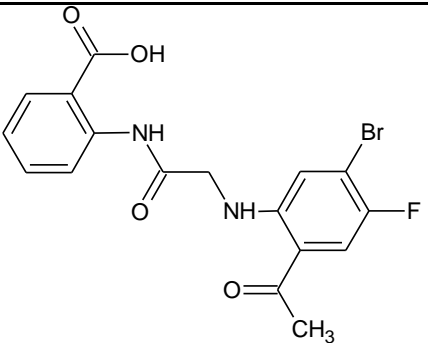
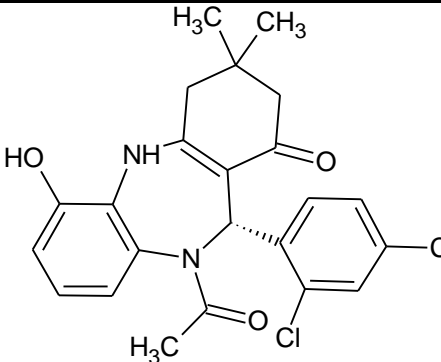
	analog, containing benzothiadiazine. (Pyridazinone motif)	10	3CVK	Gly449 Cys366 Water mediated interactions with Gly449, Gln446, Ser288 and Ser556.	et al., 2008)
	Benzothiazine-containing pyridazinone analog.	10	3CWJ	Asn411* Cys366 Ser556 Asn291 Water mediated interactions with Ser288 and Ser556.	(Ellis et al., 2008)
		10			
		15			
		10			
	1,1-dioxisothiazole	33		Asn291 Asp318 Water mediated interactions with Ser556, Ser288,	(Kim et al., 2008)

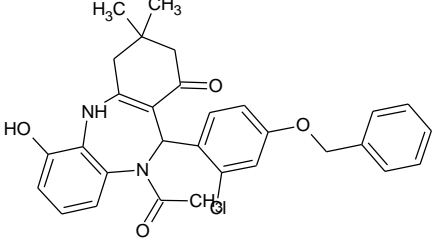
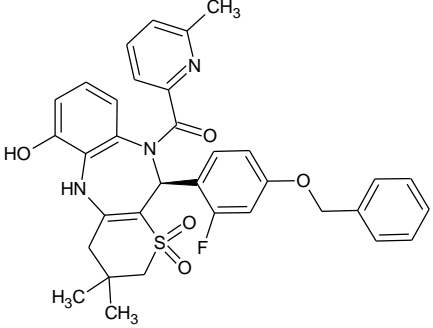
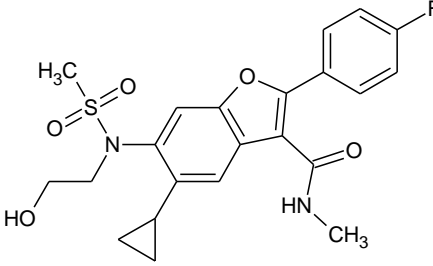
		70		Ser367, Tyr448, Tyr415, Met414, Leu384, Gln446, and Gly449.	
		10	3D5M		
		23			
		94			
		18			
		45			

	5,6-Dihydro-1H-pyridin-2-one	10		It binds to the palm pocket with no available data about the exact binding scheme.	(Ruebsam, Tran, et al., 2009)
		10			
		10			
		10			
	Proline sulfonamide	260		Try448 Ile447 Gly449 Gln446 Tyr415 Met414 Water mediated interactions with Asn441.	(Gopalsamy et al., 2006; Sofia et al., 2012)
		240			
		80			

	Acrylic acid	40		Tyr448 This class resides a lipophilic pocket that is formed by Pro197, Leu384, Met414, Tyr415, and Tyr448 residues. Water mediated interactions with Ser556 and Ser288.	(Pfefferkorn, Greene, et al., 2005; Sofia et al., 2012)
		30			
	N-acyl pyrrolidine	20		Tyr448 Ser476 Ile447 Gly449 Gln446 Trp528 Met423 Water mediated interactions with Tyr477, Arg386 and Gln446.	(Slate et al., 2007; Sofia et al., 2012)
		14			
		5			

	Benzamide	470		Tyr195 Phe551 Water mediated interactions with Asn316, Arg200, Gly192, Ser556, Ser288, Tyr448, Gly554, Gln194 and Gly449.	(Chen g, Shipp s, et al., 2010; Sofia et al., 2012)
		470			
		430			
	Nicotinamide	27		It binds to the palm pocket with no available data about the exact binding scheme.	(Chen g, Huan g, et al., 2010; Sofia et al., 2012)
		14			

	Anthranilic acid	22		Arg386 Tyr415 Tyr448 Ile447	(Nitto li et al., 2007; Sofia et al., 2012)
		17			
		10			
	Benzodiazepine	81		Tyr448 Ile447 Water mediated interactions with Asn411, Ser367 and Tyr415.	(McG owan et al., 2009; Sofia

		40			et al., 2012)
	Sulphone	26		Gly449 Gln446 Ser367 Ser556 Ile447 Arg386 Leu384 Water mediated interactions with Gln446, Arg394, Arg386 and Asn411.	(Sofia et al., 2012; Vand yck et al., 2009)
	Benzofuran	81		Met414 Ser365 Arg200 Water mediated interactions with Arg386 and Tyr415 and Tyr488.	(How e et al., 2008; Sofia et al., 2012)

*The thiophene Sulphur is the one responsible for the interaction with Asn411. Therefore, the last benzothiazine molecule is not connected with this residue.

3.2 Selection of representative PDB structure(s) for HCV ns5b-1b

At this point we need to use a protein structure that will represent HCV polymerase in the benchmarking study. We downloaded all ns5b available PDB codes (Table 2.A) and started filtering them according to the following criteria. First of all, the selected structure needs to be co-

crystallized with a palm subdomain inhibitor in order to consider any structural changes that may happen to the protein upon ligand binding. Therefore, Apo structures were omitted during the selection. Secondly, since the active set is composed of inhibitors acting on genotype 1b, the chosen structure is required to represent the HCV polymerase of genotype 1b. According to this, we selected the top five protein structures, in terms of resolution, from (Table 4). We performed a superposition analysis using MOE to figure out any deviation, either in the backbone or the side chain. Figures 10, 11 and 12, show no significant difference between the five protein structures since they show low RMSD value. At the beginning, we conducted the benchmarking using 3TYQ as it has the highest resolution. However, we found that the co-crystallized ligand is forming a covalent bond with Cys366 which may cause conformational changes to the side chain and affect the docking outcome. Thus. We finally selected the 3HHK to represent the HCV ns5b-1b proteins in our study.

Table 4: HCV ns5b structures with the highest resolution values.

PDB ID	Structure title	Ligand ID	Binding site	Resolution (Å)	Reference
3HKW	HCV ns5b genotype 1a in complex with 1,5 benzodiazepine inhibitor 6	IX6	Palm 1	1.55	(Nyanguile et al., 2010)
2HAI	Crystal structure of HCV ns5b RNA polymerase in complex with novel class of dihydropyrone-containing inhibitor	PFI	Thumb	1.58	(Li et al., 2006)
3TYQ	SAR development and discovery of potent indole-based inhibitors of the hepatitis C virus ns5b polymerase	HI4	Palm	1.6	(K. X. Chen, Lesburg, et al., 2012)
4MZ4	Discovery of an irreversible HCV ns5b polymerase inhibitor	2F3	Palm	1.63	(Zeng et al., 2013)
2GIQ	Hepatitis C virus RNA-dependent RNA polymerase ns5b with NNI-2 inhibitor	NN2	Thumb II	1.65	(Le Pogam et al., 2006)
3TYV	SAR development and discovery of potent indole-based inhibitors of the hepatitis C virus ns5b polymerase	HI3	Palm	1.65	(K. X. Chen, Vibulbhan, et al., 2012)

4KHM	HCV ns5b GT1a with GSK5852	1PV	Palm 2	1.7	(Maynard et al., 2014)
2XI3	HCV-h77 ns5b polymerase complexed with GTP	GTP		1.7	(Harrus et al., 2010)
3HHK	HCV ns5b polymerase complex with a substituted benzothiadizine	77Z		1.7	(Shaw et al., 2009)
3SKA	I. Novel HCV ns5b polymerase inhibitors: discovery of indole 2-carboxylic acids with c3-heterocycles	53	Palm	1.73	(Anilkumar et al., 2011)

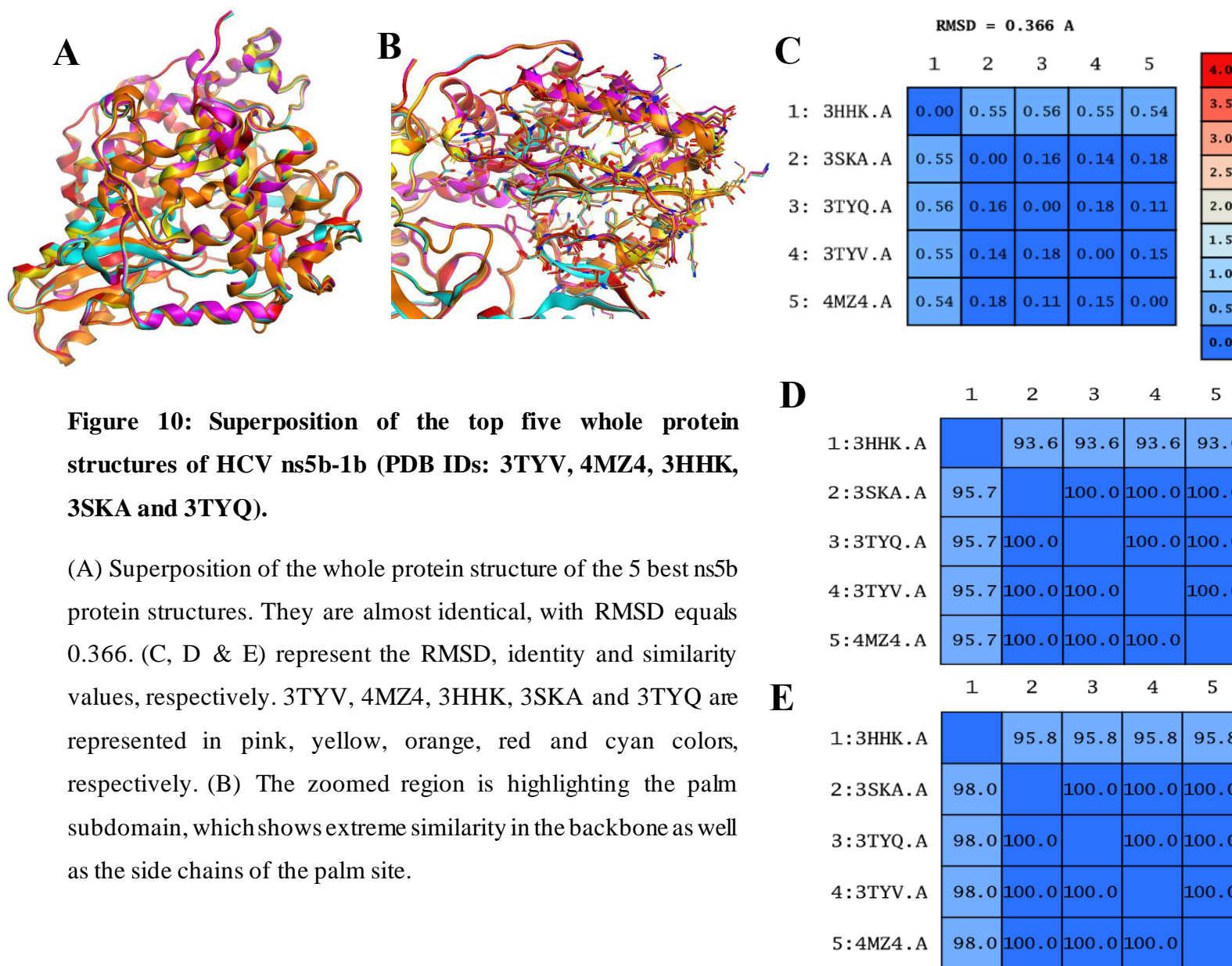


Figure 10: Superposition of the top five whole protein structures of HCV ns5b-1b (PDB IDs: 3TYV, 4MZ4, 3HHK, 3SKA and 3TYQ).

(A) Superposition of the whole protein structure of the 5 best ns5b protein structures. They are almost identical, with RMSD equals 0.366. (C, D & E) represent the RMSD, identity and similarity values, respectively. 3TYV, 4MZ4, 3HHK, 3SKA and 3TYQ are represented in pink, yellow, orange, red and cyan colors, respectively. (B) The zoomed region is highlighting the palm subdomain, which shows extreme similarity in the backbone as well as the side chains of the palm site.

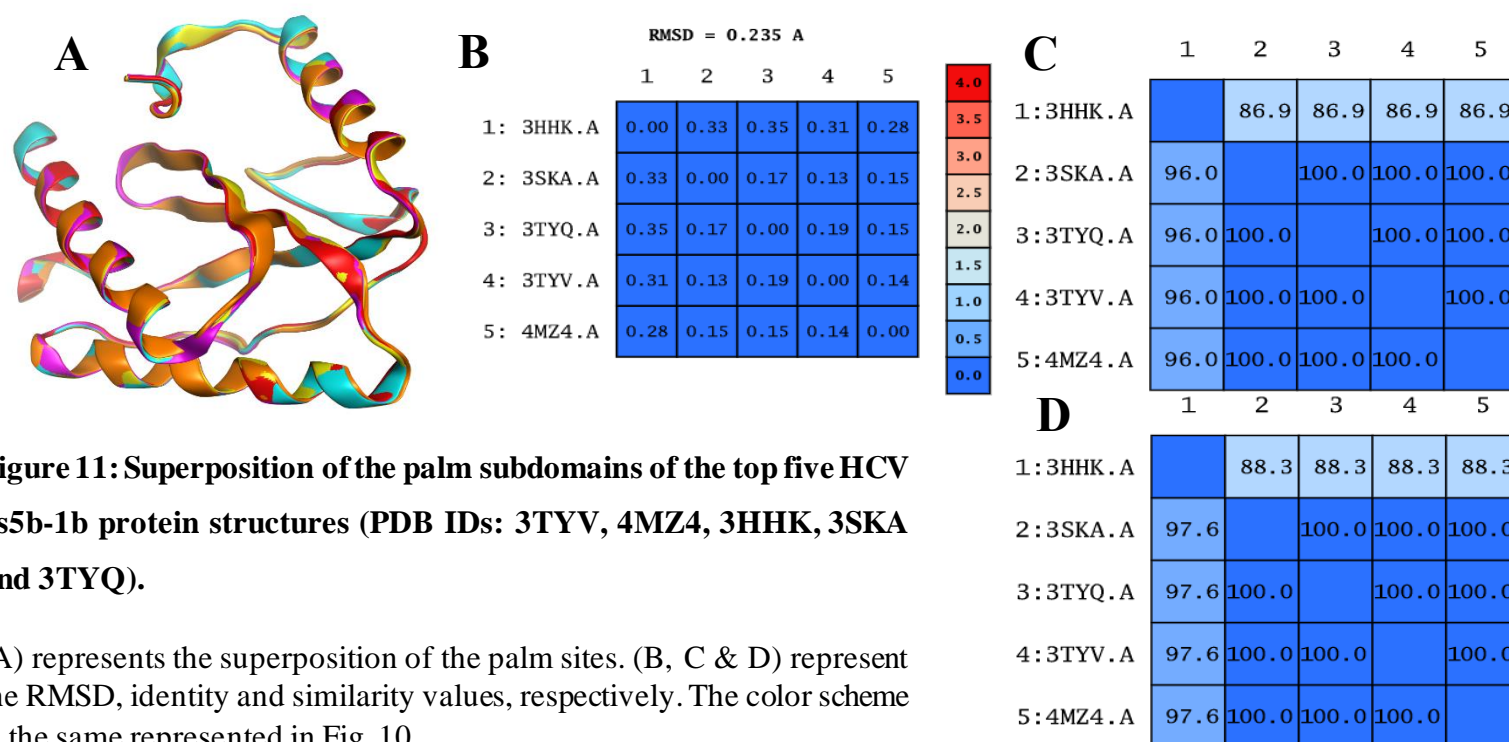


Figure 11: Superposition of the palm subdomains of the top five HCV ns5b-1b protein structures (PDB IDs: 3TYV, 4MZ4, 3HHK, 3SKA and 3TYQ).

(A) represents the superposition of the palm sites. (B, C & D) represent the RMSD, identity and similarity values, respectively. The color scheme is the same represented in Fig. 10.

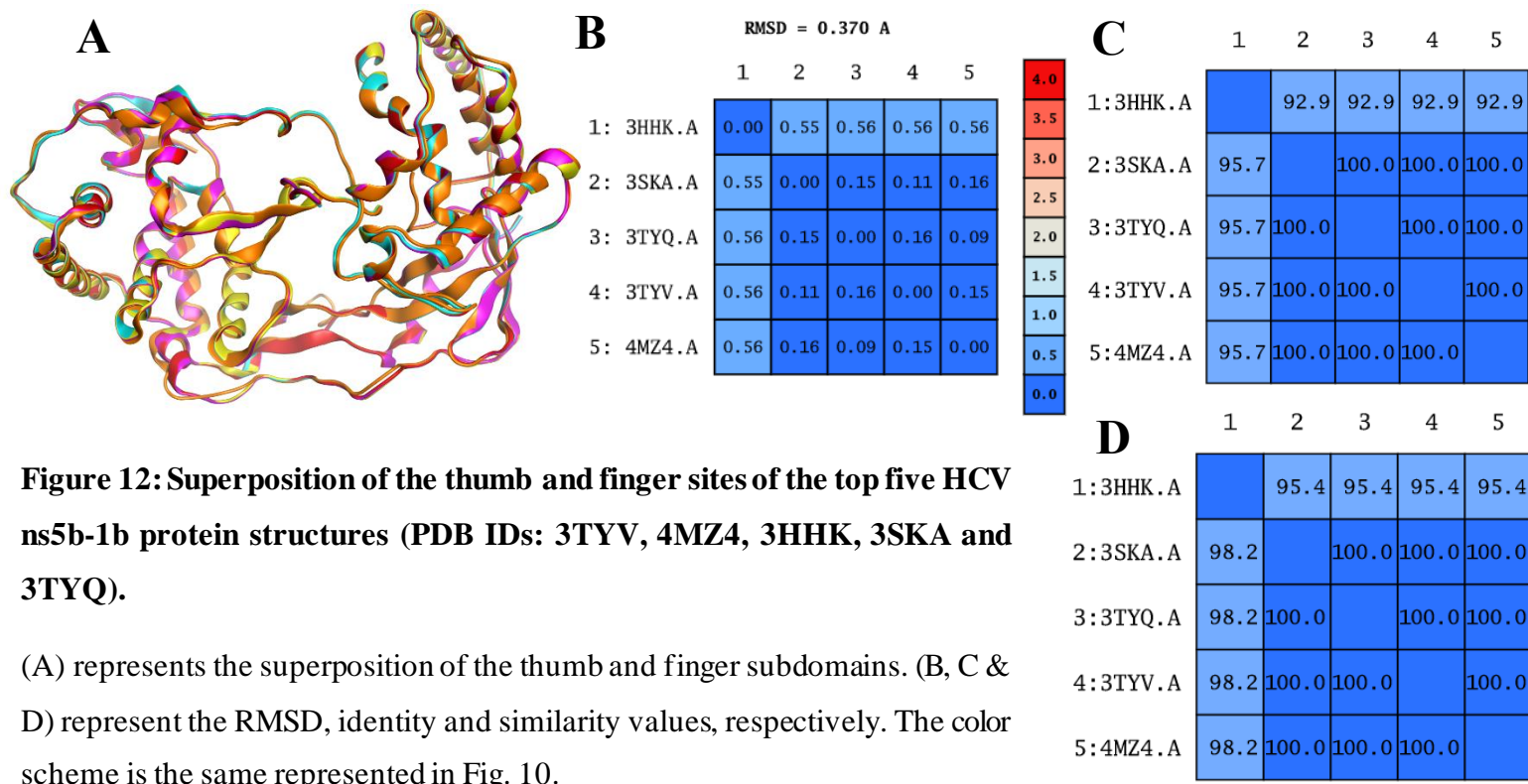


Figure 12: Superposition of the thumb and finger sites of the top five HCV ns5b-1b protein structures (PDB IDs: 3TYV, 4MZ4, 3HHK, 3SKA and 3TYQ).

(A) represents the superposition of the thumb and finger subdomains. (B, C & D) represent the RMSD, identity and similarity values, respectively. The color scheme is the same represented in Fig. 10.

3.3 Benchmarking

There are certain requirements for providing meaningful molecular benchmarking sets for structure-based VS. First, a well curated and characterized set of ligands, also often referred to as actives, has to be compiled. Second, decoy structures have to be selected based on the high-quality criteria (e.g., DEKOIS 2.0 protocol (M. R. Bauer et al., 2013; Boeckler, Bauer, Ibrahim, & Vogel, 2014; Vogel, Bauer, & Boeckler, 2011)). And finally, one (or more) well-suited 3D structure is needed to model the ligand binding site. These essential requirements confine the eligible targets for benchmark set generation.

The DEKOIS 2.0 library includes 81 new high-quality benchmark sets for 80 protein targets (2 benchmark sets for different PYGL binding sites). DEKOIS 2.0 library comprises a diverse selection of protein classes like kinases, proteases, nuclear receptors, GPCRs, oxido-reductases, transferases, hydrolases and several others, as shown in Figure 13. The DEKOIS 2.0 benchmark set protocol is automated and can generate challenging decoy set for any given active molecules (Tamer M. Ibrahim, Muhammad I. Ismail, Matthias R. Bauer, Adnan A. Bekhit, & Frank M. Boeckler, 2020).

Figure 14 (adapted from(M. R. Bauer et al., 2013)) shows the individual docking performances as color-coded pROC AUC values of three docking tools, Glide, GOLD, and AutoDock Vina within the previously presented polar dendrogram of 80 DEKOIS 2.0 targets that were clustered by their EC codes. It shows the docking performances via pROC AUC. pROC AUC is a semi-logarithmic measure that emphasizes early hit recognition.(Clark & Webster-Clark, 2008). An important conclusion from this Figure is that the docking/benchmarking performances remained target dependent. However, conserved binding sites in similar target class usually show superior performance via certain docking tool. For instance, for kinases, GLIDE appeared to be the best docking tool to discriminate between the active and decoy molecules compared to the other two docking tools, i.e., GLIDE performance shows greener color compared to the others. Similarly, for COX-1 and COX-2 enzymes, AutoDock Vina appeared to be the best performing. Inspired by these observations, we collected and compiled active set for the closely related HCV-ns5b (palm subdomain) due to the unavailability of SARS COV-2 RdRp small palm binders and the extreme resemblance of both HCV-ns5b and SARS COV-2 RdRp. We evaluated the screening performance of some highly cited docking programs FRED, AutoDock Vina and PLANTS against HCV-ns5b (palm subdomain). The outcome of this benchmarking efforts is certainly useful to gain

insights and decide which docking tool can be used for the closely related SARS COV-2 RdRp (palm subdomain).

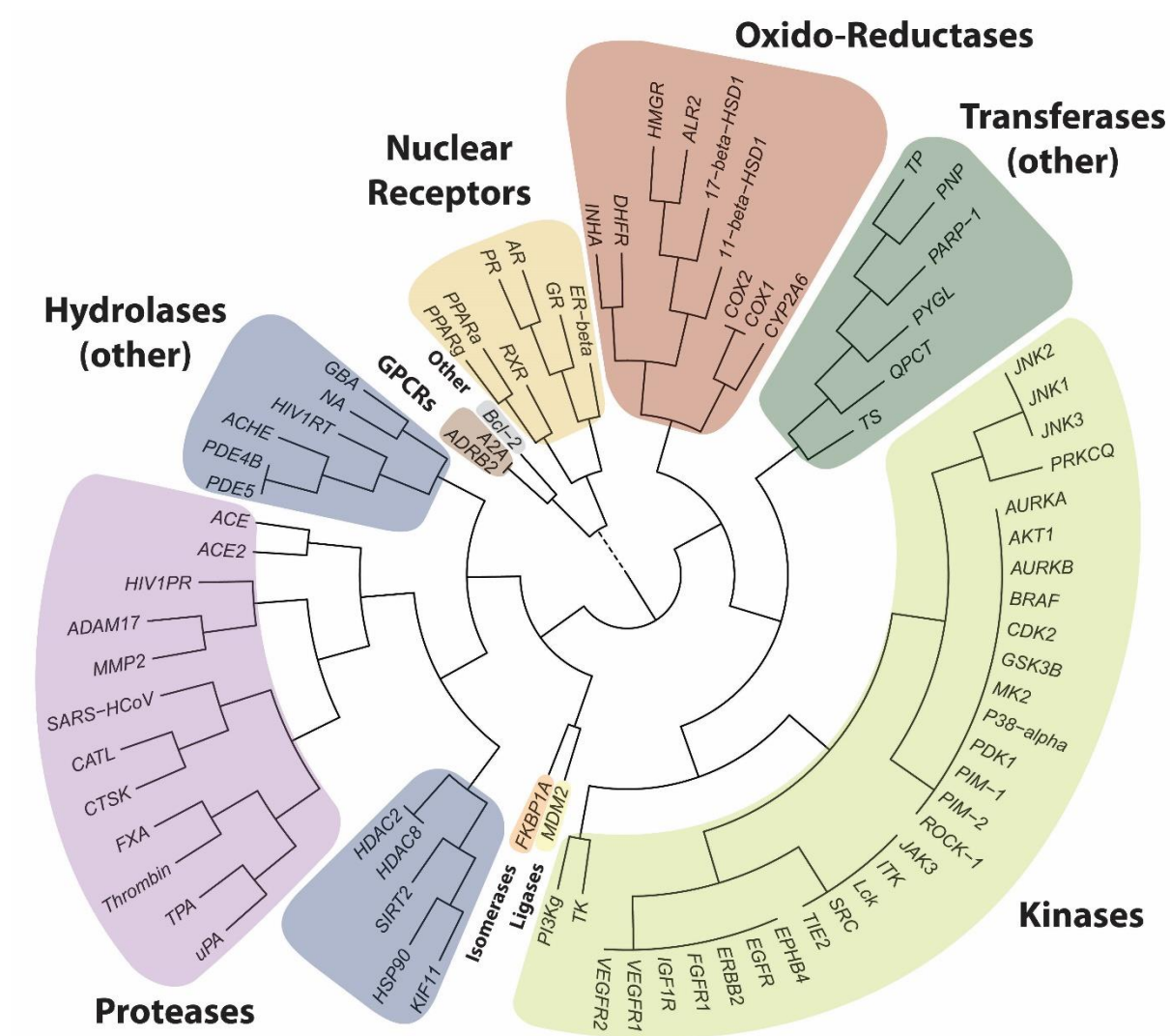


Figure 13: DEKOIS 2.0 target overview.

80 protein targets are clustered according to their enzyme commission numbers (EC) and depicted as polar dendrogram. Important enzyme groups are highlighted in the figure. (M. R. Bauer et al., 2013)

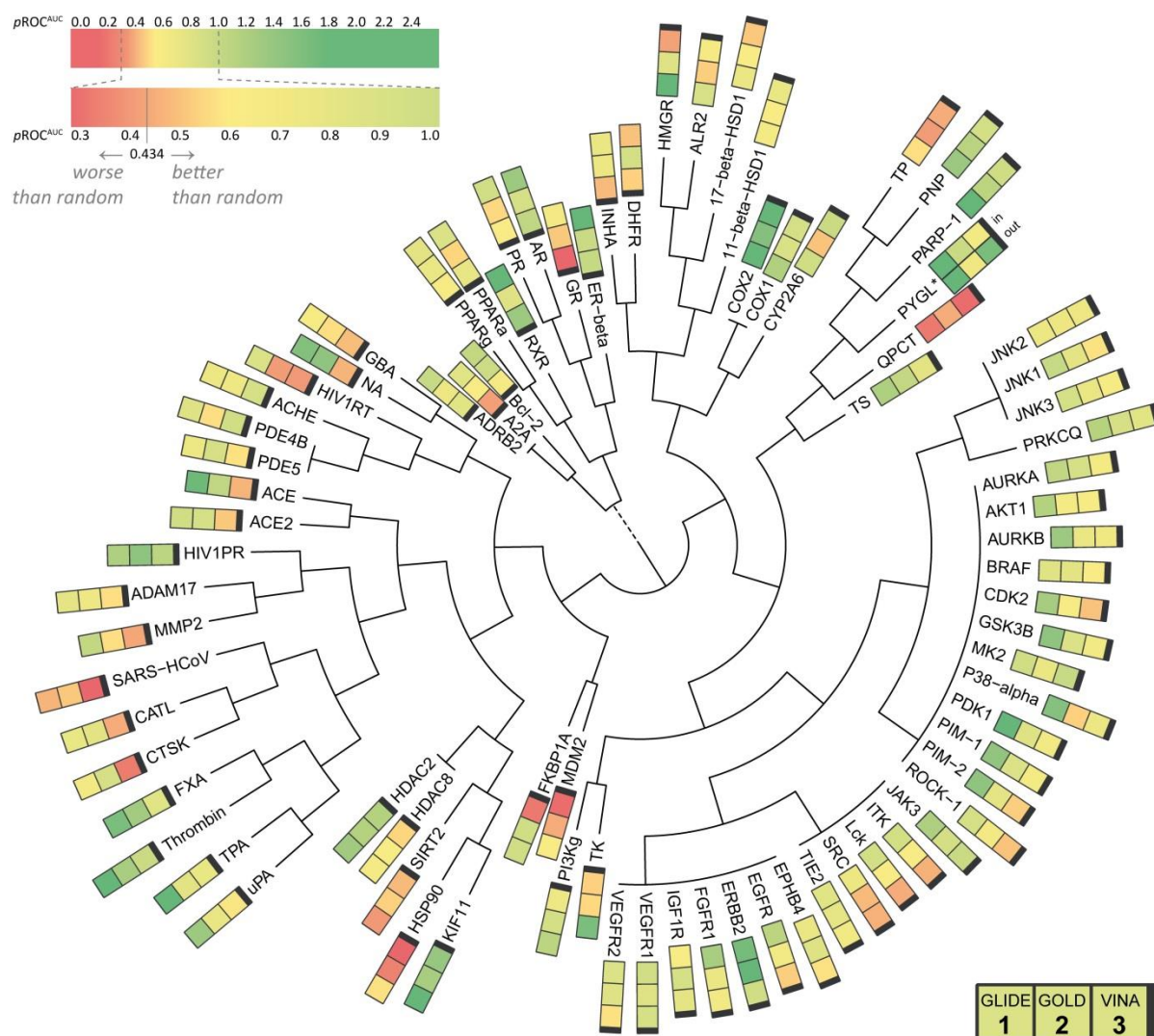


Figure 14: DEKOIS 2.0 target overview with pROC AUC enrichment results for Glide, GOLD and AutoDock Vina.

Docking calculations were conducted at default settings of the respective program. All targets are clustered by their EC codes and shown as polar dendrogram, as previously described. The calculated pROC AUC values were color-coded. A red color corresponds to a negative docking enrichment performance, orange and yellow to a random performance, and green to a reasonable or good screening performance. To facilitate the interpretation of color shades, we provide a scale for the pROC AUC values. (M. R. Bauer et al., 2013)

The HCV-ns5b (palm subdomain) benchmarking results when including key water molecules showed that PLANTS is the best performing docking tool with pROC-AUC value of 0.97. The screening performance of AutoDock Vina and FRED showed pROC-AUC values of 0.66 and 0.36, respectively (Figure 15). Additionally, PLANTS exhibited the highest screening performance when excluding the key water molecules, as shown in Figure 15. Interestingly, unlike FRED, PLANTS and AutoDock Vina performed better-than-random performance (pROC-AUC value > 0.43).

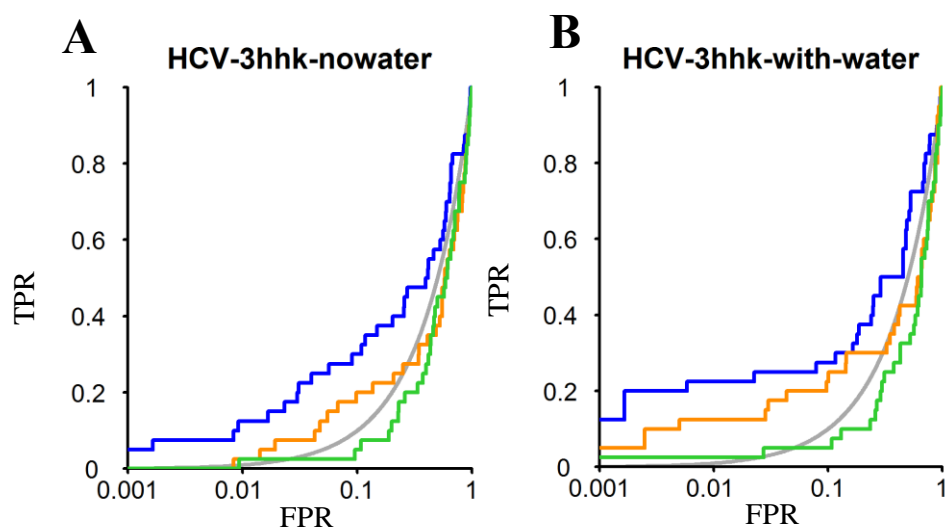


Figure 15: pROC plots of docking experiments showing the screening performance of both including and excluding key water molecules in the palm subdomain for HCV ns5b (PDB ID: 3HHK) for (A) and (B), respectively.

The benchmarking results of FRED, AutoDock Vina and PLANTS are presented by green, orange and blue lines, respectively. The random screening performance is shown as a grey line. The Y-axis is the true positive rate (TPR), which reflects the fraction of detected bioactives. While, the X-axis shows the decoys retrieved fraction that is known as false positive rate (FPR).

We examined the chemotype/scaffold enrichment with the “pROC-Chemotype”(T. M. Ibrahim et al., 2014; T. M. Ibrahim et al., 2015) plot (Figure 16) for the benchmarking of HCV-ns5b (palm subdomain) using PLANTS docking tool.

BindingDB database (Liu et al., 2007) and literature (Sofia et al., 2012) reported a variety of compounds to target HCV-NS5B (1b genotype) palm subdomain. Based on that, we selected 13 chemical scaffolds to represent the chemotype clusters of the chemical space available to target the relevant palm subdomain. This diversity of the established chemotypes highlights the challenging nature of the benchmarking against the employed docking tools.

The pROC-Chemotype plot visualized that the utilized docking procedure – by PLANTS - is expected to discover high affinity binders at early enrichment (Figure 16A). Elucidating the docking poses of the best scored actives underlines that they exhibited the key interactions of the co-crystal ligand in the palm subdomain, as shown in Figure 17. Moreover, at 1% of the score-ranked library, only two decoys were detected and many bioactives were enriched, causing an EF 1% value equals 20.0. Therefore, PLANTS can recognize actives 20 times more than the random performance (at a library cutoff 1%). It should be noted that the enrichment factor (EF) is independent of the number of actives and decoys, which were detected by the docking tool. This emphasizes encouraging prediction power of PLANTS for the closely related SARS COV-2 RdRp (palm subdomain). The bioactivity data are symbolized by *level of activity* (LOA) extending from 10^{-7} to 10^{-9} M and reported as IC_{50} as a *type of data* (TOD) (Figure 16A).

Figure 16B demonstrates the bioactives distribution with respect to their docking scores. Since fitness is the docking score multiplied by -1, the docking scores are presented by fitness values ranging from 113.87 (best score) to 58.09 (worse score). Additionally, molecules belong to scaffold 1 present in a superior region of fitness (i.e., fitness > -90). The two-best scored molecules (with docking rank 1 and 2 in in Figure 16A), demonstrate interactions with the following key residues; Asp318, Tyr448 and Cys366, in addition to water mediated interactions with; Ser288, Ser556, Gly449 and Gln446 (Figure 17). These interactions are in coherence to the respective interactions with ns5b (Table 3).

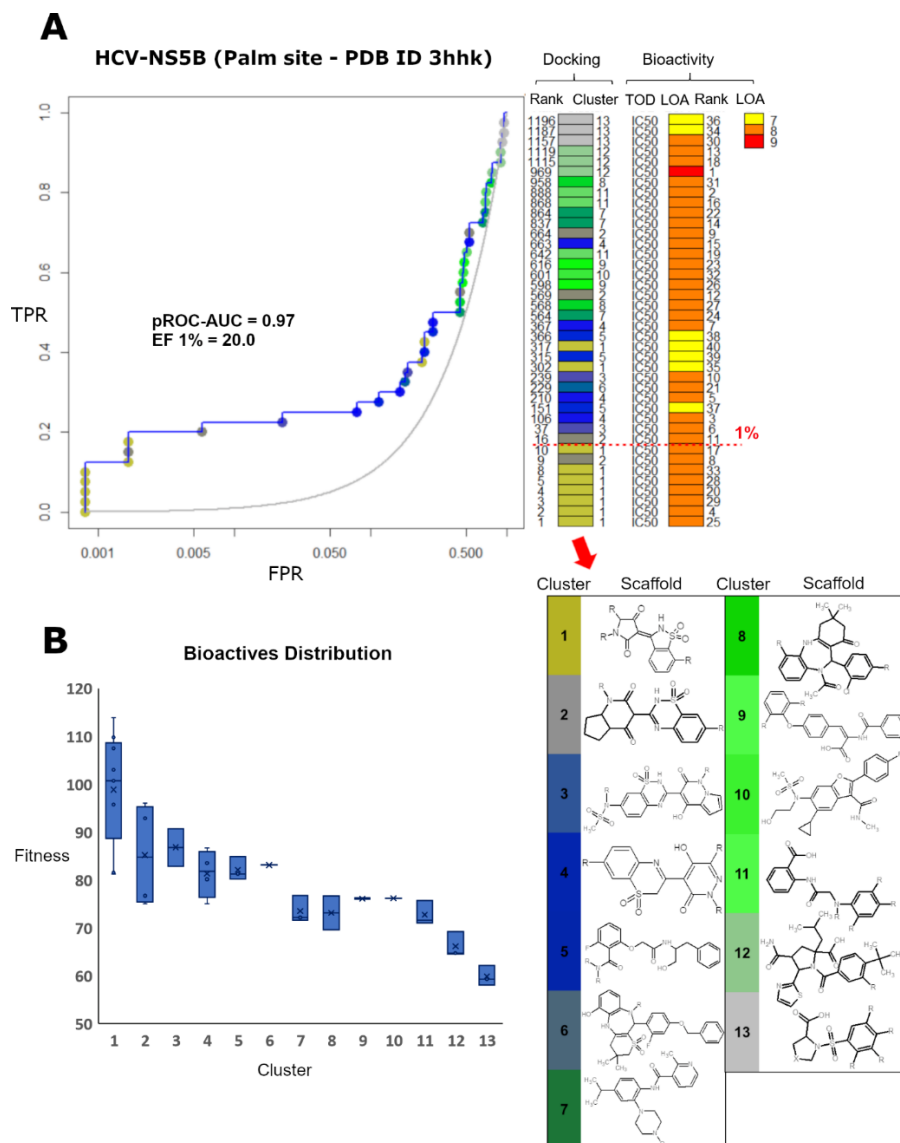


Figure 16: (A) pROC-Chemotype plot (T. M. Ibrahim et al., 2015) of the HCV-ns5b (in the palm subdomain – PDB ID: 3HHK, including key water molecules) using PLANTS docking tool.

(A) PLANTS docking information is paired with the cluster number (scaffold) and the ligand bioactivity rank. The bioactivity rank is shown as a color scale from red to yellow. The reddish the bioactivity scale the higher the potency. The 1% bioactive enrichment is shown as a red-dashed line. (B) The distribution of the bioactive molecules of each scaffold (cluster) in correlation to PLANTS score presented by fitness values.

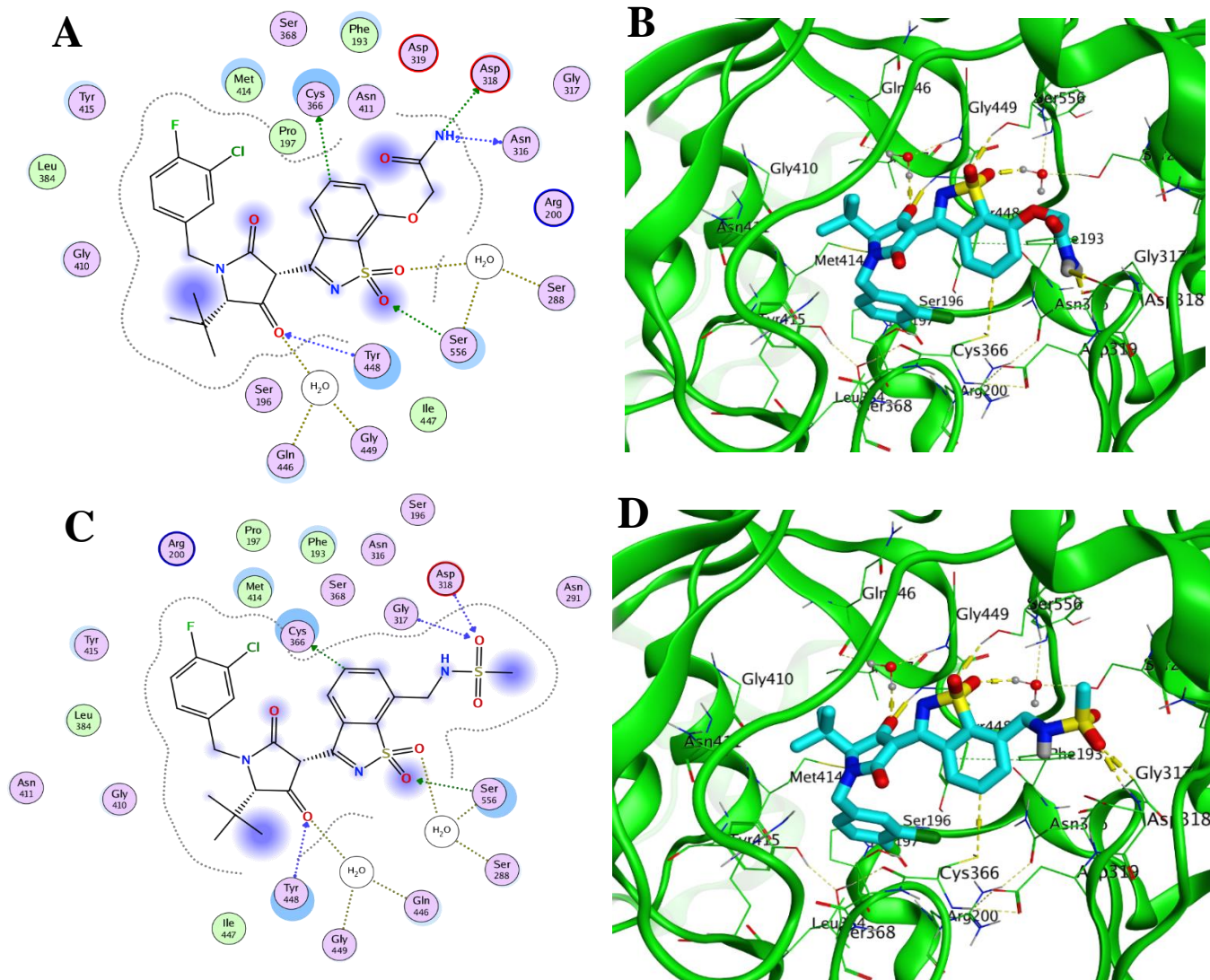


Figure 17: Docking poses of the best two scoring compounds from the active set in the palm subdomain of HCV-ns5b-1b (PDB ID: 3HHK).

Compounds are shown as cyan sticks. (A and C) Represent the 2D interactions, while (B and D) are the three-dimensional representations of the interactions. Dashed lines reveal favorable bindings. Non-polar hydrogens are omitted for clarification.

3.4 Prospective VS based on Benchmarking

Based on the promising results of the benchmarking study, we used PLANTS to screen the FDA-drugs from the DrugBank database as well as ns5b inhibitors available in the BindingDB database (Liu et al., 2007). Since the available co-crystallized nsp12 structures are found to be with nucleotide inhibitors, the virtual screening was conducted against the Apo structure of SARS-COV-2 RdRp (PDB ID: 7BV1) (Table 5). We conducted a superposition between the Apo structure of HCV polymerase genotype 1b (PDB ID: 2XHV) and the co-crystallized structure (PDB ID: 3HHK) (Figure 18). This superposition proved the high similarity between the two structures which reveals that the palm inhibitor (PDB ID: 3HHK) has a very little effect on the conformation of the protein. Since SARS COV-2 RdRp is highly similar to HCV-ns5b, the Apo structure of nsp12 is expected to have a very close conformation to the co-crystallized palm inhibitor structure.

Table 5: The available SARS COV-2 polymerase structures.

PDB ID	Structure Title	Resolution (Å)	Reference
7AAP	Nsp7-Nsp8-Nsp12 SARS-CoV2 RNA-dependent RNA polymerase in complex with template-primer dsRNA and <u>Favipiravir-RTP</u>	EM R: 2.5, R: 2.5	
7BV2	The nsp12-nsp7-nsp8 complex bound to the template-primer RNA and triphosphate form of <u>Remdesivir (RTP)</u>	EM R: 2.5, R: 2.5	(Yin et al., 2020)
7BV1	Cryo-EM structure of the apo nsp12-nsp7-nsp8 complex	EM R: 2.8, R: 2.8	(Yin et al., 2020)
6YYT	Structure of replicating SARS-CoV-2 polymerase	EM R: 2.9, R: 2.9	(Hillen et al., 2020)
6M71	SARS-Cov-2 RNA-dependent RNA polymerase in complex with cofactors	EM R: 2.9, R: 2.9	(Gao et al., 2020)
7CXM	Architecture of a SARS-CoV-2 mini replication and transcription complex	EM R: 2.9, R: 2.9	
7C2K	COVID-19 RNA-dependent RNA polymerase pre-translocated catalytic complex	EM R: 2.93, R: 2.93	(Q. Wang et al., 2020)

7BTF	SARS-CoV-2 RNA-dependent RNA polymerase in complex with cofactors in reduced condition	EM R: 2.95, R: 2.95	(Gao et al., 2020)
7CTT	Cryo-EM structure of <u>Favipiravir</u> bound to replicating polymerase complex of SARS-CoV-2 in the pre-catalytic state.	EM R: 3.2, R: 3.2	
7BZF	COVID-19 RNA-dependent RNA polymerase post-translocated catalytic complex	EM R: 3.26, R: 3.26	(Q. Wang et al., 2020)
6XQB	SARS-CoV-2 RdRp/RNA complex	EM R: 3.4, R: 3.4	
6XEZ	Structure of SARS-CoV-2 replication-transcription complex bound to nsp13 helicase - nsp13(2)-RTC	EM R: 3.5, R: 3.5	(J. Chen et al., 2020)
7CXN	Architecture of a SARS-CoV-2 mini replication and transcription complex	EM R: 3.84, R: 3.84	

Table 6 represents the best 1% of the docking outcome of the DrugBank database. While, table 7 displays the best 1% of the BindingDB database (Liu et al., 2007) docking outcome. We started analyzing the binding poses of each molecule and we found that they mainly occupy one of the four sites shown in (Figure 19). Taking HCV-ns5b palm inhibitors as a reference, it appeared that inhibition occurs when the inhibitor is residing (overlying) the palm pocket in front of the F motif in the finger subdomain (Figure 20). As was mentioned, the F motif is responsible for directing the incoming NTPs into the active site of the palm subdomain. As a consequence, the entry path to the active site will be blocked, leading to the inhibition of initiation and elongation steps during the viral replication. Accordingly, from the best ranked 1%, molecules that reside site d of the nsp12 palm subdomain (Figure 19) will be considered.

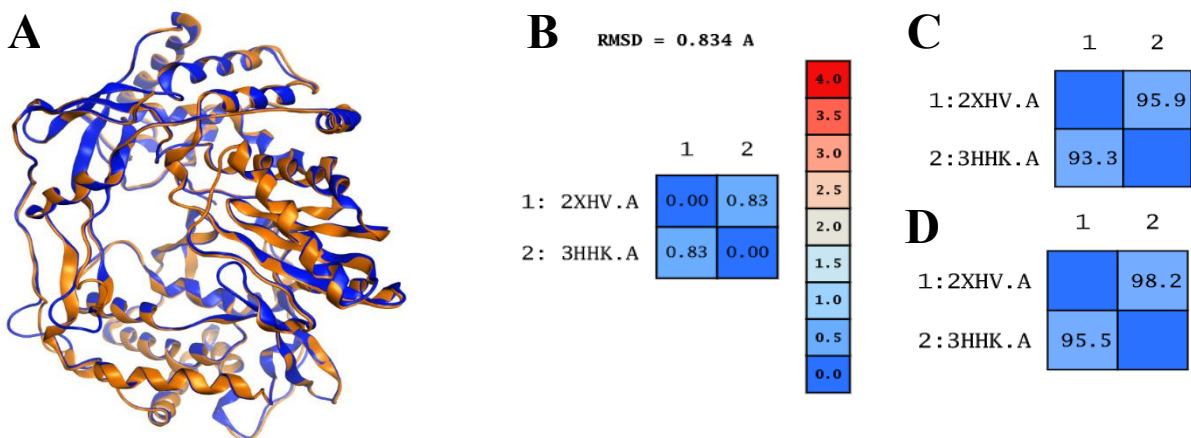
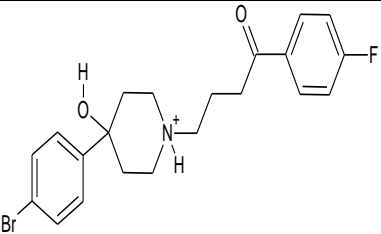
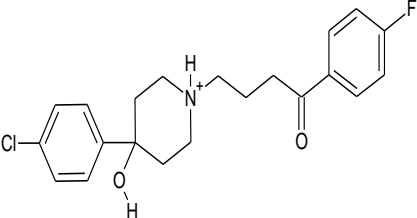
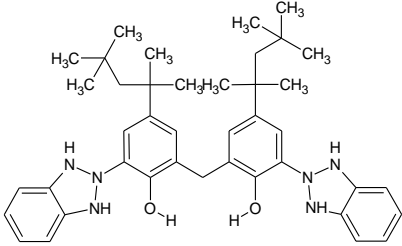
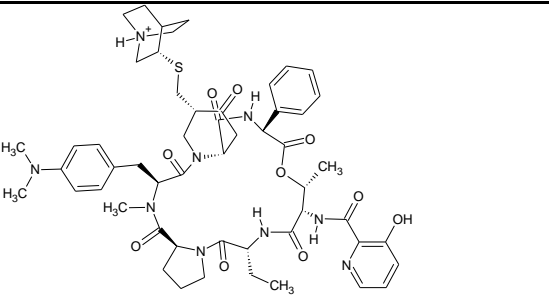
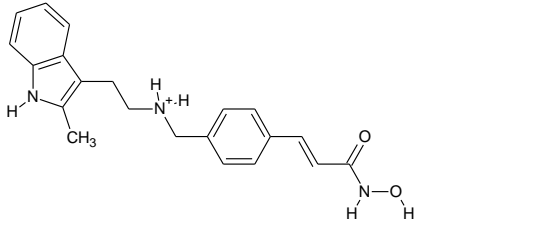
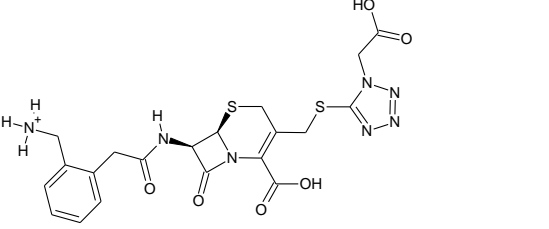
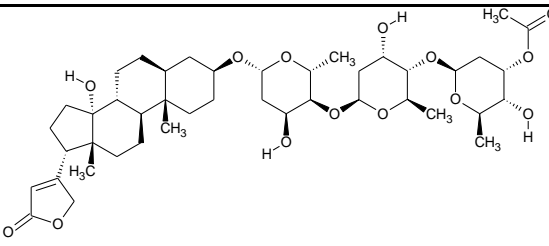


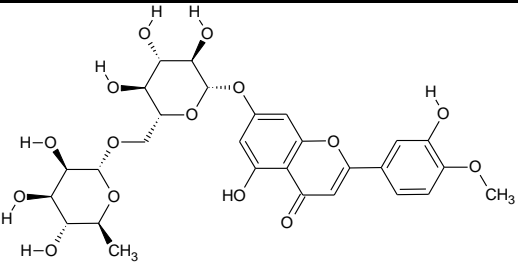
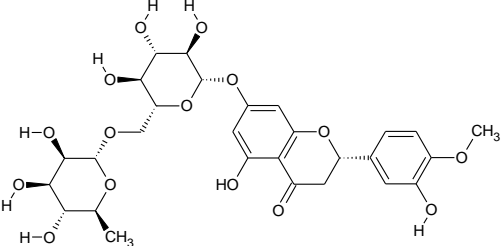
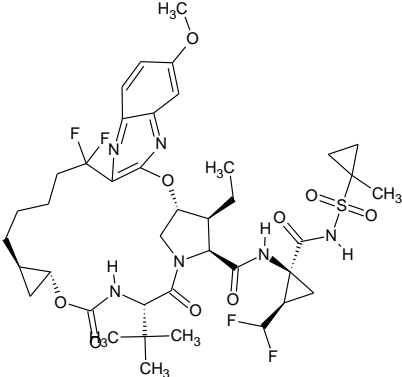
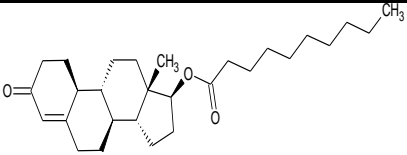
Figure 18: Superposition of HCV ns5b-1b Apo structure (PDB ID: 2XHV) and the co-crystallized form (PDB ID: 3HHK).

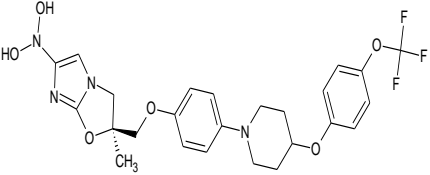
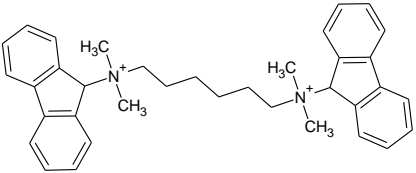
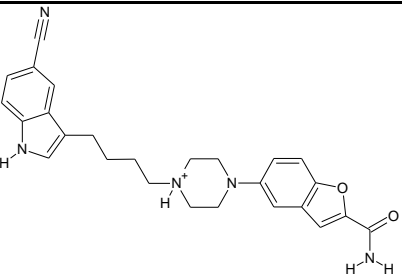
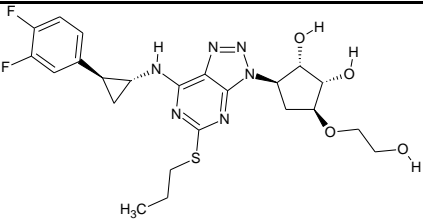
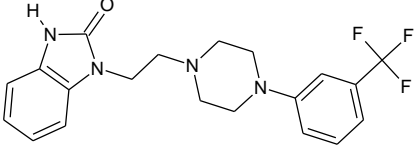
(A) Superposition of 3D structures of Apo and co-crystallized ns5b structures colored in blue and orange, respectively. (B, C & D) represent the RMSD, identity and similarity, respectively.

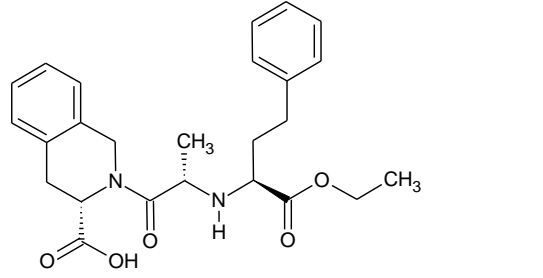
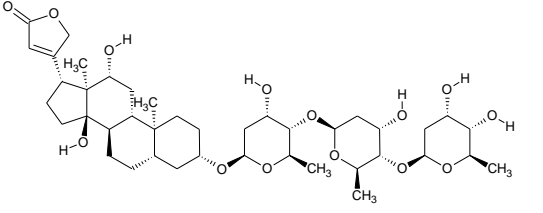
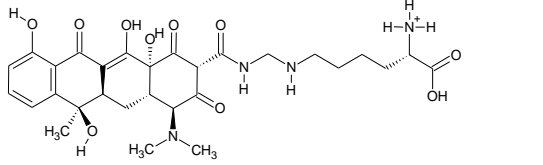
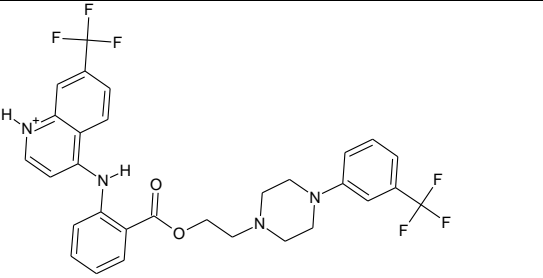
Table 6: The best ranked 1% of the VS efforts for FDA-approved drugs against the SARS COV-2 RdRp Apo form (PDB ID: 7BV1).

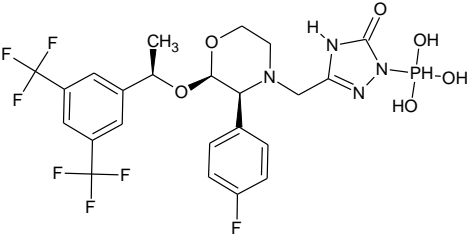
Docking rank	Structure	Drug	Docking score	Mwt	DrugBank ID	Status
1		Bromperidol	-96.029404	420.32199	DB12401	approved; investigational
2		Haloperidol	-95.175903	375.86401	DB00502	approved
3		Bisoctrizole	-94.736198	658.89099	DB11262	approved

4		Quinupristin	-93.994499	1022.23	DB01369	approved
5		Panobinostat	-93.309196	349.433 99	DB06603	approved; investigational
6		Ceforanide	-91.8731	519.554 02	DB00923	approved
7		Acetyldigitoxin	-91.872002	806.975 71	DB00511	approved

8		Diosmin	-91.546997	608.544 68	DB08995	approved; investigational
9		Hesperidin	-91.436897	610.560 61	DB04703	approved; investigational
10		Voxilaprevir	-91.391998	868.94	DB12026	approved; investigational
11		Nandrolone decanoate	-91.310501	428.647 19	DB08804	approved; illicit

12		Delamanid	-90.851501	534.492	DB11637	approved; investigational
13		Hexafluronium	-90.746902	502.745	DB00941	approved
14		Vilazodone	-90.411003	441.524 9	DB06684	approved
15		Ticagrelor	-89.165001	522.567 99	DB08816	approved
16		Flibanserin	-88.884201	390.402 1	DB04908	approved; investigational

17		Quinapril	-88.707603	438.516 11	DB00881	approved; investigational
18		Digoxin	-88.441498	780.938 48	DB00390	approved
19		Lymeccycline	-88.411201	602.632 81	DB00256	approved; investigational
20		Antrafenine	-88.2537	588.543 52	DB01419	approved

21		Fosaprepitant	-88.234802	614.406 62	DB06717	approved
----	-----------------------------------------------------------------------------------	---------------	------------	---------------	---------	----------

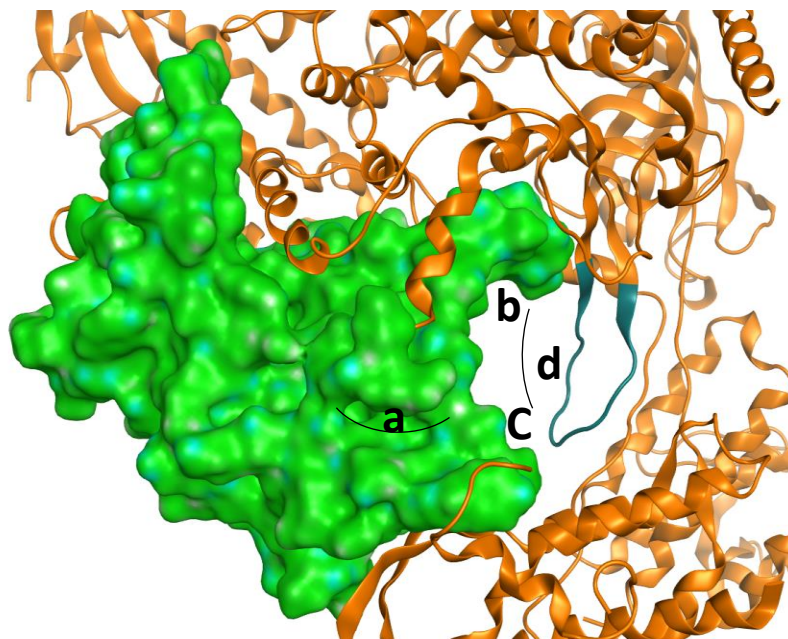


Figure 19: The binding pockets occupied by the best ranked 1% of the VS efforts against SARS COV-2 nsp12 palm site (PDB ID: 7BV1).

The palm subdomain of nsp12 is represented by a green surface and the grayish blue part of the ribbon refers to the F-motif (PDB ID: 7BV1). Ligands from the virtual screening efforts are occupying one of the four sites, a, b, c or d.

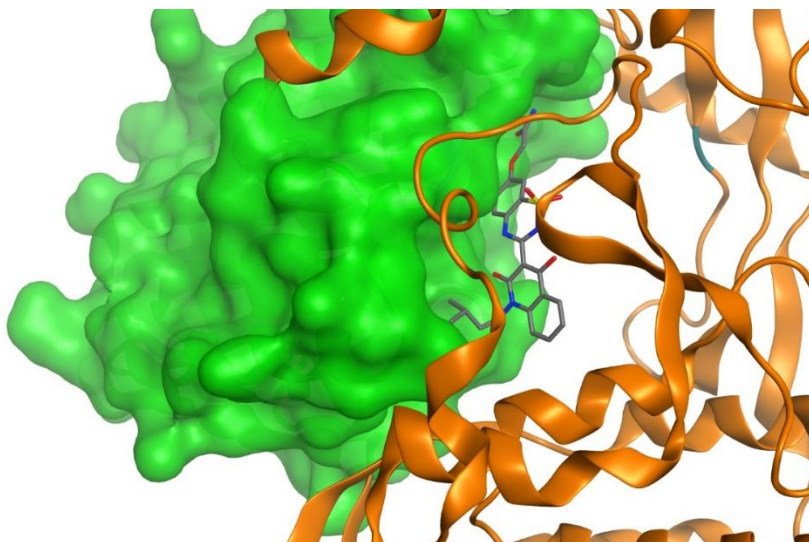


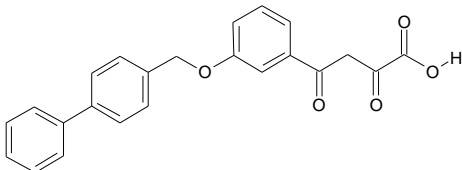
Figure 20: The palm binding pocket occupied by a benzothiadiazine ns5b inhibitor (PDB ID: 3HHK).

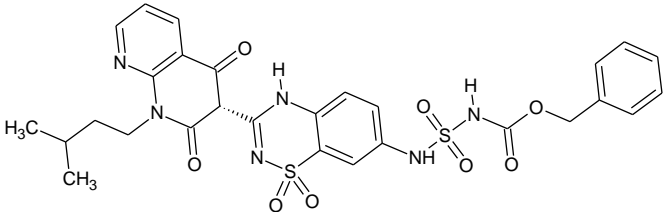
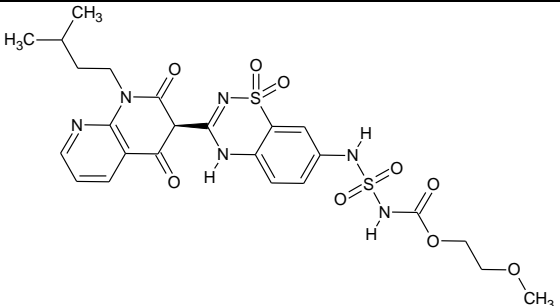
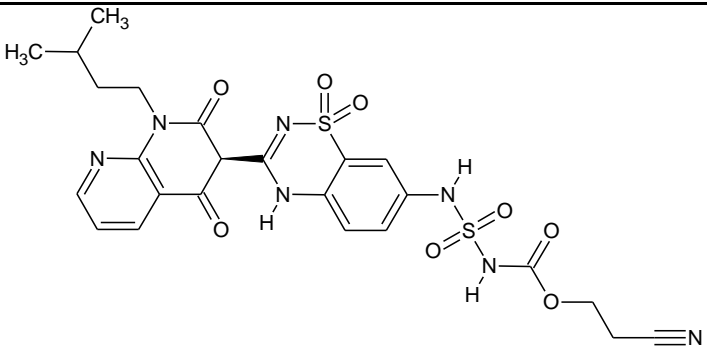
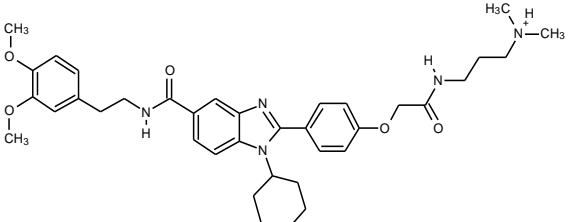
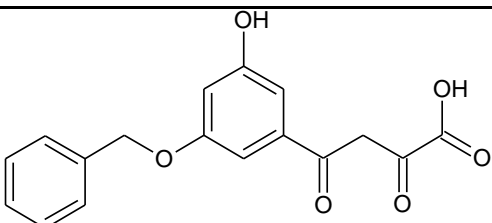
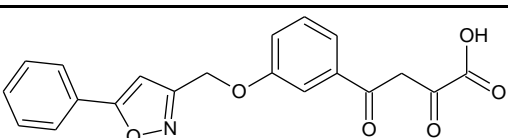
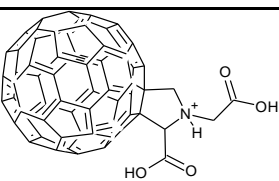
The palm subdomain of ns5b is represented by a green surface and the grayish blue part of the ribbon refers to a part of the F-motif (PDB ID: 3HHK). The ligand is completely residing the cavity facing the F-motif which resembles d-cavity in Fig. 19.

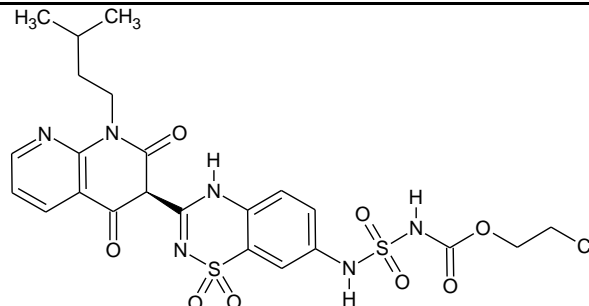
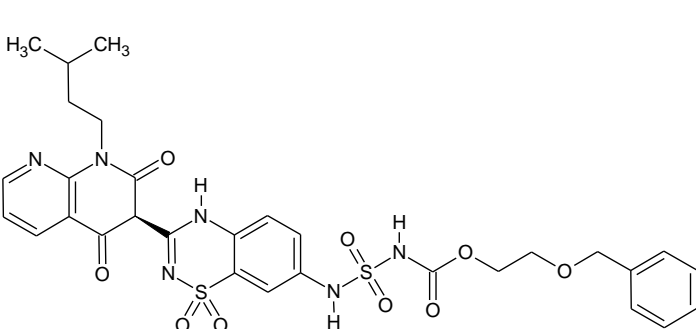
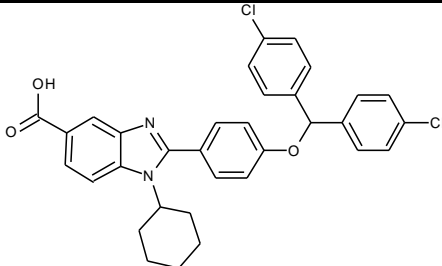
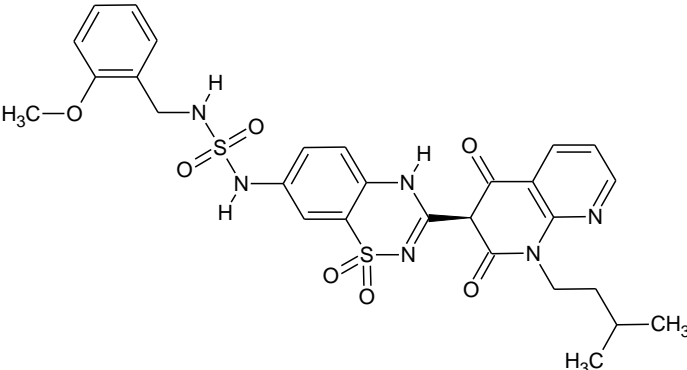
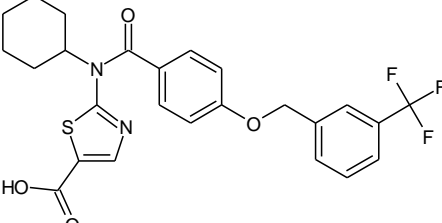
The best scored five compounds that showed better localization of the palm pocket were chosen to dig more into their poses and binding interactions. Starting with the Drug Bank results, although Amphotericin B, Nystatin and Candicidin scored the best in the rank and showed complete localization of the pocket, they were neglected. Amphotericin B, Nystatin and Candicidin are macro-molecules, therefore, they are expected to have high docking scores as their sizes allow them to better localize the cavity regardless of their real effectiveness. Consequently, Quinupristin, Acetyldigitoxin, Diosmin, Hesperidin and Voxilaprevir are the ones that met the previous criteria

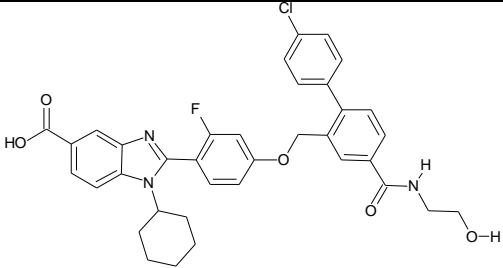
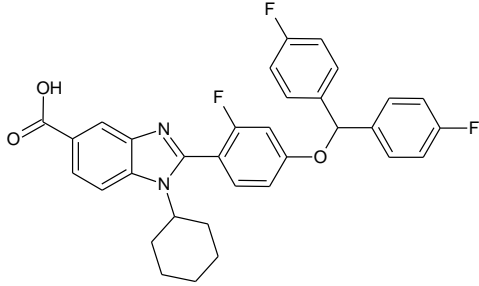
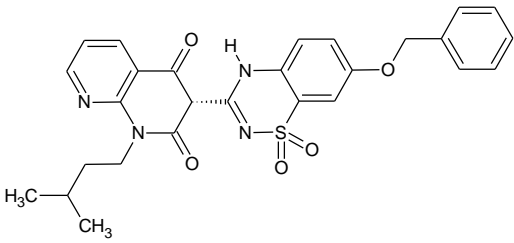
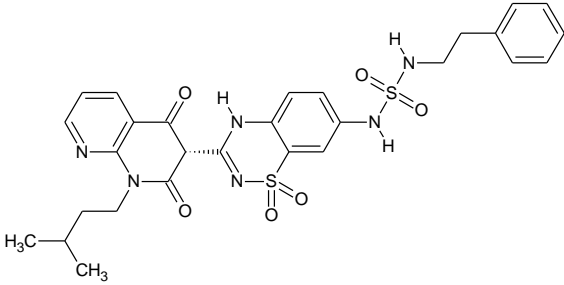
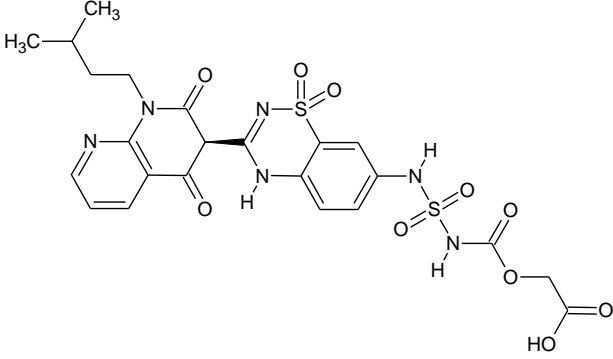
Figure 21 illustrates the pose of Quinupristin in the palm pocket of SARS-COV-2 RdRP (PDB ID: 7BV1). Quinupristin is an anti-bacterial agent that is used mainly in combination with Dalfopristin to treat bacterial infections. It binds near the 50S ribosomal subunit, therefore inhibits the late phase of protein synthesis (Allington & Rivey, 2001). Its postulated binding pose in the nsp12 (Figure 21) exhibited hydrogen bonding with the side chains Asp865, Gl590 and Asn496. Acetyldigitoxin is a cardioactive derivative of digitoxin that is used in different types of arrhythmia and congestive heart failure (Hage & Sengupta, 1999). Its binding (Figure 22) reveals hydrogen bonding with Ala685, Lys577 and Asn496 amino acid residues. Diosmin and Hesperidin are bioflavonoids, found in some plants, such as citrus fruits. Diosmin is available as nutritional supplements in the United States. Both Diosmin and Hesperidin are used in the treatment of several venous diseases, like hemorrhoids, varicose veins, and venous stasis (Hnátek, 2015). Diosmin found to participate in several H-bonds with Ser682, Asp684, Asp760, Gly590 and Ala688 (Figure 23). While Hesperidin is going through H-bonds with Ser592, Val588 and Gly590 residues (Figure 24). Interestingly, Voxilaprevir is a NS3/4A serine protease HCV inhibitor that is used against hepatitis C virus, especially with genotype 1 (Heo & Deeks, 2018). Figure 25 represents its H-binding interactions with Ala685, Asn496, Thr687 and Ala688.

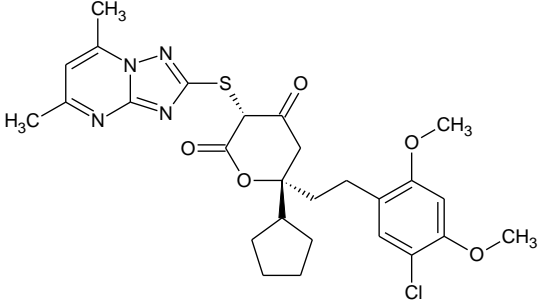
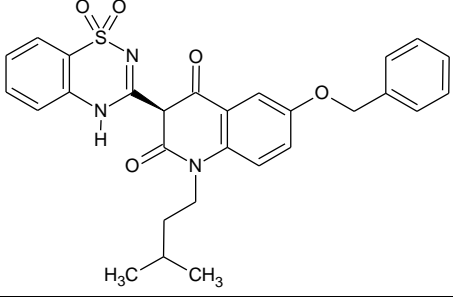
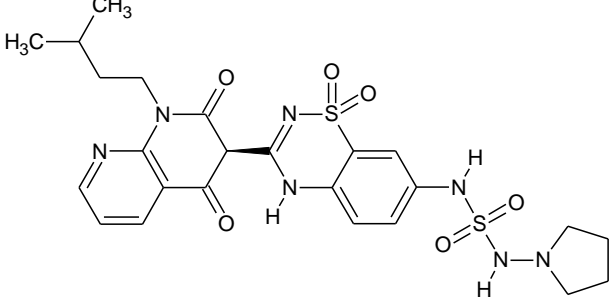
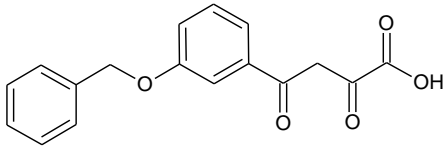
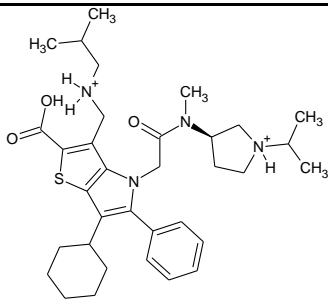
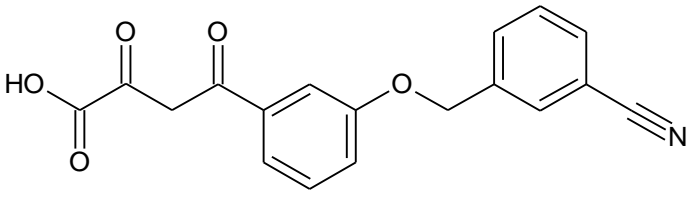
Table 7: The best ranked 1% of the VS efforts for the BindingDB database ns5b inhibitors against the SARS COV-2 RdRp Apo form (PDB ID: 7BV1).

No.	Structure	Best score	Binding DB Monomer ID	Article DOI
1		-93.2648	50174465	(Di Santo et al., 2005)

7		-89.593	50186160	(Krueger et al., 2006)
8		-89.4282	50186165	(Krueger et al., 2006)
9		-88.6499	50186141	(Krueger et al., 2006)
10		-88.4984	50137476	(Beaulieu et al., 2004)
11		-88.3516	50174478	(Di Santo et al., 2005)
12		-87.9896	50174454	(Di Santo et al., 2005)
13		-87.8785	50160864	(Mashino et al., 2005)

14		-87.8332	50186148	(Krueger et al., 2006)
15		-87.1327	50186163	(Krueger et al., 2006)
16		-86.6602	50181932	(Hirashima et al., 2006)
17		-86.5867	50222336	(Krueger et al., 2006)
18		-86.2305	50157198	(Shipps et al., 2005)

19		-86.0259	50191548	(Hirashima et al., 2006)
20		-85.5341	50181927	(Hirashima et al., 2006)
21		-85.5247	50186208	(Rockway et al., 2006)
22		-85.4918	50186139	(Krueger et al., 2006)
23		-85.4742	50186143	(Krueger et al., 2006)

24		-85.4469	50197038	(Hao et al., 2007)
25		-85.267	50181668	(Tedesco et al., 2006)
26		-85.0401	50186159	(Krueger et al., 2006)
27		-84.8217	50115572	(Summa et al., 2004)
28		-84.8189	50081636	(F. Zhao, Liu, Zhan, Jiang, & Liu, 2015)
29		-84.54	50137868	(Summa et al., 2004)

30		-84.5307	50181922	(Hirashima et al., 2006)
----	-----------------------------------------------------------------------------------	----------	----------	--------------------------

Regarding BindingDB database (Liu et al., 2007) outcome, compounds number 2, 3, 4, 5 and 6 exhibited the best localization of the palm pocket (PDB ID: 7BV1). Compounds 2, 4 and 6 contain benzothiadiazine scaffold, whereas, 3 and 5 have benzimidazole scaffold. The docking poses of each compound are represented in figures 26, 27, 28, 29 and 30 respectively. Compounds number 2 and 4 are going through hydrogen bond interaction between Gly590 and the sulphur oxygen of the benzothiadiazine ring. In addition to a hydrogen bond between Lys577 and the carbonyl oxygen of the terminal amide group. However, Lys577 is showing hydrogen bonding with the carbonyl oxygen of the carboxylic group of compound number 3. Uniquely, compound 5 has an indole ring which facilitates two interactions; one with Ala685 as a H-bond donor, and the other one is a pi interaction between the pyrrole ring and Tyr689 residue. The sixth compound is participating in a hydrogen bonding with Gly590, same as compounds 2 and 4, and another one with Asn496 amino acid.

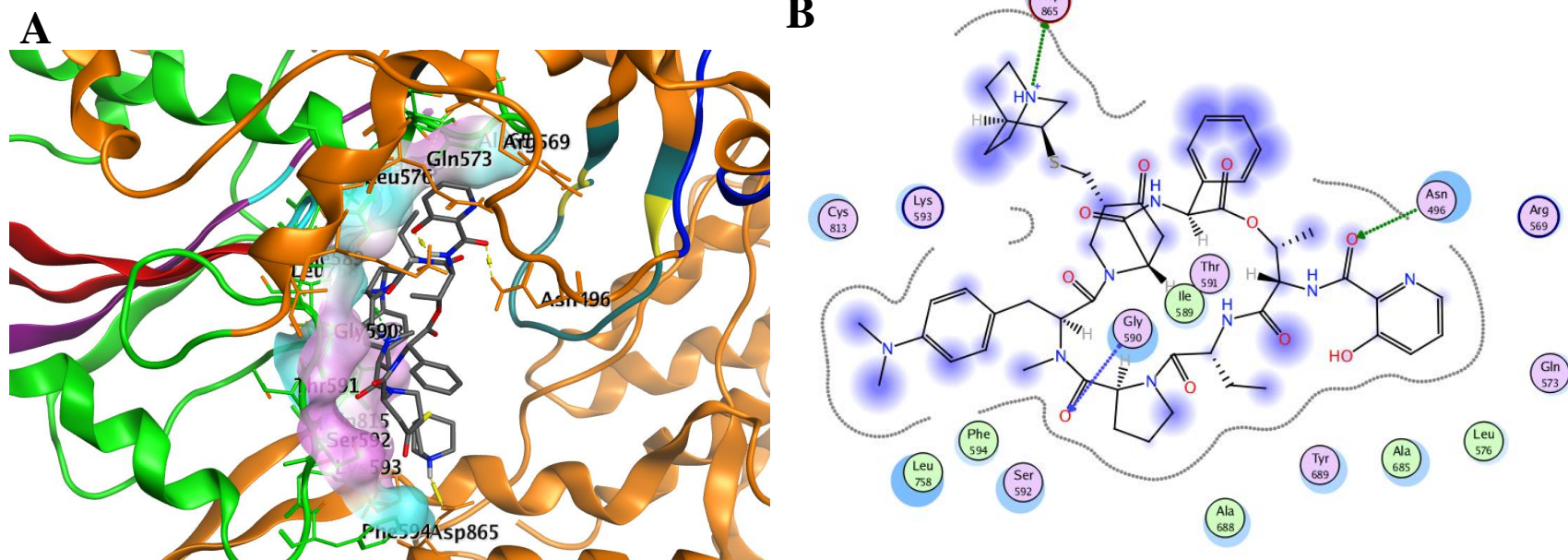


Figure 21: Docking pose of Quinupristin in the palm pocket of SARS COV-2 polymerase (PDB ID: 7BV1).

Quinupristin is shown as gray sticks. (A) The three-dimensional representation of the interactions. (B) The 2D interactions. The hydrophilic and hydrophobic regions are in purple and cyan colored molecular surfaces, respectively (A). The green ribbon part refers to the palm subdomain. The grayish blue part is for the F-motif, where you can see a yellow part representing K545, R535 and R555 amino acids that are specifically responsible for directing the NTPs into the active site, the cyan colored ribbon. A-motif and C-motif are the red and the purple ribbon parts respectively. The black part is the shared residues between A-motif and the finger subdomain. Blue region is for G-motif which participates with the F motif in forming the groove for the RNA template entry. Dashed lines show favorable bindings. Non-polar hydrogens are omitted for clarification.

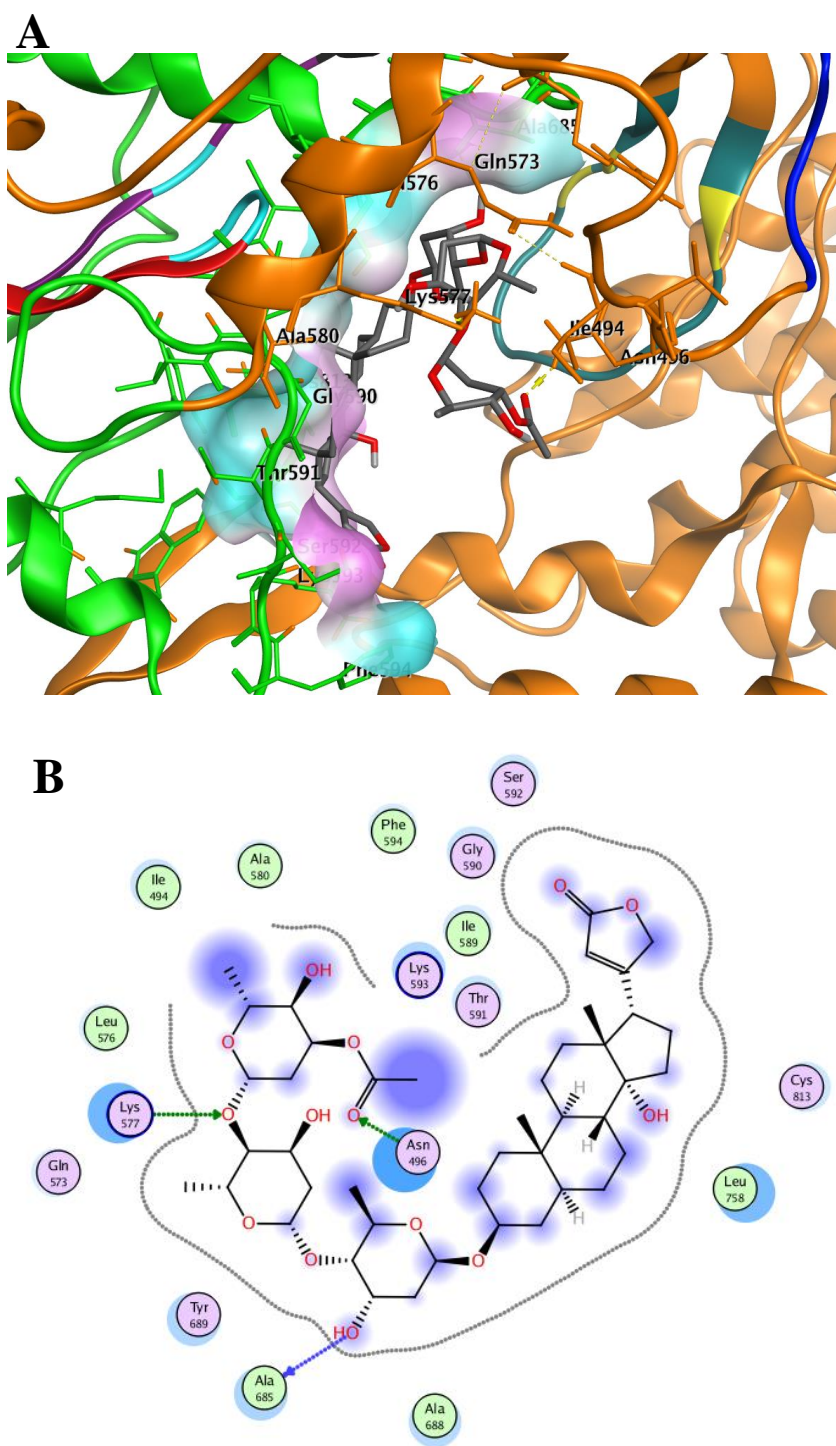


Figure 22: Docking pose of Acetyldigitoxin in the palm pocket of SARS COV-2 polymerase (PDB ID: 7BV1).

Acetyldigitoxin is shown as gray sticks. (A) The three-dimensional representation of the interactions. (B) The 2D interactions. The color scheme is same as Fig. 21.

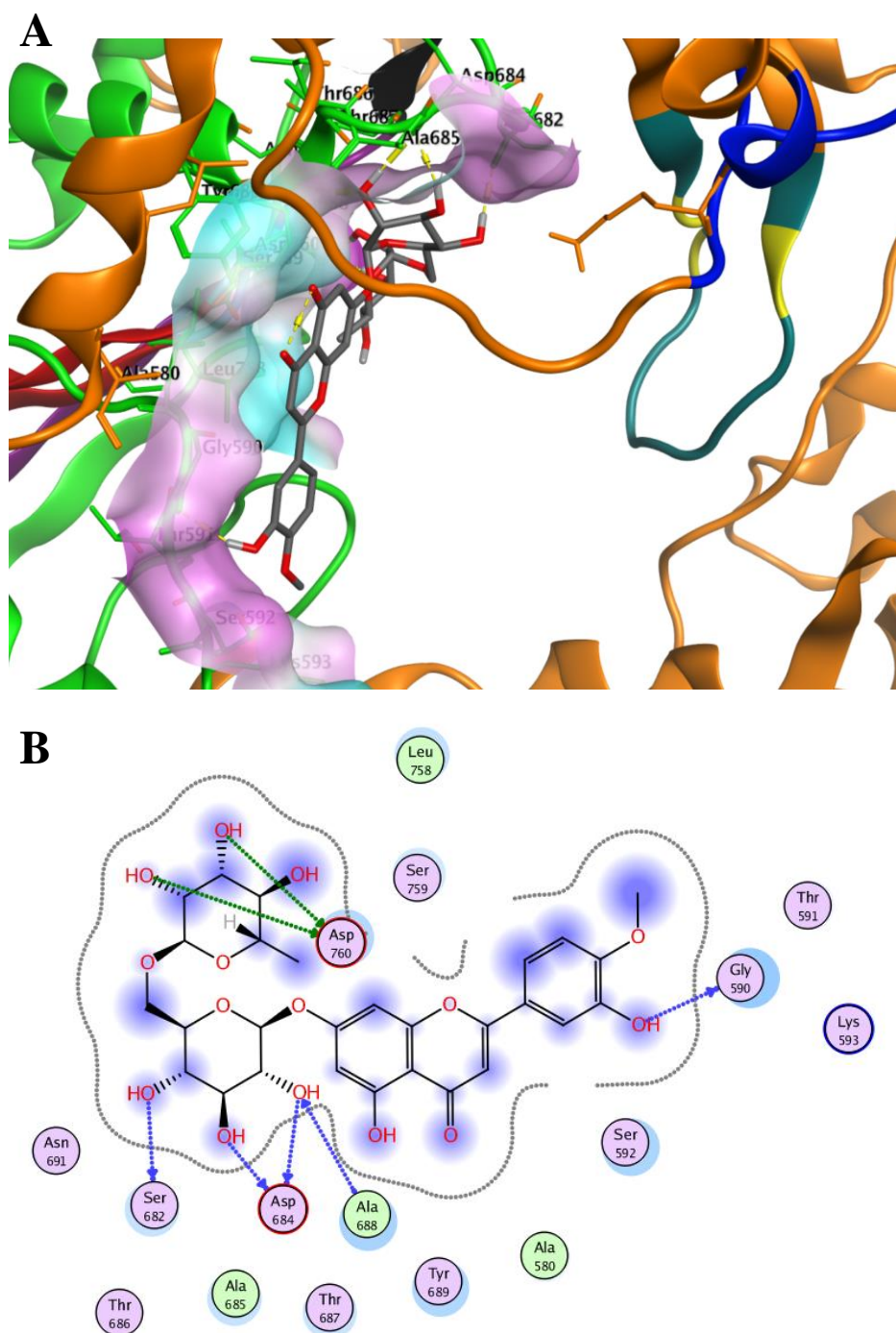


Figure 23: Docking pose of Diosmin in the palm pocket of SARS COV-2 polymerase (PDB ID: 7BV1).

Diosmin is shown as gray sticks. (A) The three-dimensional representation of the interactions. (B) The 2D interactions. The color scheme is same as Fig. 21.

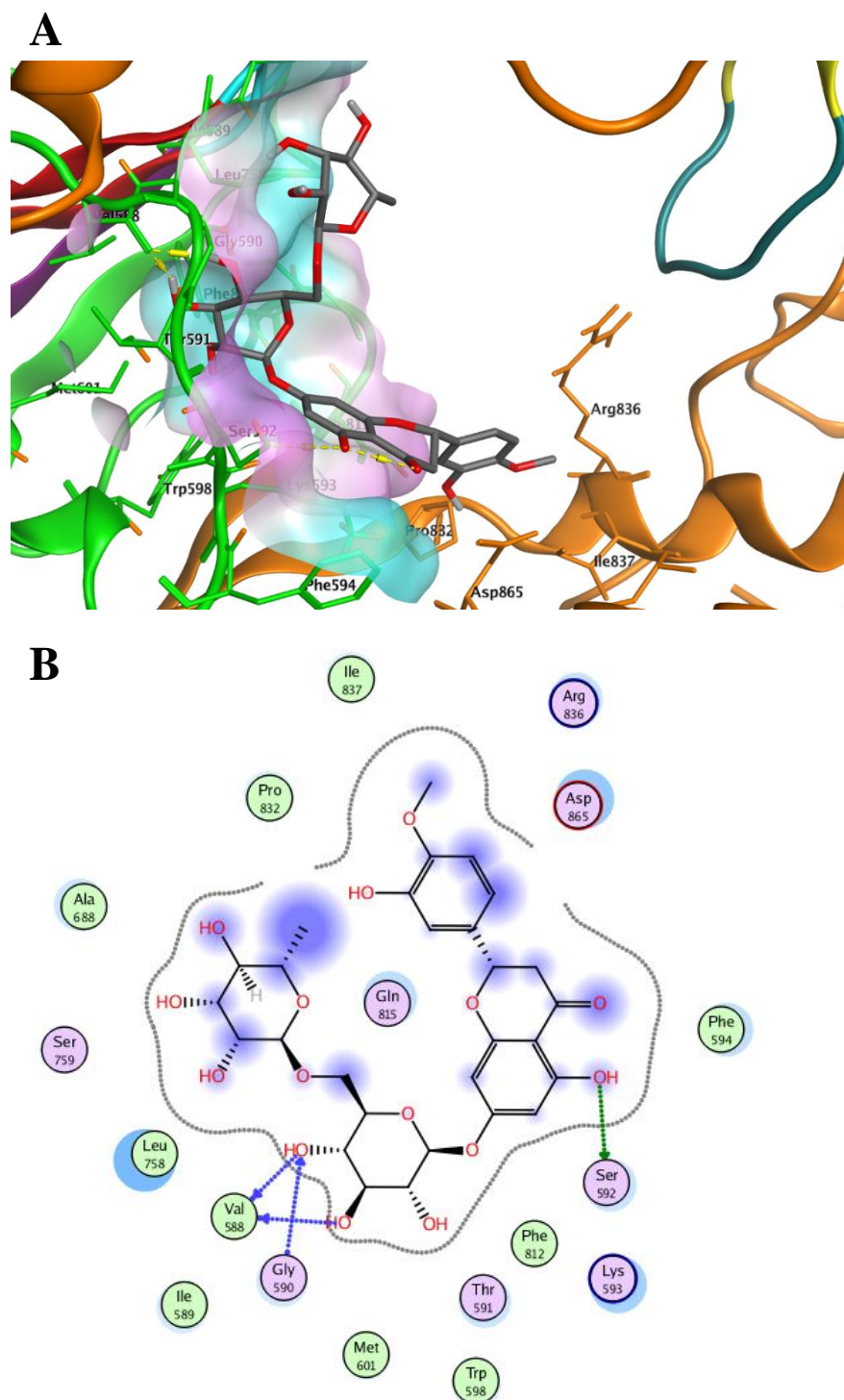


Figure 24: Docking pose of Hesperidin in the palm pocket of SARS COV-2 polymerase (PDB ID: 7BV1).

Hesperidin is shown as gray sticks. (A) The three-dimensional representation of the interactions. (B) The 2D interactions. The color scheme is same as Fig. 21.

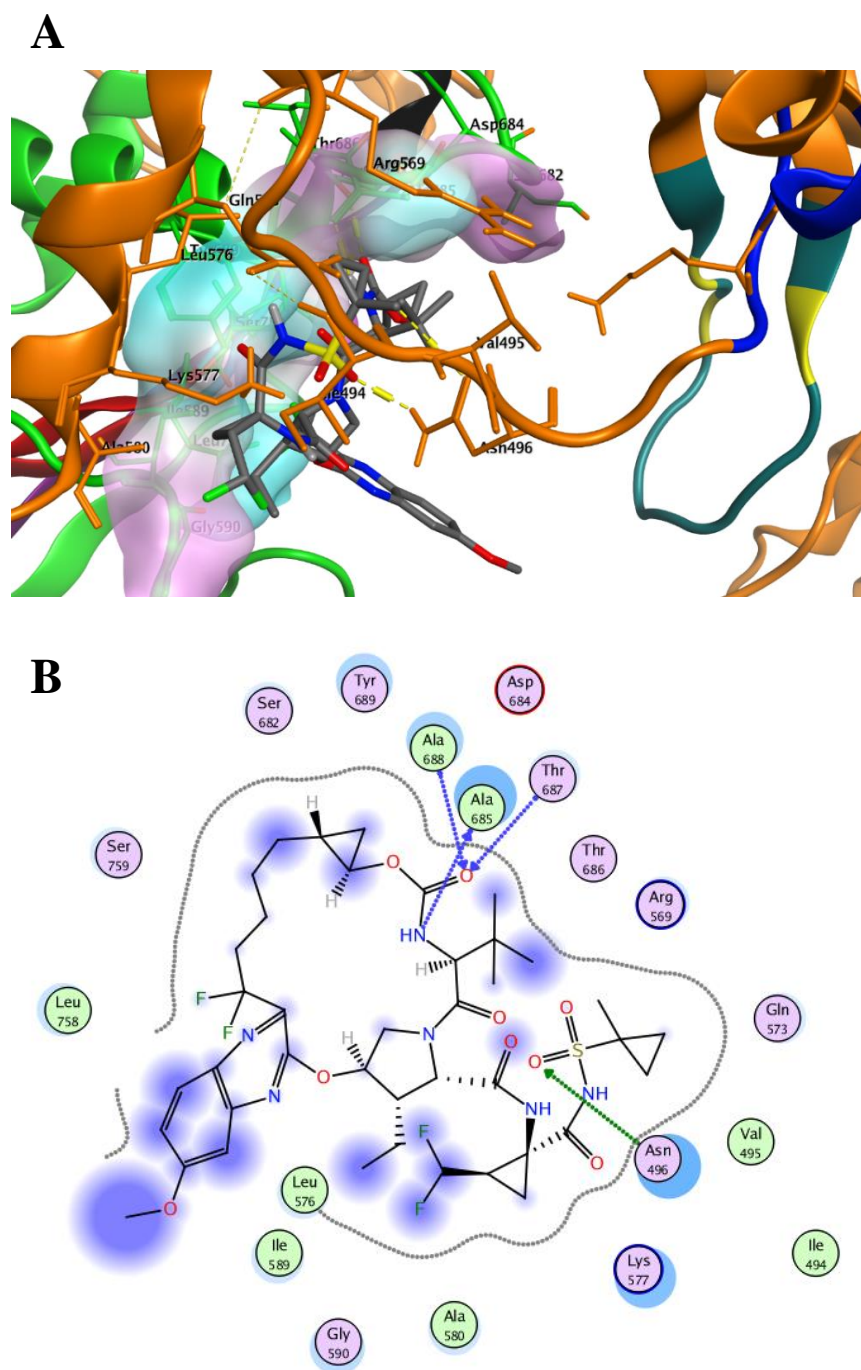


Figure 25: Docking pose of Voxilaprevir in the palm pocket of SARS COV-2 polymerase (PDB ID: 7BV1).

Voxilaprevir is shown as gray sticks. (A) The three-dimensional representation of the interactions. (B) The 2D interactions. The color scheme is same as Fig. 21.

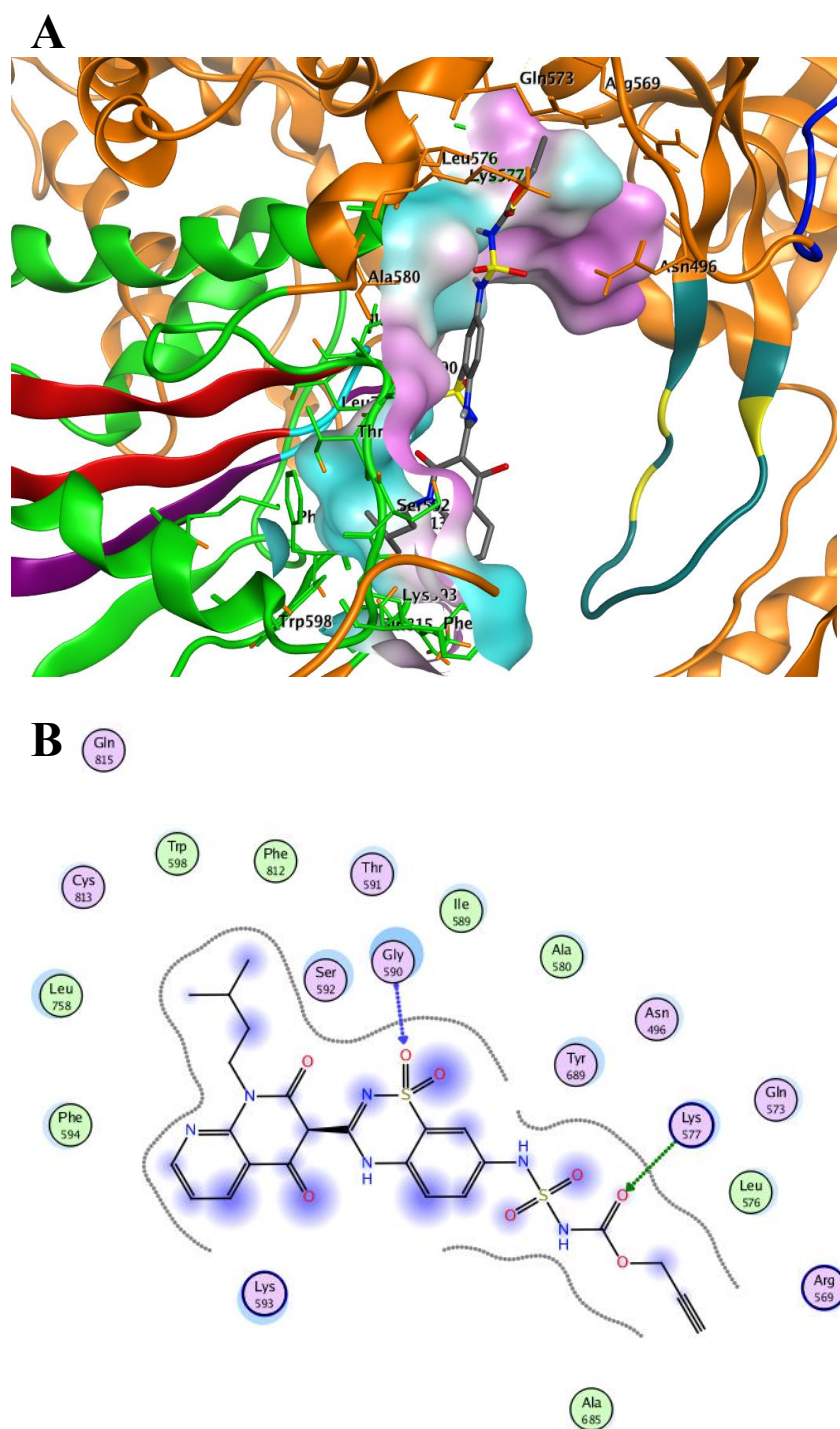


Figure 26: Docking pose of compound number 2 in the palm pocket of SARS COV-2 polymerase (PDB ID: 7BV1).

Compound 2 is shown as gray sticks. (A) The three-dimensional representation of the interactions. (B) The 2D interactions. The color scheme is same as Fig. 21.

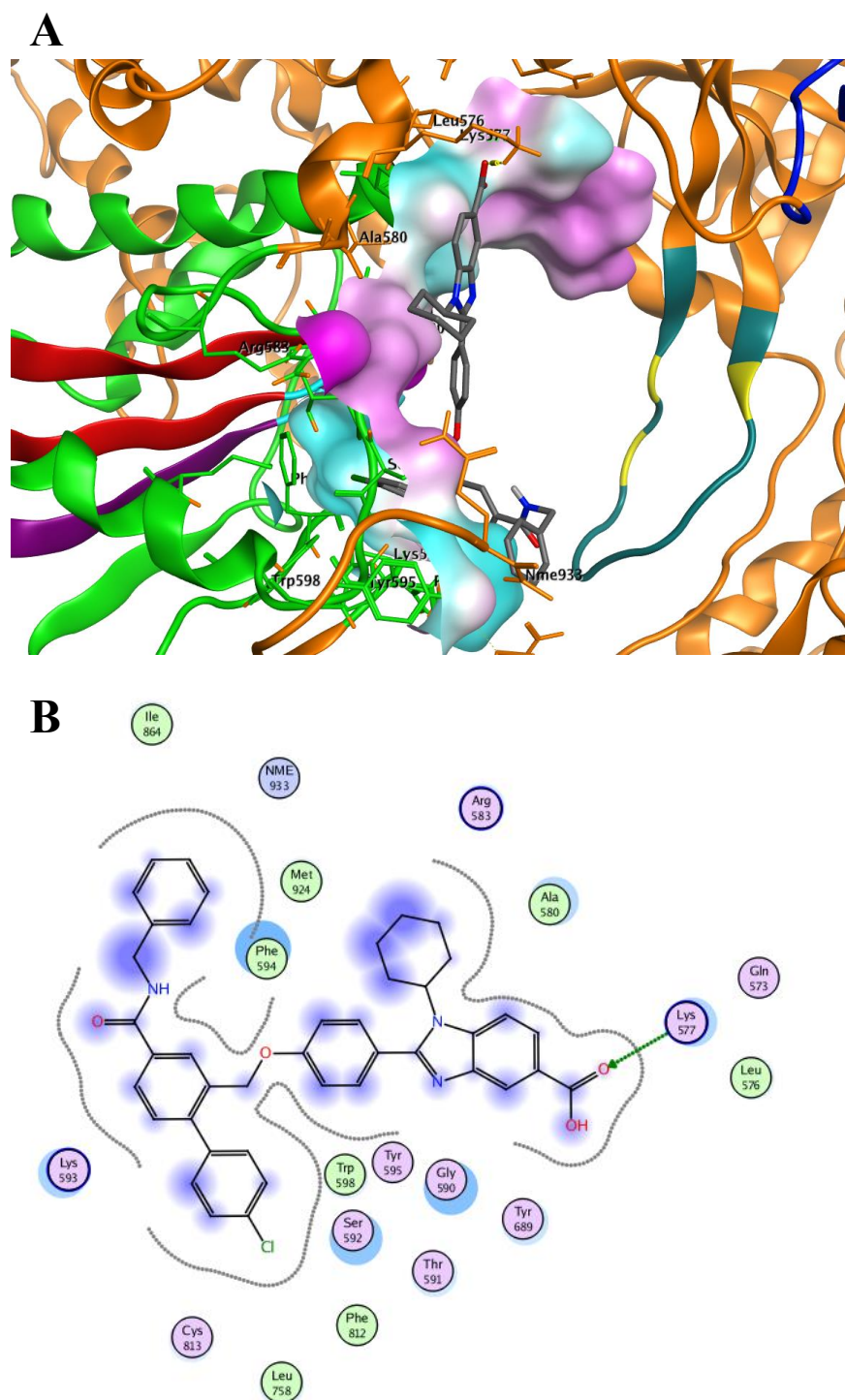


Figure 27: Docking pose of compound number 3 in the palm pocket of SARS COV-2 polymerase (PDB ID: 7BV1).

Compound 3 is shown as gray sticks. (A) The three-dimensional representation of the interactions. (B) The 2D interactions. The color scheme is same as Fig. 21.

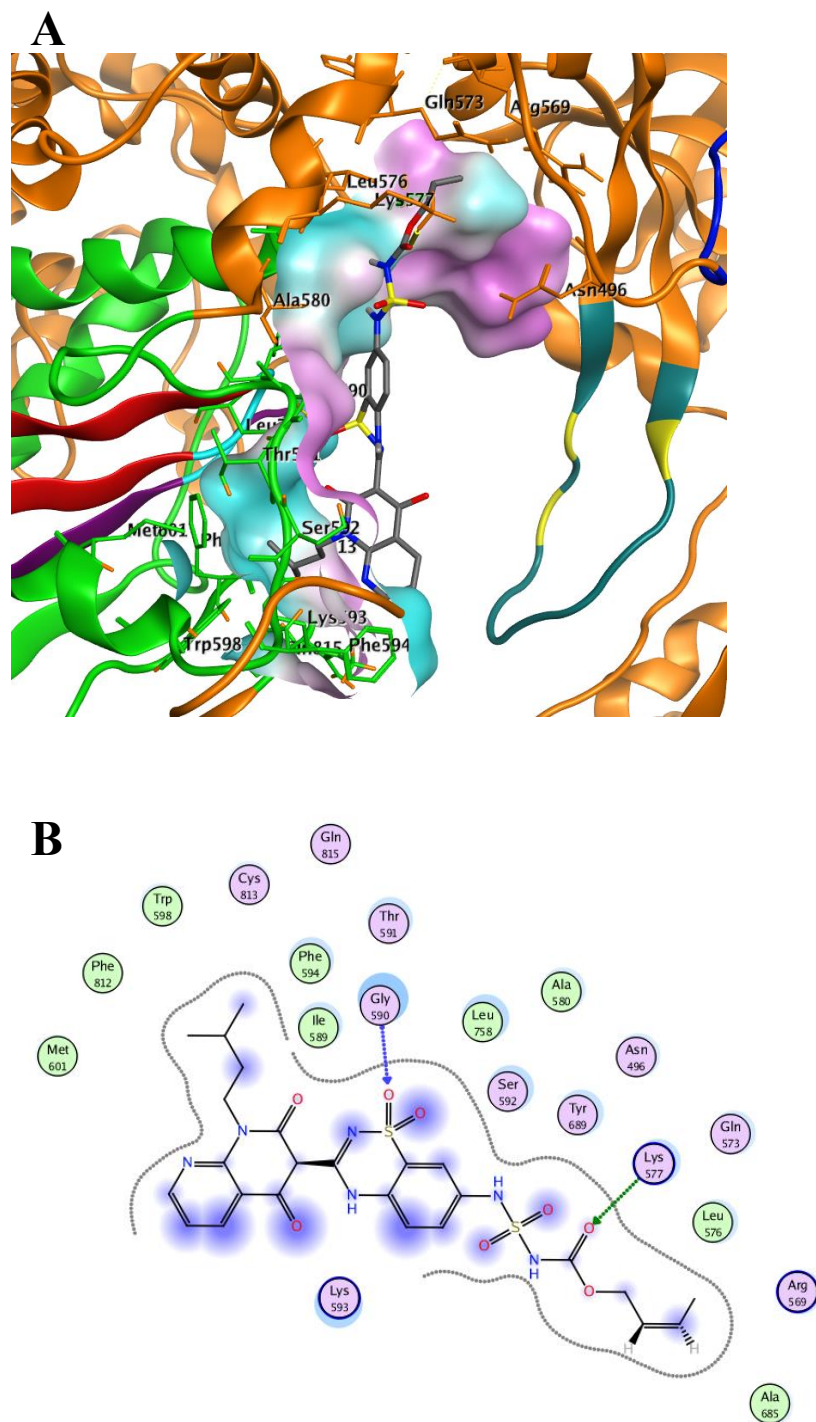


Figure 28: Docking pose of compound number 3 in the palm pocket of SARS COV-2 polymerase (PDB ID: 7BV1).

Compound 4 is shown as gray sticks. (A) The three-dimensional representation of the interactions. (B) The 2D interactions. The color scheme is same as Fig. 21.

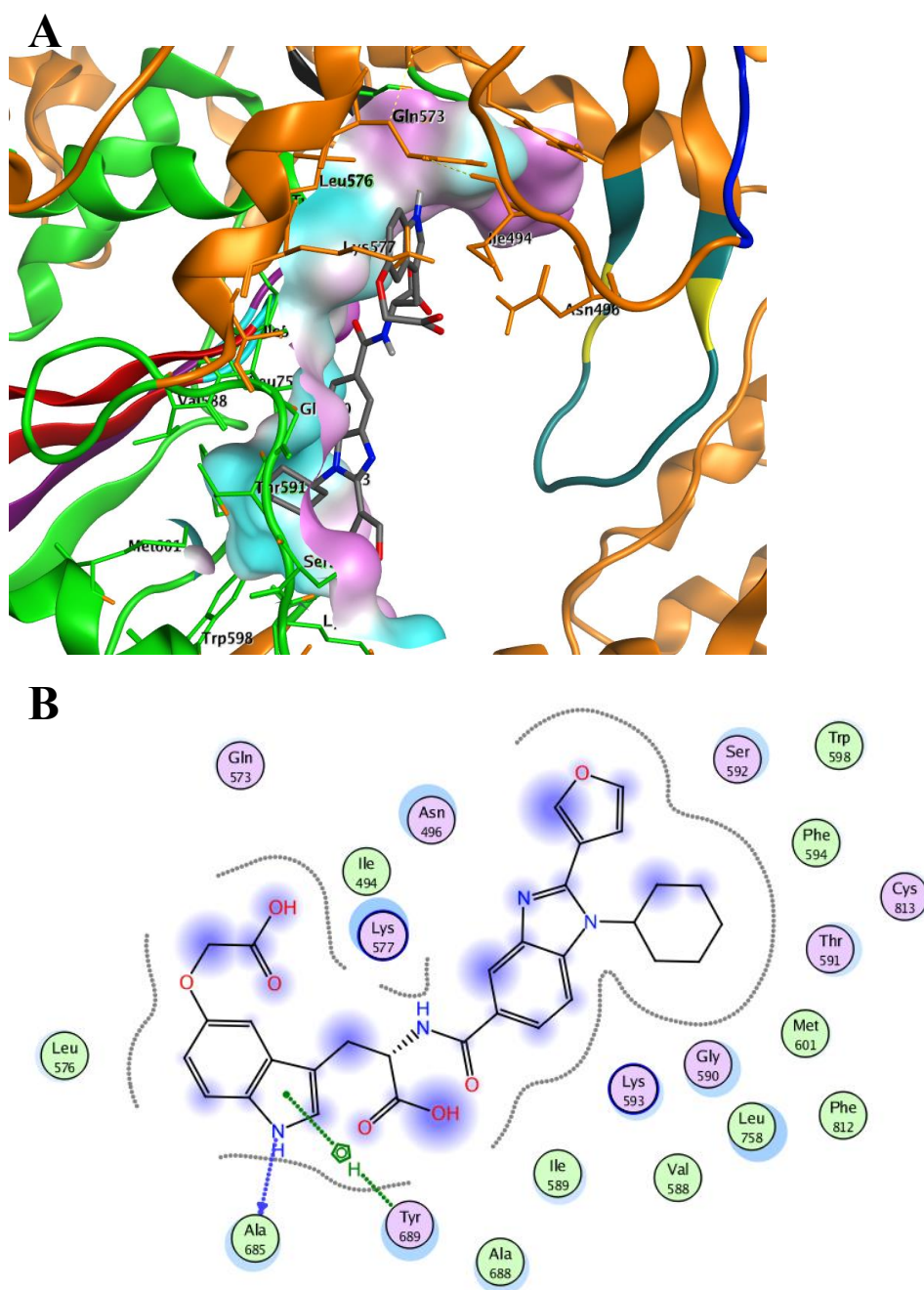


Figure 29: Docking pose of compound number 3 in the palm pocket of SARS COV-2 polymerase (PDB ID: 7BV1).

Compound 5 is shown as gray sticks. (A) The three-dimensional representation of the interactions. (B) The 2D interactions. The color scheme is same as Fig. 21.

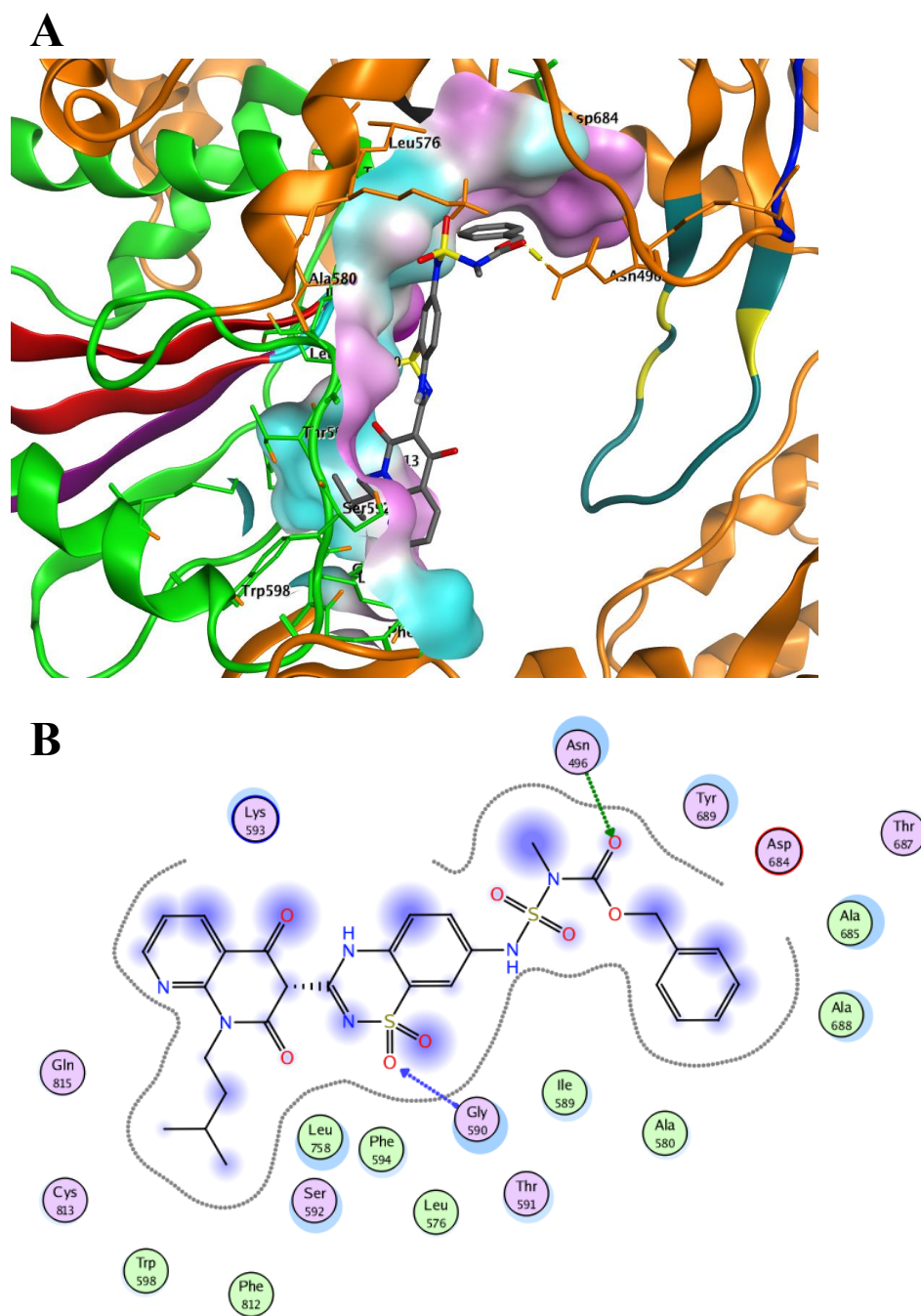


Figure 30: Docking pose of compound number 3 in the palm pocket of SARS COV-2 polymerase (PDB ID: 7BV1).

Compound 6 is shown as gray sticks. (A) The three-dimensional representation of the interactions. (B) The 2D interactions. The color scheme is same as Fig. 21.

4. CONCLUSION AND FUTURE PERSPECTIVES

To conclude, we relied on the high similarity between SARS COV-2 polymerase and HCV-1b polymerase to build a benchmark set from HCV ns5b-1b palm inhibitors. Afterwards, based on the benchmarking outcome, we conducted SBVS efforts against SARS COV-2 RdRp palm subdomain.

This was achieved via generating high-quality DEKOIS 2.0 benchmark set to use it in the benchmarking against HCV ns5b-1b palm subdomain (PDB ID: 3HHK). To generate the decoy set, we created a highly diverse active set that contains 13 different scaffolds, namely benzothiadiazine, Benzothiazine, 1,1-dioxoisothiazole, 5,6-Dihydro-1H-pyridin-2-one, Proline sulfonamide, Acrylic acid, N-acyl pyrrolidine, Benzamide, Nicotinamide, Anthranilic acid, Benzodiazepine, Sulphone and Benzofuran. The HCV ns5b-1b protein structure was selected after superposing the top five, in terms of resolution, ns5b-1b protein structures, 3TYV, 4MZ4, 3HHK, 3SKA and 3TYQ. Since they were almost identical with RMSD value equals 0.366 Å, we selected 3HHK to start the analysis. The three highly cited docking tools, FRED, PLANTS and AutoDock Vina, were utilized in the benchmarking study against the model. The benchmarking analysis via pROC-AUC, EF and pROC-Chemotype plot suggested that PLANTS is the best performing docking tool, while, both PLANTS and AutoDock Vina exhibited better-than-random performance. Accordingly, PLANTS was selected to perform prospective VS campaigns using FDA-approved drugs (from DrugBank) and HCV ns5b-1b palm inhibitors (from BindingDB) against SARS COV-2 RdRp (PDB ID: 7BV1).

Our present study displays a clear example of how to implement a DEKOIS 2.0 benchmark set against a crucial SARS COV-2 target. This aids in enhancing the success rate of VS campaigns against SARS COV-2 resolved targets. Furthermore, molecular dynamics (using NAMD, Desmond or GROMACS) can be employed to elucidate the dynamic nature of the nsp12 palm site, after selection of certain hits provided by the best performing tool (PLANTS). Additionally, Quinupristin, the best docking scored compound, and other top ranked compounds from DrugBank and BindingDB databases are recommended to be subjected for further in vitro and in vivo investigations and repurposing against COVID-19.

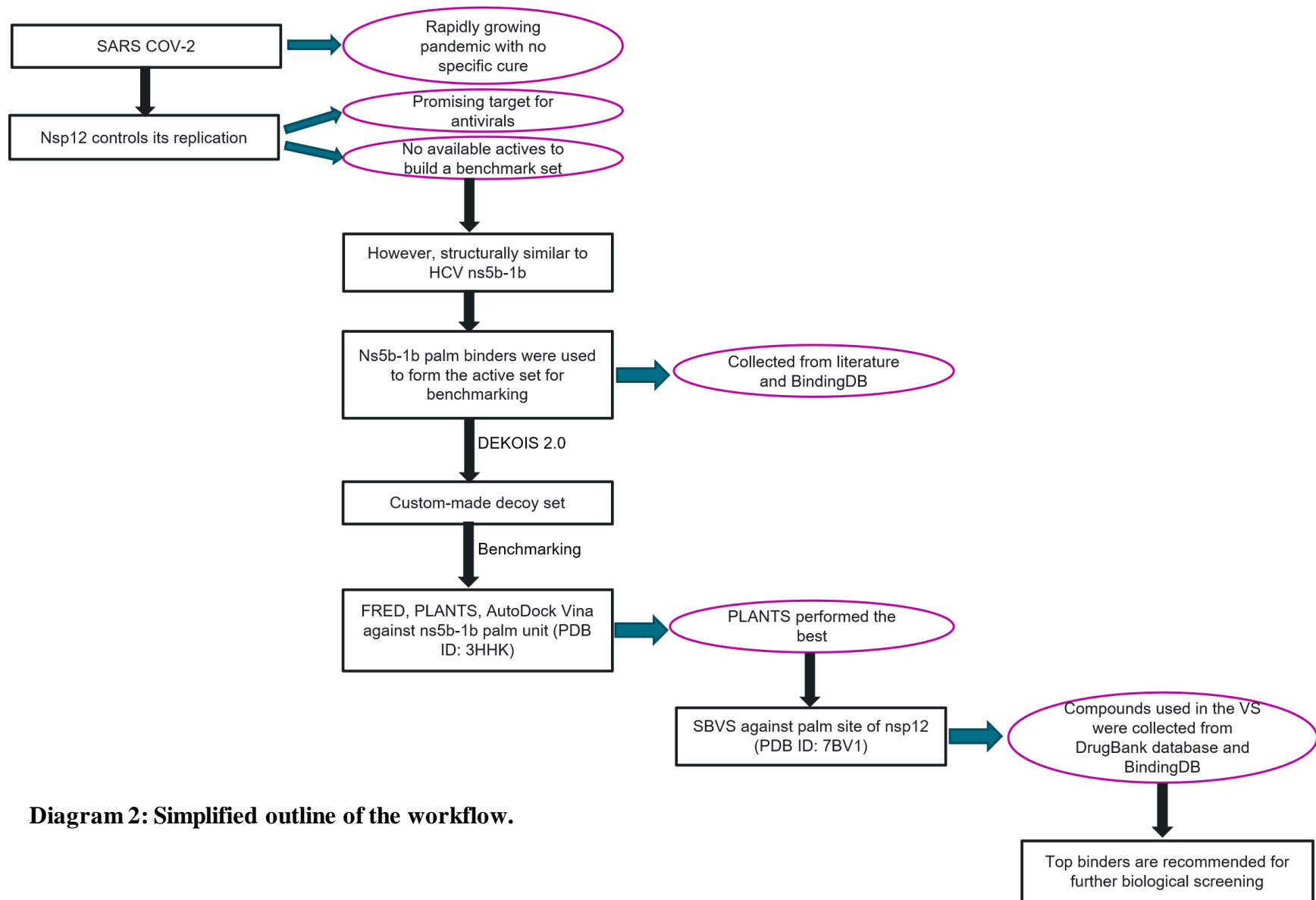


Diagram 2: Simplified outline of the workflow.

References

- DrugBank webserver - <https://www.drugbank.ca/>.
- Molecular Operating Environment (MOE 2018), Chemical Computing Group Inc.: Montreal, <http://www.chemcomp.com>.
- ACD/ChemSketch Freeware <https://www.acdlabs.com/resources/freeware/chemsketch/>.
- Ahmed-Belkacem, A., Guichou, J. F., Brillet, R., Ahnou, N., Hernandez, E., Pallier, C., & Pawlotsky, J. M. (2014). Inhibition of RNA binding to hepatitis C virus RNA-dependent RNA polymerase: a new mechanism for antiviral intervention. *Nucleic Acids Res*, 42(14), 9399-9409. doi:10.1093/nar/gku632
- Allington, D. R., & Rivey, M. P. (2001). Quinupristin/dalfopristin: a therapeutic review. *Clin Ther*, 23(1), 24-44. doi:10.1016/s0149-2918(01)80028-x
- Ando, I., Adachi, T., Ogura, N., Toyonaga, Y., Sugimoto, K., Abe, H., . . . Noguchi, T. (2012). Preclinical characterization of JTK-853, a novel nonnucleoside inhibitor of the hepatitis C virus RNA-dependent RNA polymerase. *Antimicrob Agents Chemother*, 56(8), 4250-4256. doi:10.1128/aac.00312-12
- Anilkumar, G. N., Lesburg, C. A., Selyutin, O., Rosenblum, S. B., Zeng, Q., Jiang, Y., . . . Kozlowski, J. A. (2011). I. Novel HCV NS5B polymerase inhibitors: discovery of indole 2-carboxylic acids with C3-heterocycles. *Bioorg Med Chem Lett*, 21(18), 5336-5341. doi:10.1016/j.bmcl.2011.07.021
- Anilkumar, G. N., Selyutin, O., Rosenblum, S. B., Zeng, Q., Jiang, Y., Chan, T. Y., . . . Kozlowski, J. A. (2012). II. Novel HCV NS5B polymerase inhibitors: discovery of indole C2 acyl sulfonamides. *Bioorg Med Chem Lett*, 22(1), 713-717. doi:10.1016/j.bmcl.2011.10.041
- Antonyamy, S. S., Aubol, B., Blaney, J., Browner, M. F., Giannetti, A. M., Harris, S. F., . . . Wright, T. (2008). Fragment-based discovery of hepatitis C virus NS5b RNA polymerase inhibitors. *Bioorg Med Chem Lett*, 18(9), 2990-2995. doi:10.1016/j.bmcl.2008.03.056
- Appleby, T. C., Perry, J. K., Murakami, E., Barauskas, O., Feng, J., Cho, A., . . . Edwards, T. E. (2015). Viral replication. Structural basis for RNA replication by the hepatitis C virus polymerase. *Science*, 347(6223), 771-775. doi:10.1126/science.1259210
- Barnes-Seeman, D., Boisselle, C., Capacci-Daniel, C., Chopra, R., Hoffmaster, K., Jones, C. T., . . . Fu, J. (2014). Design and synthesis of lactam-thiophene carboxylic acids as potent hepatitis C virus polymerase inhibitors. *Bioorg Med Chem Lett*, 24(16), 3979-3985. doi:10.1016/j.bmcl.2014.06.031
- Bauer, M. R., Ibrahim, T. M., Vogel, S. M., & Boeckler, F. M. (2013). Evaluation and optimization of virtual screening workflows with DEKOIS 2.0--a public library of challenging docking benchmark sets. *J Chem Inf Model*, 53(6), 1447-1462. doi:10.1021/ci400115b
- Bauer, M. R., Ibrahim, T. M., Vogel, S. M., & Boeckler, F. M. (2013). Evaluation and optimization of virtual screening workflows with DEKOIS 2.0--a public library of challenging docking benchmark sets. *Journal of chemical information and modeling*, 53(6), 1447-1462.
- Beaulieu, P. L., Bös, M., Bousquet, Y., DeRoy, P., Fazal, G., Gauthier, J., . . . Kukolj, G. (2004). Non-nucleoside inhibitors of the hepatitis C virus NS5B polymerase: discovery of benzimidazole 5-carboxylic amide derivatives with low-nanomolar potency. *Bioorg Med Chem Lett*, 14(4), 967-971. doi:10.1016/j.bmcl.2003.12.032
- Beaulieu, P. L., Coulombe, R., Duan, J., Fazal, G., Godbout, C., Hucke, O., . . . Stammers, T. A. (2013). Structure-based design of novel HCV NS5B thumb pocket 2 allosteric inhibitors with submicromolar gt1 replicon potency: discovery of a quinazolinone chemotype. *Bioorg Med Chem Lett*, 23(14), 4132-4140. doi:10.1016/j.bmcl.2013.05.037

- Berthold, M. R., Cebon, N., Dill, F., Gabriel, T. R., Kötter, T., Meinl, T., . . . Wiswedel, B. (2007). KNIME: The Konstanz Information Miner. *Studies in Classification, Data Analysis, and Knowledge Organization (GfKL 2007)*, Heidelberg-Berlin: Springer-Verlag.
- Biswal, B. K., Cherney, M. M., Wang, M., Chan, L., Yannopoulos, C. G., Bilimoria, D., . . . James, M. N. (2005). Crystal structures of the RNA-dependent RNA polymerase genotype 2a of hepatitis C virus reveal two conformations and suggest mechanisms of inhibition by non-nucleoside inhibitors. *J Biol Chem*, 280(18), 18202-18210. doi:10.1074/jbc.M413410200
- Biswal, B. K., Wang, M., Cherney, M. M., Chan, L., Yannopoulos, C. G., Bilimoria, D., . . . James, M. N. (2006). Non-nucleoside inhibitors binding to hepatitis C virus NS5B polymerase reveal a novel mechanism of inhibition. *J Mol Biol*, 361(1), 33-45. doi:10.1016/j.jmb.2006.05.074
- Boeckler, F. M., Bauer, M. R., Ibrahim, T. M., & Vogel, S. M. (2014). Use of DEKOIS 2.0 to gain insights for virtual screening. *J Cheminform*, 6(Suppl 1), O24. doi:10.1186/1758-2946-6-S1-O24
- Bressanelli, S., Tomei, L., Roussel, A., Incitti, I., Vitale, R. L., Mathieu, M., . . . Rey, F. A. (1999). Crystal structure of the RNA-dependent RNA polymerase of hepatitis C virus. *Proc Natl Acad Sci U S A*, 96(23), 13034-13039. doi:10.1073/pnas.96.23.13034
- Buonaguro, L., Tagliamonte, M., Tornesello, M. L., & Buonaguro, F. M. (2020). SARS-CoV-2 RNA polymerase as target for antiviral therapy. *J Transl Med*, 18(1), 185. doi:10.1186/s12967-020-02355-3
- Canales, E., Carlson, J. S., Appleby, T., Fenaux, M., Lee, J., Tian, Y., . . . Watkins, W. J. (2012). Tri-substituted acylhydrazines as tertiary amide bioisosteres: HCV NS5B polymerase inhibitors. *Bioorg Med Chem Lett*, 22(13), 4288-4292. doi:10.1016/j.bmcl.2012.05.025
- Chen, J., Malone, B., Llewellyn, E., Grasso, M., Shelton, P. M. M., Olinares, P. D. B., . . . Campbell, E. A. (2020). Structural Basis for Helicase-Polymerase Coupling in the SARS-CoV-2 Replication-Transcription Complex. *Cell*, 182(6), 1560-1573.e1513. doi:10.1016/j.cell.2020.07.033
- Chen, K. X., Lesburg, C. A., Vibulbhan, B., Yang, W., Chan, T. Y., Venkatraman, S., . . . Njoroge, F. G. (2012). A novel class of highly potent irreversible hepatitis C virus NS5B polymerase inhibitors. *J Med Chem*, 55(5), 2089-2101. doi:10.1021/jm201322r
- Chen, K. X., Venkatraman, S., Anilkumar, G. N., Zeng, Q., Lesburg, C. A., Vibulbhan, B., . . . Njoroge, F. G. (2014). Discovery of SCH 900188: A Potent Hepatitis C Virus NS5B Polymerase Inhibitor Prodrug As a Development Candidate. *ACS Med Chem Lett*, 5(3), 244-248. doi:10.1021/ml400192w
- Chen, K. X., Vibulbhan, B., Yang, W., Sannigrahi, M., Velazquez, F., Chan, T. Y., . . . Njoroge, F. G. (2012). Structure-activity relationship (SAR) development and discovery of potent indole-based inhibitors of the hepatitis C virus (HCV) NS5B polymerase. *J Med Chem*, 55(2), 754-765. doi:10.1021/jm201258k
- Cheng, C. C., Huang, X., Shipps, G. W., Jr., Wang, Y. S., Wyss, D. F., Soucy, K. A., . . . Huang, H. C. (2010). Pyridine Carboxamides: Potent Palm Site Inhibitors of HCV NS5B Polymerase. *ACS Med Chem Lett*, 1(9), 466-471. doi:10.1021/ml100128h
- Cheng, C. C., Shipps, G. W., Jr., Yang, Z., Kawahata, N., Lesburg, C. A., Duca, J. S., . . . Huang, H. C. (2010). Inhibitors of hepatitis C virus polymerase: synthesis and characterization of novel 2-oxy-6-fluoro-N-((S)-1-hydroxy-3-phenylpropan-2-yl)-benzamides. *Bioorg Med Chem Lett*, 20(7), 2119-2124. doi:10.1016/j.bmcl.2010.02.054
- Cherry, A. L., Dennis, C. A., Baron, A., Eisele, L. E., Thommes, P. A., & Jaeger, J. (2015). Hydrophobic and charged residues in the C-terminal arm of hepatitis C virus RNA-dependent RNA polymerase regulate initiation and elongation. *J Virol*, 89(4), 2052-2063. doi:10.1128/jvi.01106-14
- Chong, P. Y., Shotwell, J. B., Miller, J., Price, D. J., Maynard, A., Voitenleitner, C., . . . Peat, A. J. (2019). Design of N-Benzoxaborole Benzofuran GSK8175-Optimization of Human Pharmacokinetics Inspired by Metabolites of a Failed Clinical HCV Inhibitor. *J Med Chem*, 62(7), 3254-3267. doi:10.1021/acs.jmedchem.8b01719

- Clark, R. D., & Webster-Clark, D. J. (2008). Managing bias in ROC curves. *J Comput Aided Mol Des*, 22(3-4), 141-146. doi:10.1007/s10822-008-9181-z
- Das, D., Hong, J., Chen, S. H., Wang, G., Beigelman, L., Seiwert, S. D., & Buckman, B. O. (2011). Recent advances in drug discovery of benzothiadiazine and related analogs as HCV NS5B polymerase inhibitors. *Bioorg Med Chem*, 19(16), 4690-4703. doi:10.1016/j.bmc.2011.06.079
- de Vicente, J., Hendricks, R. T., Smith, D. B., Fell, J. B., Fischer, J., Spencer, S. R., . . . Farrell, R. (2009). Non-nucleoside inhibitors of HCV polymerase NS5B. Part 4: structure-based design, synthesis, and biological evaluation of benzo[d]isothiazole-1,1-dioxides. *Bioorg Med Chem Lett*, 19(19), 5652-5656. doi:10.1016/j.bmcl.2009.08.022
- de Vicente, J., Hendricks, R. T., Smith, D. B., Fell, J. B., Fischer, J., Spencer, S. R., . . . Xu, B. (2009). Non-nucleoside inhibitors of HCV polymerase NS5B. Part 2: Synthesis and structure-activity relationships of benzothiazine-substituted quinolinediones. *Bioorg Med Chem Lett*, 19(13), 3642-3646. doi:10.1016/j.bmcl.2009.05.004
- de Vicente, J., Hendricks, R. T., Smith, D. B., Fell, J. B., Fischer, J., Spencer, S. R., . . . Voronin, T. (2009). Non-nucleoside inhibitors of HCV polymerase NS5B. Part 3: synthesis and optimization studies of benzothiazine-substituted tetramic acids. *Bioorg Med Chem Lett*, 19(19), 5648-5651. doi:10.1016/j.bmcl.2009.08.023
- Di Maio, V. C., Cento, V., Mirabelli, C., Artese, A., Costa, G., Alcaro, S., . . . Ceccherini-Silberstein, F. (2014). Hepatitis C virus genetic variability and the presence of NS5B resistance-associated mutations as natural polymorphisms in selected genotypes could affect the response to NS5B inhibitors. *Antimicrob Agents Chemother*, 58(5), 2781-2797. doi:10.1128/aac.02386-13
- Di Marco, S., Volpari, C., Tomei, L., Altamura, S., Harper, S., Narjes, F., . . . Carfi, A. (2005). Interdomain communication in hepatitis C virus polymerase abolished by small molecule inhibitors bound to a novel allosteric site. *J Biol Chem*, 280(33), 29765-29770. doi:10.1074/jbc.M505423200
- Di Santo, R., Fermeglia, M., Ferrone, M., Paneni, M. S., Costi, R., Artico, M., . . . Pricl, S. (2005). Simple but highly effective three-dimensional chemical-feature-based pharmacophore model for diketo acid derivatives as hepatitis C virus RNA-dependent RNA polymerase inhibitors. *J Med Chem*, 48(20), 6304-6314. doi:10.1021/jm0504454
- Dragovich, P. S., Blazel, J. K., Ellis, D. A., Han, Q., Kamran, R., Kissinger, C. R., . . . Zhou, Y. (2008). Novel HCV NS5B polymerase inhibitors derived from 4-(1',1'-dioxo-1',4'-dihydro-1'lambda(6)-benzo[1',2',4']thiadiazin-3'-yl)-5-hydroxy-2H-pyridazin-3-ones. Part 5: Exploration of pyridazinones containing 6-amino-substituents. *Bioorg Med Chem Lett*, 18(20), 5635-5639. doi:10.1016/j.bmcl.2008.08.094
- Drosten, C., Günther, S., Preiser, W., Van Der Werf, S., Brodt, H.-R., Becker, S., . . . Fouchier, R. A. (2003). Identification of a novel coronavirus in patients with severe acute respiratory syndrome. *New England journal of medicine*, 348(20), 1967-1976.
- Eastman, K. J., Parcella, K., Yeung, K. S., Grant-Young, K. A., Zhu, J., Wang, T., . . . Kadow, J. F. (2017). The discovery of a pan-genotypic, primer grip inhibitor of HCV NS5B polymerase. *Medchemcomm*, 8(4), 796-806. doi:10.1039/c6md00636a
- Ellis, D. A., Blazel, J. K., Tran, C. V., Ruebsam, F., Murphy, D. E., Li, L. S., . . . Kirkovsky, L. (2009). 5,5'- and 6,6'-dialkyl-5,6-dihydro-1H-pyridin-2-ones as potent inhibitors of HCV NS5B polymerase. *Bioorg Med Chem Lett*, 19(21), 6047-6052. doi:10.1016/j.bmcl.2009.09.051
- Ellis, D. A., Blazel, J. K., Webber, S. E., Tran, C. V., Dragovich, P. S., Sun, Z., . . . Kirkovsky, L. (2008). 4-(1,1-Dioxo-1,4-dihydro-1lambda6-benzo[1,4]thiazin-3-yl)-5-hydroxy-2H-pyridazin-3-ones as potent inhibitors of HCV NS5B polymerase. *Bioorg Med Chem Lett*, 18(16), 4628-4632. doi:10.1016/j.bmcl.2008.07.014

- Furman, P. A., Lam, A. M., & Murakami, E. (2009). Nucleoside analog inhibitors of hepatitis C viral replication: recent advances, challenges and trends. *Future Med Chem*, 1(8), 1429-1452. doi:10.4155/fmc.09.88
- Gao, Y., Yan, L., Huang, Y., Liu, F., Zhao, Y., Cao, L., . . . Rao, Z. (2020). Structure of the RNA-dependent RNA polymerase from COVID-19 virus. *Science*, 368(6492), 779-782. doi:10.1126/science.abb7498
- Gentles, R. G., Ding, M., Bender, J. A., Bergstrom, C. P., Grant-Young, K., Hewawasam, P., . . . Kadow, J. F. (2014). Discovery and preclinical characterization of the cyclopropylindolobenzazepine BMS-791325, a potent allosteric inhibitor of the hepatitis C virus NS5B polymerase. *J Med Chem*, 57(5), 1855-1879. doi:10.1021/jm4016894
- Gentles, R. G., Sheriff, S., Beno, B. R., Wan, C., Kish, K., Ding, M., . . . Kadow, J. F. (2011). Investigation of the mode of binding of a novel series of N-benzyl-4-heteroaryl-1-(phenylsulfonyl)piperazine-2-carboxamides to the hepatitis C virus polymerase. *Bioorg Med Chem Lett*, 21(8), 2212-2215. doi:10.1016/j.bmcl.2011.03.011
- Gopalsamy, A., Chopra, R., Lim, K., Ciszewski, G., Shi, M., Curran, K. J., . . . Mansour, T. S. (2006). Discovery of proline sulfonamides as potent and selective hepatitis C virus NS5b polymerase inhibitors. Evidence for a new NS5b polymerase binding site. *J Med Chem*, 49(11), 3052-3055. doi:10.1021/jm060168g
- Gordon, D. E., Jang, G. M., Bouhaddou, M., Xu, J., Obernier, K., White, K. M., . . . Krogan, N. J. (2020). A SARS-CoV-2 protein interaction map reveals targets for drug repurposing. *Nature*, 583(7816), 459-468. doi:10.1038/s41586-020-2286-9
- Hage, D. S., & Sengupta, A. (1999). Characterisation of the binding of digitoxin and acetyldigitoxin to human serum albumin by high-performance affinity chromatography. *J Chromatogr B Biomed Sci Appl*, 724(1), 91-100. doi:10.1016/s0378-4347(98)00589-1
- Hang, J. Q., Yang, Y., Harris, S. F., Leveque, V., Whittington, H. J., Rajyaguru, S., . . . Klumpp, K. (2009). Slow binding inhibition and mechanism of resistance of non-nucleoside polymerase inhibitors of hepatitis C virus. *J Biol Chem*, 284(23), 15517-15529. doi:10.1074/jbc.M808889200
- Hao, W., Herlihy, K. J., Zhang, N. J., Fuhrman, S. A., Doan, C., Patick, A. K., & Duggal, R. (2007). Development of a novel dicistronic reporter-selectable hepatitis C virus replicon suitable for high-throughput inhibitor screening. *Antimicrob Agents Chemother*, 51(1), 95-102. doi:10.1128/aac.01008-06
- Harrus, D., Ahmed-El-Sayed, N., Simister, P. C., Miller, S., Triconnet, M., Hagedorn, C. H., . . . Bressanelli, S. (2010). Further insights into the roles of GTP and the C terminus of the hepatitis C virus polymerase in the initiation of RNA synthesis. *J Biol Chem*, 285(43), 32906-32918. doi:10.1074/jbc.M110.151316
- Heo, Y. A., & Deeks, E. D. (2018). Sofosbuvir/Velpatasvir/Voxilaprevir: A Review in Chronic Hepatitis C. *Drugs*, 78(5), 577-587. doi:10.1007/s40265-018-0895-5
- Hillen, H. S., Kokic, G., Farnung, L., Dienemann, C., Tegunov, D., & Cramer, P. (2020). Structure of replicating SARS-CoV-2 polymerase. *Nature*, 584(7819), 154-156. doi:10.1038/s41586-020-2368-8
- Hirashima, S., Suzuki, T., Ishida, T., Noji, S., Yata, S., Ando, I., . . . Hashimoto, H. (2006). Benzimidazole derivatives bearing substituted biphenyls as hepatitis C virus NS5B RNA-dependent RNA polymerase inhibitors: structure-activity relationship studies and identification of a potent and highly selective inhibitor JTK-109. *J Med Chem*, 49(15), 4721-4736. doi:10.1021/jm060269e
- Hnátek, L. (2015). [Therapeutic potential of micronized purified flavonoid fraction (MPFF) of diosmin and hesperidin in treatment chronic venous disorder]. *Vnitr Lek*, 61(9), 807-814.
- Howe, A. Y., Cheng, H., Johann, S., Mullen, S., Chunduru, S. K., Young, D. C., . . . O'Connell, J. (2008). Molecular mechanism of hepatitis C virus replicon variants with reduced susceptibility to a

- benzofuran inhibitor, HCV-796. *Antimicrob Agents Chemother*, 52(9), 3327-3338. doi:10.1128/aac.00238-08
- Hucke, O., Coulombe, R., Bonneau, P., Bertrand-Laperle, M., Brochu, C., Gillard, J., . . . Stammers, T. A. (2014). Molecular dynamics simulations and structure-based rational design lead to allosteric HCV NS5B polymerase thumb pocket 2 inhibitor with picomolar cellular replicon potency. *J Med Chem*, 57(5), 1932-1943. doi:10.1021/jm4004522
- Ibrahim, T. M., Bauer, M. R., & Boeckler, F. M. (2014). Probing the impact of protein and ligand preparation procedures on chemotype enrichment in structure-based virtual screening using DEKOIS 2.0 benchmark sets. *J Cheminform*, 6(Suppl 1), p19. doi:10.1186/1758-2946-6-S1-P19
- Ibrahim, T. M., Bauer, M. R., & Boeckler, F. M. (2015). Applying DEKOIS 2.0 in structure-based virtual screening to probe the impact of preparation procedures and score normalization. *Journal of cheminformatics*, 7(1), 21.
- Ibrahim, T. M., Bauer, M. R., Dorr, A., Veyisoglu, E., & Boeckler, F. M. (2015). pROC-Chemotype Plots Enhance the Interpretability of Benchmarking Results in Structure-Based Virtual Screening. *J Chem Inf Model*, 55(11), 2297-2307. doi:10.1021/acs.jcim.5b00475
- Ibrahim, T. M., Ismail, M. I., Bauer, M. R., Bekhit, A. A., & Boeckler, F. M. (2020). Supporting SARS-CoV-2 Papain-Like Protease Drug Discovery: In silico Methods and Benchmarking. 8(996). doi:10.3389/fchem.2020.592289
- Ibrahim, T. M., Ismail, M. I., Bauer, M. R., Bekhit, A. A., & Boeckler, F. M. (2020). Supporting SARS-CoV-2 Papain-Like Protease Drug Discovery: In silico Methods and Benchmarking. *Front Chem*, 8, 592289. doi:10.3389/fchem.2020.592289
- Ikegashira, K., Oka, T., Hirashima, S., Noji, S., Yamanaka, H., Hara, Y., . . . Hashimoto, H. (2006). Discovery of conformationally constrained tetracyclic compounds as potent hepatitis C virus NS5B RNA polymerase inhibitors. *J Med Chem*, 49(24), 6950-6953. doi:10.1021/jm0610245
- Jiang, Y., Yin, W., & Xu, H. E. (2020). RNA-dependent RNA polymerase: Structure, mechanism, and drug discovery for COVID-19. *Biochem Biophys Res Commun*. doi:10.1016/j.bbrc.2020.08.116
- Kim, S. H., Tran, M. T., Ruebsam, F., Xiang, A. X., Ayida, B., McGuire, H., . . . Kissinger, C. R. (2008). Structure-based design, synthesis, and biological evaluation of 1,1-dioxisothiazole and benzo[b]thiophene-1,1-dioxide derivatives as novel inhibitors of hepatitis C virus NS5B polymerase. *Bioorg Med Chem Lett*, 18(14), 4181-4185. doi:10.1016/j.bmcl.2008.05.083
- Kirchdoerfer, R. N., & Ward, A. B. (2019). Structure of the SARS-CoV nsp12 polymerase bound to nsp7 and nsp8 co-factors. *Nat Commun*, 10(1), 2342. doi:10.1038/s41467-019-10280-3
- Kirschberg, T. A., Metobo, S., Clarke, M. O., Aktoudianakis, V., Babusis, D., Barauskas, O., . . . Kim, C. U. (2017). Discovery of a 2'-fluoro-2'-C-methyl C-nucleotide HCV polymerase inhibitor and a phosphoramidate prodrug with favorable properties. *Bioorg Med Chem Lett*, 27(8), 1840-1847. doi:10.1016/j.bmcl.2017.02.037
- Korb, O., Stutzle, T., & Exner, T. E. (2009). Empirical scoring functions for advanced protein-ligand docking with PLANTS. *J Chem Inf Model*, 49(1), 84-96. doi:10.1021/ci800298z
- Krueger, A. C., Madigan, D. L., Jiang, W. W., Kati, W. M., Liu, D., Liu, Y., . . . Kempf, D. J. (2006). Inhibitors of HCV NS5B polymerase: synthesis and structure-activity relationships of N-alkyl-4-hydroxyquinolon-3-yl-benzothiadiazine sulfamides. *Bioorg Med Chem Lett*, 16(13), 3367-3370. doi:10.1016/j.bmcl.2006.04.015
- Kuiken, C., & Simmonds, P. (2009). Nomenclature and numbering of the hepatitis C virus. *Methods Mol Biol*, 510, 33-53. doi:10.1007/978-1-59745-394-3_4
- Kumar, D. V., Rai, R., Brameld, K. A., Somoza, J. R., Rajagopalan, R., Janc, J. W., . . . Green, M. J. (2011). Quinolones as HCV NS5B polymerase inhibitors. *Bioorg Med Chem Lett*, 21(1), 82-87. doi:10.1016/j.bmcl.2010.11.068

- Lam, A. M., Edwards, T. E., Mosley, R. T., Murakami, E., Bansal, S., Lugo, C., . . . Furman, P. A. (2014). Molecular and structural basis for the roles of hepatitis C virus polymerase NS5B amino acids 15, 223, and 321 in viral replication and drug resistance. *Antimicrob Agents Chemother*, 58(11), 6861-6869. doi:10.1128/aac.03847-14
- LaPlante, S. R., Forgione, P., Boucher, C., Coulombe, R., Gillard, J., Hucke, O., . . . Stammers, T. (2014). Enantiomeric atropisomers inhibit HCV polymerase and/or HIV matrix: characterizing hindered bond rotations and target selectivity. *J Med Chem*, 57(5), 1944-1951. doi:10.1021/jm401202a
- LaPlante, S. R., Gillard, J. R., Jakalian, A., Aubry, N., Coulombe, R., Brochu, C., . . . Beaulieu, P. L. (2010). Importance of ligand bioactive conformation in the discovery of potent indole-diamide inhibitors of the hepatitis C virus NS5B. *J Am Chem Soc*, 132(43), 15204-15212. doi:10.1021/ja101358s
- Le Pogam, S., Kang, H., Harris, S. F., Leveque, V., Giannetti, A. M., Ali, S., . . . Nájera, I. (2006). Selection and characterization of replicon variants dually resistant to thumb- and palm-binding nonnucleoside polymerase inhibitors of the hepatitis C virus. *J Virol*, 80(12), 6146-6154. doi:10.1128/jvi.02628-05
- Lesburg, C. A., Cable, M. B., Ferrari, E., Hong, Z., Mannarino, A. F., & Weber, P. C. (1999). Crystal structure of the RNA-dependent RNA polymerase from hepatitis C virus reveals a fully encircled active site. *Nat Struct Biol*, 6(10), 937-943. doi:10.1038/13305
- Li, H., Tatlock, J., Linton, A., Gonzalez, J., Jewell, T., Patel, L., . . . Lewis, C. (2009). Discovery of (R)-6-cyclopentyl-6-(2-(2,6-diethylpyridin-4-yl)ethyl)-3-((5,7-dimethyl-[1,2,4]triazolo[1,5-a]pyrimidin-2-yl)methyl)-4-hydroxy-5,6-dihydropyran-2-one (PF-00868554) as a potent and orally available hepatitis C virus polymerase inhibitor. *J Med Chem*, 52(5), 1255-1258. doi:10.1021/jm8014537
- Li, L. S., Zhou, Y., Murphy, D. E., Stankovic, N., Zhao, J., Dragovich, P. S., . . . Kissinger, C. R. (2008). Novel HCV NS5B polymerase inhibitors derived from 4-(1',1'-dioxo-1',4'-dihydro-1'lambda(6)-benzo[1',2',4']thiadiazin-3'-yl)-5-hydroxy-2H-pyridazin-3-ones. Part 3: Further optimization of the 2-, 6-, and 7'-substituents and initial pharmacokinetic assessments. *Bioorg Med Chem Lett*, 18(11), 3446-3455. doi:10.1016/j.bmcl.2008.02.072
- Littler, D. R., Gully, B. S., Colson, R. N., & Rossjohn, J. (2020). Crystal Structure of the SARS-CoV-2 Non-structural Protein 9, Nsp9. *iScience*, 23(7), 101258. doi:10.1016/j.isci.2020.101258
- Liu, T., Lin, Y., Wen, X., Jorissen, R. N., & Gilson, M. K. (2007). BindingDB: a web-accessible database of experimentally determined protein-ligand binding affinities. *Nucleic Acids Res*, 35(Database issue), D198-201. doi:gkl999 [pii]10.1093/nar/gkl999
- Love, R. A., Parge, H. E., Yu, X., Hickey, M. J., Diehl, W., Gao, J., . . . Fuhrman, S. A. (2003). Crystallographic identification of a noncompetitive inhibitor binding site on the hepatitis C virus NS5B RNA polymerase enzyme. *J Virol*, 77(13), 7575-7581. doi:10.1128/jvi.77.13.7575-7581.2003
- Malik, Y. A. (2020). Properties of Coronavirus and SARS-CoV-2. *Malays J Pathol*, 42(1), 3-11.
- MartinHernando, J. I., Ontoria, J. M., Malancona, S., Attenni, B., Fiore, F., Bonelli, F., . . . Narjes, F. (2009). Optimization of thienopyrrole-based finger-loop inhibitors of the hepatitis C virus NS5B polymerase. *ChemMedChem*, 4(10), 1695-1713. doi:10.1002/cmdc.200900184
- Mashino, T., Shimotohno, K., Ikegami, N., Nishikawa, D., Okuda, K., Takahashi, K., . . . Mochizuki, M. (2005). Human immunodeficiency virus-reverse transcriptase inhibition and hepatitis C virus RNA-dependent RNA polymerase inhibition activities of fullerene derivatives. *Bioorg Med Chem Lett*, 15(4), 1107-1109. doi:10.1016/j.bmcl.2004.12.030
- Maynard, A., Crosby, R. M., Ellis, B., Hamatake, R., Hong, Z., Johns, B. A., . . . Shotwell, J. B. (2014). Discovery of a potent boronic acid derived inhibitor of the HCV RNA-dependent RNA polymerase. *J Med Chem*, 57(5), 1902-1913. doi:10.1021/jm400317w

- McComas, C. C., Palani, A., Chang, W., Holloway, M. K., Lesburg, C. A., Li, P., . . . Ludmerer, S. W. (2017). Development of a New Structural Class of Broadly Acting HCV Non-Nucleoside Inhibitors Leading to the Discovery of MK-8876. *ChemMedChem*, 12(17), 1436-1448. doi:10.1002/cmdc.201700228
- McGann, M. (2011). FRED pose prediction and virtual screening accuracy. *Journal of chemical information and modeling*, 51(3), 578-596.
- McGann, M. (2012). FRED and HYBRID docking performance on standardized datasets. *Journal of computer-aided molecular design*, 26(8), 897-906.
- McGowan, D., Nyanguile, O., Cummings, M. D., Vendeville, S., Vandyck, K., Van den Broeck, W., . . . Raboisson, P. (2009). 1,5-Benzodiazepine inhibitors of HCV NS5B polymerase. *Bioorg Med Chem Lett*, 19(9), 2492-2496. doi:10.1016/j.bmcl.2009.03.035
- Mosley, R. T., Edwards, T. E., Murakami, E., Lam, A. M., Grice, R. L., Du, J., . . . Otto, M. J. (2012). Structure of hepatitis C virus polymerase in complex with primer-template RNA. *J Virol*, 86(12), 6503-6511. doi:10.1128/jvi.00386-12
- Nakano, T., Lau, G. M., Lau, G. M., Sugiyama, M., & Mizokami, M. (2012). An updated analysis of hepatitis C virus genotypes and subtypes based on the complete coding region. *Liver Int*, 32(2), 339-345. doi:10.1111/j.1478-3231.2011.02684.x
- Narjes, F., Crescenzi, B., Ferrara, M., Habermann, J., Colarusso, S., Ferreira Mdel, R., . . . Rowley, M. (2011). Discovery of (7R)-14-cyclohexyl-7-[[2-(dimethylamino)ethyl](methyl) amino]-7,8-dihydro-6H-indolo[1,2-e][1,5]benzoxazocine-11-carboxylic acid (MK-3281), a potent and orally bioavailable finger-loop inhibitor of the hepatitis C virus NS5B polymerase. *J Med Chem*, 54(1), 289-301. doi:10.1021/jm1013105
- Nittoli, T., Curran, K., Insaft, S., DiGrandi, M., Orlowski, M., Chopra, R., . . . Bloom, J. (2007). Identification of anthranilic acid derivatives as a novel class of allosteric inhibitors of hepatitis C NS5B polymerase. *J Med Chem*, 50(9), 2108-2116. doi:10.1021/jm061428x
- Nyanguile, O., Devogelaere, B., Vijgen, L., Van den Broeck, W., Pauwels, F., Cummings, M. D., . . . Fanning, G. C. (2010). 1a/1b subtype profiling of nonnucleoside polymerase inhibitors of hepatitis C virus. *J Virol*, 84(6), 2923-2934. doi:10.1128/jvi.01980-09
- Nyanguile, O., Pauwels, F., Van den Broeck, W., Boutton, C. W., Quirynen, L., Ivens, T., . . . Raboisson, P. (2008). 1,5-benzodiazepines, a novel class of hepatitis C virus polymerase nonnucleoside inhibitors. *Antimicrob Agents Chemother*, 52(12), 4420-4431. doi:10.1128/aac.00669-08
- O'Boyle, N. M., Banck, M., James, C. A., Morley, C., Vandermeersch, T., & Hutchison, G. R. (2011). Open Babel: An open chemical toolbox. *J Cheminform*, 3, 33. doi:10.1186/1758-2946-3-33
- Ontoria, J. M., Rydberg, E. H., Di Marco, S., Tomei, L., Attenni, B., Malancona, S., . . . Carfi, A. (2009). Identification and biological evaluation of a series of 1H-benzo[de]isoquinoline-1,3(2H)-diones as hepatitis C virus NS5B polymerase inhibitors. *J Med Chem*, 52(16), 5217-5227. doi:10.1021/jm900517t
- Parcella, K., Nickel, A., Beno, B. R., Sheriff, S., Wan, C., Wang, Y. K., . . . Kadow, J. F. (2017). Discovery and initial optimization of alkoxyanthranilic acid derivatives as inhibitors of HCV NS5B polymerase. *Bioorg Med Chem Lett*, 27(2), 295-298. doi:10.1016/j.bmcl.2016.11.054
- Pfefferkorn, J. A., Greene, M. L., Nugent, R. A., Gross, R. J., Mitchell, M. A., Finzel, B. C., . . . Schwende, F. J. (2005). Inhibitors of HCV NS5B polymerase. Part 1: Evaluation of the southern region of (2Z)-2-(benzoylamino)-3-(5-phenyl-2-furyl)acrylic acid. *Bioorg Med Chem Lett*, 15(10), 2481-2486. doi:10.1016/j.bmcl.2005.03.066
- Pfefferkorn, J. A., Nugent, R., Gross, R. J., Greene, M., Mitchell, M. A., Reding, M. T., . . . Schwende, F. J. (2005). Inhibitors of HCV NS5B polymerase. Part 2: Evaluation of the northern region of (2Z)-2-benzoylamino-3-(4-phenoxy-phenyl)-acrylic acid. *Bioorg Med Chem Lett*, 15(11), 2812-2818. doi:10.1016/j.bmcl.2005.03.106

- Pierra Rouvière, C., Amador, A., Badaroux, E., Convard, T., Da Costa, D., Dukhan, D., . . . Dousson, C. (2016). Synthesis of potent and broad genotypically active NS5B HCV non-nucleoside inhibitors binding to the thumb domain allosteric site 2 of the viral polymerase. *Bioorg Med Chem Lett*, 26(18), 4536-4541. doi:10.1016/j.bmcl.2016.01.042
- Pillon, M. C., Frazier, M. N., Dillard, L. B., Williams, J. G., Kocaman, S., Krahn, J. M., . . . Stanley, R. E. (2020). Cryo-EM Structures of the SARS-CoV-2 Endoribonuclease Nsp15. *bioRxiv*. doi:10.1101/2020.08.11.244863
- Powers, J. P., Piper, D. E., Li, Y., Mayorga, V., Anzola, J., Chen, J. M., . . . Wang, Z. (2006). SAR and mode of action of novel non-nucleoside inhibitors of hepatitis C NS5b RNA polymerase. *J Med Chem*, 49(3), 1034-1046. doi:10.1021/jm050859x
- Rabi, F. A., Al Zoubi, M. S., Kasasbeh, G. A., Salameh, D. M., & Al-Nasser, A. D. (2020). SARS-CoV-2 and coronavirus disease 2019: What we know so far. *Pathogens*, 9(3), 231.
- Rockway, T. W., Zhang, R., Liu, D., Betebenner, D. A., McDaniel, K. F., Pratt, J. K., . . . Kempf, D. J. (2006). Inhibitors of HCV NS5B polymerase: synthesis and structure-activity relationships of N-1-benzyl and N-1-[3-methylbutyl]-4-hydroxy-1,8-naphthyridon-3-yl benzothiadiazine analogs containing substituents on the aromatic ring. *Bioorg Med Chem Lett*, 16(14), 3833-3838. doi:10.1016/j.bmcl.2006.04.022
- Ruebsam, F., Murphy, D. E., Tran, C. V., Li, L. S., Zhao, J., Dragovich, P. S., . . . Kirkovsky, L. (2009). Discovery of tricyclic 5,6-dihydro-1H-pyridin-2-ones as novel, potent, and orally bioavailable inhibitors of HCV NS5B polymerase. *Bioorg Med Chem Lett*, 19(22), 6404-6412. doi:10.1016/j.bmcl.2009.09.045
- Ruebsam, F., Sun, Z., Ayida, B. K., Webber, S. E., Zhou, Y., Zhao, Q., . . . Kirkovsky, L. (2008). Hexahydro-pyrrolo- and hexahydro-1H-pyrido[1,2-b]pyridazin-2-ones as potent inhibitors of HCV NS5B polymerase. *Bioorg Med Chem Lett*, 18(18), 5002-5005. doi:10.1016/j.bmcl.2008.08.017
- Ruebsam, F., Tran, C. V., Li, L. S., Kim, S. H., Xiang, A. X., Zhou, Y., . . . Kirkovsky, L. (2009). 5,6-Dihydro-1H-pyridin-2-ones as potent inhibitors of HCV NS5B polymerase. *Bioorg Med Chem Lett*, 19(2), 451-458. doi:10.1016/j.bmcl.2008.11.048
- Ruebsam, F., Webber, S. E., Tran, M. T., Tran, C. V., Murphy, D. E., Zhao, J., . . . Kirkovsky, L. (2008). Pyrrolo[1,2-b]pyridazin-2-ones as potent inhibitors of HCV NS5B polymerase. *Bioorg Med Chem Lett*, 18(12), 3616-3621. doi:10.1016/j.bmcl.2008.04.066
- Rydberg, E. H., Cellucci, A., Bartholomew, L., Mattu, M., Barbato, G., Ludmerer, S. W., . . . Carfi, A. (2009). Structural basis for resistance of the genotype 2b hepatitis C virus NS5B polymerase to site A non-nucleoside inhibitors. *J Mol Biol*, 390(5), 1048-1059. doi:10.1016/j.jmb.2009.06.012
- Sanner, M. F. (1999). Python: a programming language for software integration and development. *J Mol Graph Model*, 17(1), 57-61.
- Santiago, D. N., Pevzner, Y., Durand, A. A., Tran, M., Scheerer, R. R., Daniel, K., . . . Brooks, W. H. (2012). Virtual target screening: validation using kinase inhibitors. *Journal of chemical information and modeling*, 52(8), 2192-2203.
- Schapira, M., Abagyan, R., & Totrov, M. (2003). Nuclear hormone receptor targeted virtual screening. *J Med Chem*, 46(14), 3045-3059.
- Schmitt, M., Scrima, N., Radujkovic, D., Caillet-Saguy, C., Simister, P. C., Friebe, P., . . . Bressanelli, S. (2011). A comprehensive structure-function comparison of hepatitis C virus strain JFH1 and J6 polymerases reveals a key residue stimulating replication in cell culture across genotypes. *J Virol*, 85(6), 2565-2581. doi:10.1128/jvi.02177-10
- Schneider, G. (2010). Virtual screening: an endless staircase? *Nature Reviews Drug Discovery*, 9(4), 273-276.

- Schoenfeld, R. C., Bourdet, D. L., Brameld, K. A., Chin, E., de Vicente, J., Fung, A., . . . Zhao, J. (2013). Discovery of a novel series of potent non-nucleoside inhibitors of hepatitis C virus NS5B. *J Med Chem*, 56(20), 8163-8182. doi:10.1021/jm401266k
- Scior, T., Bender, A., Tresadern, G., Medina-Franco, J. L., Martínez-Mayorga, K., Langer, T., . . . Agrafiotis, D. K. (2012). Recognizing pitfalls in virtual screening: a critical review. *Journal of chemical information and modeling*, 52(4), 867-881.
- Scrima, N., Caillet-Saguy, C., Ventura, M., Harrus, D., Astier-Gin, T., & Bressanelli, S. (2012). Two crucial early steps in RNA synthesis by the hepatitis C virus polymerase involve a dual role of residue 405. *J Virol*, 86(13), 7107-7117. doi:10.1128/jvi.00459-12
- Shaw, A. N., Tedesco, R., Bambal, R., Chai, D., Concha, N. O., Darcy, M. G., . . . Zimmerman, M. N. (2009). Substituted benzothiadiazine inhibitors of Hepatitis C virus polymerase. *Bioorg Med Chem Lett*, 19(15), 4350-4353. doi:10.1016/j.bmcl.2009.05.091
- Shipps, G. W., Jr., Deng, Y., Wang, T., Popovici-Muller, J., Curran, P. J., Rosner, K. E., . . . Cable, M. (2005). Aminothiazole inhibitors of HCV RNA polymerase. *Bioorg Med Chem Lett*, 15(1), 115-119. doi:10.1016/j.bmcl.2004.10.024
- Simister, P., Schmitt, M., Geitmann, M., Wicht, O., Danielson, U. H., Klein, R., . . . Lohmann, V. (2009). Structural and functional analysis of hepatitis C virus strain JFH1 polymerase. *J Virol*, 83(22), 11926-11939. doi:10.1128/jvi.01008-09
- Slater, M. J., Amphlett, E. M., Andrews, D. M., Bravi, G., Burton, G., Cheasty, A. G., . . . Wonacott, A. (2007). Optimization of novel acyl pyrrolidine inhibitors of hepatitis C virus RNA-dependent RNA polymerase leading to a development candidate. *J Med Chem*, 50(5), 897-900. doi:10.1021/jm061207r
- Sofia, M. J., Chang, W., Furman, P. A., Mosley, R. T., & Ross, B. S. (2012). Nucleoside, nucleotide, and non-nucleoside inhibitors of hepatitis C virus NS5B RNA-dependent RNA-polymerase. *J Med Chem*, 55(6), 2481-2531. doi:10.1021/jm201384j
- Stammers, T. A., Coulombe, R., Duplessis, M., Fazal, G., Gagnon, A., Garneau, M., . . . Beaulieu, P. L. (2013). Anthranilic acid-based Thumb Pocket 2 HCV NS5B polymerase inhibitors with sub-micromolar potency in the cell-based replicon assay. *Bioorg Med Chem Lett*, 23(24), 6879-6885. doi:10.1016/j.bmcl.2013.09.102
- Stammers, T. A., Coulombe, R., Rancourt, J., Thavonekham, B., Fazal, G., Goulet, S., . . . Beaulieu, P. L. (2013). Discovery of a novel series of non-nucleoside thumb pocket 2 HCV NS5B polymerase inhibitors. *Bioorg Med Chem Lett*, 23(9), 2585-2589. doi:10.1016/j.bmcl.2013.02.110
- Subissi, L., Posthuma, C. C., Collet, A., Zevenhoven-Dobbe, J. C., Gorbalenya, A. E., Decroly, E., . . . Imbert, I. (2014). One severe acute respiratory syndrome coronavirus protein complex integrates processive RNA polymerase and exonuclease activities. *Proc Natl Acad Sci U S A*, 111(37), E3900-3909. doi:10.1073/pnas.1323705111
- Summa, V., Petrocchi, A., Pace, P., Matassa, V. G., De Francesco, R., Altamura, S., . . . Neuner, P. (2004). Discovery of alpha,gamma-diketo acids as potent selective and reversible inhibitors of hepatitis C virus NS5b RNA-dependent RNA polymerase. *J Med Chem*, 47(1), 14-17. doi:10.1021/jm0342109
- Talamas, F. X., Abbot, S. C., Anand, S., Brameld, K. A., Carter, D. S., Chen, J., . . . Weller, P. E. (2014). Discovery of N-[4-[6-tert-butyl-5-methoxy-8-(6-methoxy-2-oxo-1H-pyridin-3-yl)-3-quinolyl]phenyl]methanesulfonamide (RG7109), a potent inhibitor of the hepatitis C virus NS5B polymerase. *J Med Chem*, 57(5), 1914-1931. doi:10.1021/jm401329s
- Talamas, F. X., Ao-leong, G., Brameld, K. A., Chin, E., de Vicente, J., Dunn, J. P., . . . Wong, A. (2013). De novo fragment design: a medicinal chemistry approach to fragment-based lead generation. *J Med Chem*, 56(7), 3115-3119. doi:10.1021/jm4002605

- Tedesco, R., Shaw, A. N., Bambal, R., Chai, D., Concha, N. O., Darcy, M. G., . . . Duffy, K. J. (2006). 3-(1,1-dioxo-2H-(1,2,4)-benzothiadiazin-3-yl)-4-hydroxy-2(1H)-quinolinones, potent inhibitors of hepatitis C virus RNA-dependent RNA polymerase. *J Med Chem*, 49(3), 971-983. doi:10.1021/jm050855s
- Tosstorff, A., Cole, J. C., Taylor, R., Harris, S. F., & Kuhn, B. (2020). Identification of Noncompetitive Protein-Ligand Interactions for Structural Optimization. *J Chem Inf Model*. doi:10.1021/acs.jcim.0c00858
- Trott, O., & Olson, A. J. (2010). AutoDock Vina: improving the speed and accuracy of docking with a new scoring function, efficient optimization, and multithreading. *J. Comput. Chem.*, 31(2), 455-461. doi:10.1002/jcc.21334
- Vandyck, K., Cummings, M. D., Nyanguile, O., Boutton, C. W., Vendeville, S., McGowan, D., . . . Raboisson, P. (2009). Structure-based design of a benzodiazepine scaffold yields a potent allosteric inhibitor of hepatitis C NS5B RNA polymerase. *J Med Chem*, 52(14), 4099-4102. doi:10.1021/jm9005548
- Velázquez, F., Venkatraman, S., Lesburg, C. A., Duca, J., Rosenblum, S. B., Kozlowski, J. A., & Njoroge, F. G. (2012). Synthesis of new 4,5-dihydrofuranoindoles and their evaluation as HCV NS5B polymerase inhibitors. *Org Lett*, 14(2), 556-559. doi:10.1021/ol203177g
- Vogel, S. M., Bauer, M. R., & Boeckler, F. M. (2011). DEKOIS: demanding evaluation kits for objective in silico screening—a versatile tool for benchmarking docking programs and scoring functions. *J Chem Inf Model*, 51(10), 2650-2665. doi:10.1021/ci2001549
- Wang, G., Lei, H., Wang, X., Das, D., Hong, J., Mackinnon, C. H., . . . Beigelman, L. (2009). HCV NS5B polymerase inhibitors 2: Synthesis and in vitro activity of (1,1-dioxo-2H-[1,2,4]benzothiadiazin-3-yl) azolo[1,5-a]pyridine and azolo[1,5-a]pyrimidine derivatives. *Bioorg Med Chem Lett*, 19(15), 4480-4483. doi:10.1016/j.bmcl.2009.05.022
- Wang, M., Ng, K. K., Cherney, M. M., Chan, L., Yannopoulos, C. G., Bedard, J., . . . James, M. N. (2003). Non-nucleoside analogue inhibitors bind to an allosteric site on HCV NS5B polymerase. Crystal structures and mechanism of inhibition. *J Biol Chem*, 278(11), 9489-9495. doi:10.1074/jbc.M209397200
- Wang, Q., Wu, J., Wang, H., Gao, Y., Liu, Q., Mu, A., . . . Rao, Z. (2020). Structural Basis for RNA Replication by the SARS-CoV-2 Polymerase. *Cell*, 182(2), 417-428.e413. doi:10.1016/j.cell.2020.05.034
- Wei, B. Q., Baase, W. A., Weaver, L. H., Matthews, B. W., & Shoichet, B. K. (2002). A model binding site for testing scoring functions in molecular docking. *J Mol Biol*, 322(2), 339-355.
- Wu, F., Zhao, S., Yu, B., Chen, Y. M., Wang, W., Song, Z. G., . . . Zhang, Y. Z. (2020). A new coronavirus associated with human respiratory disease in China. *Nature*, 579(7798), 265-269. doi:10.1038/s41586-020-2008-3
- Yan, S., Appleby, T., Gunic, E., Shim, J. H., Tasu, T., Kim, H., . . . Yao, N. (2007). Isothiazoles as active-site inhibitors of HCV NS5B polymerase. *Bioorg Med Chem Lett*, 17(1), 28-33. doi:10.1016/j.bmcl.2006.10.002
- Yan, S., Appleby, T., Larson, G., Wu, J. Z., Hamatake, R., Hong, Z., & Yao, N. (2006). Structure-based design of a novel thiazolone scaffold as HCV NS5B polymerase allosteric inhibitors. *Bioorg Med Chem Lett*, 16(22), 5888-5891. doi:10.1016/j.bmcl.2006.08.056
- Yan, S., Appleby, T., Larson, G., Wu, J. Z., Hamatake, R. K., Hong, Z., & Yao, N. (2007). Thiazolone-acylsulfonamides as novel HCV NS5B polymerase allosteric inhibitors: convergence of structure-based drug design and X-ray crystallographic study. *Bioorg Med Chem Lett*, 17(7), 1991-1995. doi:10.1016/j.bmcl.2007.01.024

- Yan, S., Larson, G., Wu, J. Z., Appleby, T., Ding, Y., Hamatake, R., . . . Yao, N. (2007). Novel thiazolones as HCV NS5B polymerase allosteric inhibitors: Further designs, SAR, and X-ray complex structure. *Bioorg Med Chem Lett*, 17(1), 63-67. doi:10.1016/j.bmcl.2006.09.095
- Yang, D., & Leibowitz, J. L. (2015). The structure and functions of coronavirus genomic 3' and 5' ends. *Virus research*, 206, 120-133.
- Yang, H., Hendricks, R. T., Arora, N., Nitzan, D., Yee, C., Lucas, M. C., . . . Tavares, G. A. (2010). Cyclic amide bioisosterism: strategic application to the design and synthesis of HCV NS5B polymerase inhibitors. *Bioorg Med Chem Lett*, 20(15), 4614-4619. doi:10.1016/j.bmcl.2010.06.008
- Yeung, K. S., Beno, B. R., Mosure, K., Zhu, J., Grant-Young, K. A., Parcella, K., . . . Kadow, J. F. (2018). Structure-Property Basis for Solving Transporter-Mediated Efflux and Pan-Genotypic Inhibition in HCV NS5B Inhibitors. *ACS Med Chem Lett*, 9(12), 1217-1222. doi:10.1021/acsmchemlett.8b00379
- Yeung, K. S., Beno, B. R., Parcella, K., Bender, J. A., Grant-Young, K. A., Nickel, A., . . . Kadow, J. F. (2017). Discovery of a Hepatitis C Virus NS5B Replicase Palm Site Allosteric Inhibitor (BMS-929075) Advanced to Phase 1 Clinical Studies. *J Med Chem*, 60(10), 4369-4385. doi:10.1021/acs.jmedchem.7b00328
- Yin, W., Mao, C., Luan, X., Shen, D. D., Shen, Q., Su, H., . . . Xu, H. E. (2020). Structural basis for inhibition of the RNA-dependent RNA polymerase from SARS-CoV-2 by remdesivir. *Science*, 368(6498), 1499-1504. doi:10.1126/science.abc1560
- Zaki, A. M., Van Boheemen, S., Bestebroer, T. M., Osterhaus, A. D., & Fouchier, R. A. (2012). Isolation of a novel coronavirus from a man with pneumonia in Saudi Arabia. *New England journal of medicine*, 367(19), 1814-1820.
- Zeng, Q., Nair, A. G., Rosenblum, S. B., Huang, H. C., Lesburg, C. A., Jiang, Y., . . . Kozlowski, J. A. (2013). Discovery of an irreversible HCV NS5B polymerase inhibitor. *Bioorg Med Chem Lett*, 23(24), 6585-6587. doi:10.1016/j.bmcl.2013.10.060
- Zhao, F., Liu, N., Zhan, P., Jiang, X., & Liu, X. (2015). Discovery of HCV NS5B thumb site I inhibitors: core-refining from benzimidazole to indole scaffold. *Eur J Med Chem*, 94, 218-228. doi:10.1016/j.ejmech.2015.03.012
- Zhao, Z., & Bourne, P. E. (2020). Structural Insights into the Binding Modes of Viral RNA-Dependent RNA Polymerases Using a Function-Site Interaction Fingerprint Method for RNA Virus Drug Discovery. *J Proteome Res*, 19(11), 4698-4705. doi:10.1021/acs.jproteome.0c00623
- Zheng, X., Hudyma, T. W., Martin, S. W., Bergstrom, C., Ding, M., He, F., . . . Gentles, R. G. (2011). Syntheses and initial evaluation of a series of indolo-fused heterocyclic inhibitors of the polymerase enzyme (NS5B) of the hepatitis C virus. *Bioorg Med Chem Lett*, 21(10), 2925-2929. doi:10.1016/j.bmcl.2011.03.067
- Zhou, Y., Webber, S. E., Murphy, D. E., Li, L. S., Dragovich, P. S., Tran, C. V., . . . Kirkovsky, L. (2008). Novel HCV NS5B polymerase inhibitors derived from 4-(1',1'-dioxo-1',4'-dihydro-1'lambda6-benzo[1',2',4']thiadiazin-3'-yl)-5-hydroxy-2H-pyridazin-3-ones. Part 1: exploration of 7'-substitution of benzothiadiazine. *Bioorg Med Chem Lett*, 18(4), 1413-1418. doi:10.1016/j.bmcl.2008.01.007
- Ziebuhr, J. (2005). The coronavirus replicase. *Curr Top Microbiol Immunol*, 287, 57-94. doi:10.1007/3-540-26765-4_3

Appendix

Table 1.A: AutoDock Vina, PLANTS and FRED scoring functions.

Docking tool	Scoring function	Reference
AutoDock Vina (version 1.1.2)	$c = \sum_{i < j} f_{t_i t_j}(r_{ij})$ <p>The equation represents the conformation dependent part of the scoring function; \sum is the sum total of all the atomic pairs that can move relatively, i is the atom, t_i is the atom type, $f_{t_i t_j}$ is a symmetric set of interaction functions, r_{ij} is the intermolecular distance.</p> <p>C is also calculated from</p> $c = c_{inter} + c_{intra}$ <p>While the conformation independent part is calculated as g function based on the following equation;</p> $g(c_{inter}) = \frac{c_{inter}}{1 + wN_{rot}}$ <p>N_{rot} is the number of rotatable bonds between heavy atoms, so w refers to the atomic weight.</p>	(Trott & Olson, 2010)
PLANTS	<p><i>f</i>PLANTSCHEMPLP</p> $= f_{PLP} + f_{hb} + f_{hb-ch} + f_{hb-CHO} + f_{met} + f_{met-coord} + f_{met-ch} + f_{met-coord-ch} + f_{clash} + f_{tors} + C_{site}$ <p><i>f</i>_{PLP}: Piecewise linear potential. <i>f</i>_{hb}, <i>f</i>_{hb-ch} and <i>f</i>_{hb-CHO}: Hydrogen bonding dependent distance and angle. <i>f</i>_{met}, <i>f</i>_{met-coord}, <i>f</i>_{met-ch} and <i>f</i>_{met-coord-ch}: Metal interactions potentials. <i>f</i>_{clash}: Empirical heavy metal potential. <i>f</i>_{tors}: Torsional potential. <i>C</i>_{site}: Reflects the contribution of the interesting regions around the binding site.</p>	(Korb et al., 2009)
FRED (OEDocking v3.2.0.2 docking)	FRED uses Chemgauss scoring function which uses Guassian smoothed potentials. It basically measures the complementarity of the different ligand poses within the active site taking into consideration the hydrogen bonding interactions, shape interactions and metal chelator interactions.	(McGamm, 2011, 2012)

Table 2.A: All HCV ns5b available structures in the protein data bank (PDB).

PDB ID	Structure title	Ligand ID	Binding site	Resolution (Å)	Reference
3HKW	HCV ns5b genotype 1a in complex with 1,5 benzodiazepine inhibitor 6	IX6	Palm 1	1.55	(Nyanguile et al., 2010)
2HAI	Crystal structure of HCV ns5b RNA polymerase in complex with novel class of dihydropyrone-containing inhibitor	PFI	Thumb	1.58	(Li et al., 2006)
3TYQ	Sar development and discovery of potent indole-based inhibitors of the hepatitis C virus ns5b polymerase	HI4	Palm	1.6	(K. X. Chen, Lesburg, et al., 2012)
4MZ4	Discovery of an irreversible HCV ns5b polymerase inhibitor	2F3	Palm	1.63	(Zeng et al., 2013)
2GIQ	Hepatitis C virus RNA-dependent RNA polymerase ns5b with nni-2 inhibitor	NN2	Thumb II	1.65	(Le Pogam et al., 2006)
3TYV	SAR development and discovery of potent indole-based inhibitors of the hepatitis C virus ns5b polymerase	HI3	Palm	1.65	(K. X. Chen, Vibulbhan, et al., 2012)
4KHM	HCV ns5b gt1a with GSK5852	1PV	Palm 2	1.7	(Maynard et al., 2014)
2XI3	HCV-h77 ns5b polymerase complexed with GTP	GTP		1.7	(Harrus et al., 2010)
3HHK	HCV ns5b polymerase complex with a substituted benzothiadizine	77Z		1.7	(Shaw et al., 2009)
3SKA	I. Novel HCV ns5b polymerase inhibitors: discovery of indole 2-carboxylic acids with c3-heterocycles	53	Palm	1.73	(Anilkumar et al., 2011)
3CJ2	Crystal structure of hepatitis C virus RNA-dependent RNA polymerase ns5b in complex with optimized small molecule fragments	SX3	Thumb	1.75	(Antony samy et al., 2008)
2YOJ	HCV ns5b polymerase complexed with pyridonylindole compound	8Y6	Palm	1.76	(K. X. Chen et al., 2014)

3U4O	Novel HCV ns5b polymerase inhibitors: discovery of indole c2 acyl sulfonamides	08E	Palm	1.77	(Anilkumar et al., 2012)
2XYM	Hcv-jfh1 ns5b t385a mutant	PO4		1.774	(Schmitt et al., 2011)
4EO6	HCV ns5b polymerase inhibitors: tri-substituted acylhydrazines as tertiary amide bioisosteres	0S2	Thumb 2	1.791	(Canales et al., 2012)
4EO8	HCV ns5b polymerase inhibitors: tri-substituted acylhydrazines as tertiary amide bioisosteres	0S3	Thumb 2	1.798	(Canales et al., 2012)
3FQL	Hepatitis C virus polymerase ns5b (con1 1-570) with hcv-796 inhibitor	79Z	Palm 2	1.8	(Hang et al., 2009)
2D3Z	X-ray crystal structure of hepatitis C virus RNA-dependent RNA polymerase in complex with non-nucleoside analogue inhibitor	FIH	Thumb	1.8	(Biswal et al., 2006)
2XWH	HCV-J6 ns5b polymerase structure at 1.8 angstrom	PEG		1.8	(Schmitt et al., 2011)
4AEP	Hcv-jfh1 ns5b polymerase structure at 1.8 angstrom	PO4		1.8	(Scrima et al., 2012)
2XI2	Hcv-h77 ns5b apo polymerase	SO4		1.8	(Harrus et al., 2010)
3QGI	Crystal structure of the hepatitis C virus ns5b RNA-dependent RNA polymerase genotype 1a complex with n-[(2s)-butan-2-yl]-6-[(3r)-3-{[4-(trifluoromethoxy) benzyl] carbamoyl}-4-{[4-(trifluoromethoxy) phenyl] sulfonyl} piperazin-1-yl] pyridazine-3-carboxamide	33F	Thumb	1.8	(Gentles et al., 2011)
4KB7	HCV ns5b gt1b n316y with CMPD 32	690	Palm 2	1.85	(Maynard et al., 2014)
4TLR	Ns5b in complex with lactam-thiophene carboxylic acids	33H	Thumb 2	1.86	(Barnes-Seeman et al., 2014)
4TLR	Ns5b in complex with lactam-thiophene carboxylic acids	79Z	Thumb 2	1.86	(Barnes-Seeman et al., 2014)
3FRZ	Crystal structure of HCV ns5b RNA polymerase in complex with pf868554	AG0	Thumb	1.86	(H. Li et al., 2009)

3FRZ	Crystal structure of HCV ns5b RNA polymerase in complex with pf868554	AG6	Thumb	1.86	(H. Li et al., 2009)
3CJ3	Crystal structure of hepatitis C virus RNA-dependent RNA polymerase ns5b in complex with optimized small molecule fragments	SX4	Thumb	1.87	(Antonysamy et al., 2008)
3CIZ	Crystal structure of hepatitis C virus RNA-dependent RNA polymerase ns5b in complex with small molecule fragments	SX1	Thumb	1.87	(Antonysamy et al., 2008)
2XXD	HCV-JFH1 ns5b polymerase structure at 1.9 angstrom	PO4		1.881	(Schmitt et al., 2011)
2XHV	HCV-J4 ns5b polymerase point mutant orthorhombic crystal form	SO4		1.9	(Harrus et al., 2010)
3CJ0	Crystal structure of hepatitis C virus RNA-dependent RNA polymerase ns5b in complex with small molecule fragments	SX2	Thumb	1.9	(Antonysamy et al., 2008)
3H2L	Crystal structure of HCV ns5b polymerase in complex with a novel bicyclic dihydro-pyridinone inhibitor	YAK	Palm	1.9	(Ruebsam, Murphy, et al., 2009)
4MKB	Hepatitis C virus polymerase ns5b genotype 1b (bk) in complex with inhibitor 14 (n-(4-((e)-2-[3-tert-butyl-2-methoxy-5-(3-oxo-2,3-dihydropyridazin-4-yl) phenyl] ethenyl) phenyl) methanesulfonamide)	28V	Palm I	1.9	(Schoenfeld et al., 2013)
1C2P	Hepatitis C virus ns5b RNA-dependent RNA polymerase			1.9	(Lesburg et al., 1999)
2GIR	Hepatitis C virus RNA -dependent RNA polymerase ns5b with nni-1 inhibitor	NN3	Thumb I	1.9	(Le Pogam et al., 2006)
1YUY	Hepatitis C virus ns5b RNA -dependent RNA polymerase genotype 2a	SO4	Thumb	1.9	(Biswal et al., 2005)
3BSA	Crystal structure of HCV ns5b polymerase with a novel pyridazinone inhibitor	N35	Palm	1.9	(Dragovich et al., 2008)
3HKY	HCV ns5b polymerase genotype 1b in complex with 1,5 benzodiazepine 6	IX6	Palm 1	1.9	(Nyanguile et al., 2010)

3H98	Crystal structure of HCV ns5b 1b with (1,1-dioxo-2h- [1,2,4] benzothiadiazin-3-yl) azolo[1,5-a] pyrimidine derivative	B5P	Palm	1.9	(G. Wang et al., 2009)
4IH5	Hepatitis C virus polymerase ns5b (bk) with fragment-based compounds	12R	Palm 1	1.9	(Talamas et al., 2013)
3GSZ	Structure of the genotype 2b HCV polymerase			1.9	(Rydberg et al., 2009)
3VQS	Crystal structure of HCV ns5b RNA polymerase with a novel piperazine inhibitor	JT1	Palm site and -hairpin region	1.9	(Ando et al., 2012)
4ADP	Hcv-j6 ns5b polymerase v405i mutant			1.902	(Scrima et al., 2012)
4JJU	Crystal structure of HCV ns5b polymerase in complex with compound 29	1MB	Thumb 2	1.91	(Beaulieu et al., 2013)
3CJ5	Crystal structure of hepatitis C virus RNA -dependent RNA polymerase ns5b in complex with optimized small molecule fragments	SX6	Thumb	1.92	(Antony samy et al., 2008)
3H5U	Hepatitis C virus polymerase ns5b with saccharin inhibitor 1	H5U	Palm	1.95	(Antony samy et al., 2008)
6MVO	HCV ns5b 1a y316 bound to compound 49	K4P		1.95	(Chong et al., 2019)
6W4G	Hepatitis C virus polymerase ns5b with RO inhibitor for SAR studies	SL4		1.95	(Tosstorff, Cole, Taylor, Harris, & Kuhn, 2020)
2WRM	Identification of novel allosteric inhibitors of hepatitis C virus ns5b polymerase thumb domain (site ii) by structure-based design	QQ3		1.95	
2ZKU	Structure of hepatitis C virus ns5b polymerase in a new crystal form	ACY		1.95	
5CZB	HCV ns5b in complex with ligand IDX 17119-5	55W	Thumb 2	1.96	(Pierra Rouvière et al., 2016)
3SKE	I. Novel HCV ns5b polymerase inhibitors: discovery of indole 2- carboxylic acids with c3-heterocycles	54	Palm	1.97	(Anilkumar et al., 2011)

5TWM	Crystal structure of the hepatitis C virus genotype 2a strain jfh1 l30s ns5b RNA -dependent RNA polymerase in complex with 5-[3-(tert-butylcarbamoyl) phenyl]-6-(ethylamino)-2-(4-fluorophenyl)-n-methylfuro[2,3-b] pyridine-3-carboxamide	7NG	Primer grip site	1.97	(Eastman et al., 2017)
2D3U	X-ray crystal structure of hepatitis C virus RNA dependent RNA polymerase in complex with non-nucleoside analogue inhibitor	CCT	Thumb	2	(Biswal et al., 2006)
1NHU	Hepatitis C virus RNA polymerase in complex with non-nucleoside analogue inhibitor	153	Thumb about 35 Å from the active site.	2	(M. Wang et al., 2003)
2HWI	HCV ns5b allosteric inhibitor complex	VRX	Thumb	2	(Yan et al., 2006)
2WHO	Crystal structure of hepatitis C virus ns5b polymerase from 1b genotype in complex with a non-nucleoside inhibitor	VGI	Thumb site ii	2	(Ontoria et al., 2009)
2AX0	Hepatitis C virus ns5b RNA polymerase in complex with a covalent inhibitor (5x)	5X	Inhibitors bound covalently to Cys366 in the palm domain	2	(Powers et al., 2006)
3U4R	Novel HCV ns5b polymerase inhibitors: discovery of indole c2 acyl sulfonamides	08F	Palm	2	(Anilkumar et al., 2012)
4J06	Crystal structure of HCV ns5b polymerase in complex with 2-{[(5-bromothiophen-2-yl) sulfonyl] amino }-4-chlorobenzoic acid	1JG	Thumb 2	2	(Stammers, Coulombe, Rancourt, et al., 2013)
3H5S	Hepatitis C virus polymerase ns5b with saccharin inhibitor	H5S	Palm	2	(de Vicente, Hendricks, Smith, Fell, Fischer, Spencer, Stengel, Mohr, Robinson, Blake, Hilgenkamp, Yee,

					Adjabeng, Elworthy, Li, et al., 2009)
4J02	Crystal structure of HCV ns5b polymerase in complex with [(1r)-5,8-dichloro-1-propyl-1,3,4,9-tetrahydropyrano[3,4-b] indol-1-yl] acetic acid	1JE	Thumb	2	(Stammers, Coulombe, Rancourt, et al., 2013)
4J04	Crystal structure of HCV ns5b polymerase in complex with 4-chloro-2-[(2,4,5-trichlorophenyl) sulfonyl] amino } benzoic acid	1JF	Thumb	2	(Stammers, Coulombe, Rancourt, et al., 2013)
3MF5	Hepatitis C virus polymerase ns5b (bk) with amide bioisostere thumb site inhibitor	HJZ	Thumb 2	2	(H. Yang et al., 2010)
2WCX	Crystal structure of hepatitis C virus ns5b polymerase in complex with thienopyrrole-based finger-loop inhibitors	VGC	Thumb	2	(Martin Hernando et al., 2009)
4JU3	Crystal structure of HCV ns5b polymerase in complex with compound 8	1O1	Thumb 2	2	(Stammers, Coulombe, Duplessis, et al., 2013)
6MVP	HCV ns5b 1b n316 bound to compound 18	K4S		2	(Chong et al., 2019)
3UPH	Synthesis of novel 4,5-dihydrofurano indoles and their evaluation as HCV ns5b polymerase inhibitors	0C1	Active site	2	(Velázquez et al., 2012)
3UPI	Synthesis of novel 4,5-dihydrofurano indoles and their evaluation as HCV ns5b polymerase inhibitors	0C2	Active site	2	(Velázquez et al., 2012)
1YVX	Hepatitis C virus RNA polymerase genotype 2a in complex with non-nucleoside analogue inhibitor	IPC	Thumb	2	(Biswal et al., 2005)
4WTL	Crystal structure of HCV ns5b genotype 2a jfh-1 isolate with s15g e86q e87q c223h v321i mutations in complex with RNA template 5'-uacc, RNA primer 5'-pgg, mn2+, and UDP	B3P		2	(Appleby et al., 2015)
4EAW	HCV ns5b in complex with idx375	0NQ		2	

3HVO	Structure of the genotype 2b HCV polymerase bound to a NNI	VGI	Thumb II	2	
2FVC	Crystal structure of ns5b bk strain (delta 24) in complex with a 3-(1,1-dioxo-2h-(1,2,4)-benzothiadiazin-3-yl)-4-hydroxy-2(1h)-quinolinone	888	Palm/thumb domain region	2	(Tedesco et al., 2006)
4MK9	Hepatitis C virus polymerase ns5b genotype 1b (bk) in complex with inhibitor 12 (n-{2-[3-tert-butyl-2-methoxy-5-(2-oxo-1,2-dihydropyridin-3-yl) phenyl]-1,3-benzoxazol-5-yl} methanesulfonamide)	28R	Palm I	2.05	(Schoenfeld et al., 2013)
4MKA	Hepatitis C virus polymerase ns5b genotype 1b (bk) in complex with inhibitor 13 (n-{2-[3-tert-butyl-2-methoxy-5-(2-oxo-1,2-dihydropyridin-3-yl) phenyl]-1,3-benzoxazol-5-yl} methanesulfonamide)	2AY	Palm I	2.05	(Schoenfeld et al., 2013)
3LKH	Inhibitors of hepatitis C virus polymerase: synthesis and characterization of novel 6-fluoro-n-[2-hydroxy-1(s)-benzamides	LT6	Palm	2.05	(Cheng, Shipps, et al., 2010)
5PZL	Crystal structure of the hepatitis C virus ns5b RNA -dependent RNA polymerase in complex with 2-({3-[1-(2-cyclopropylethyl)-6-fluoro-4-hydroxy-2-oxo-1,2-dihydroquinolin-3-yl]-1,1-dioxo-1,4-dihydro-1lambda~6~,2,4-benzothiadiazin-7-yl} oxy) acetamide	23E	Thumb	2.06	(Yeung et al., 2017)
5PZL	Crystal structure of the hepatitis C virus ns5b RNA -dependent RNA polymerase in complex with 2-({3-[1-(2-cyclopropylethyl)-6-fluoro-4-hydroxy-2-oxo-1,2-dihydroquinolin-3-yl]-1,1-dioxo-1,4-dihydro-1lambda~6~,2,4-benzothiadiazin-7-yl} oxy) acetamide	8XV	Palm	2.06	(Yeung et al., 2017)
5TRK	Crystal structure of the hepatitis C virus ns5b RNA - dependent RNA polymerase in complex with n-{3-[(benzenecarbonyl)amino]-4-[(4-	23E	Thumb	2.06	(Parcella et al., 2017)

	chlorophenyl) methoxy] benzene-1-carbonyl} glycine				
5TRK	Crystal structure of the hepatitis C virus ns5b RNA - dependent RNA polymerase in complex with n-{3-[(benzenecarbonyl)amino]-4-[(4-chlorophenyl) methoxy] benzene-1-carbonyl} glycine	7HH	An allosteric site located at the convergence of the palm and thumb regions.	2.06	(Parcella et al., 2017)
4KBI	HCV ns5b gt1b n316y with CMPD 4	1C0	Palm 2	2.06	(Maynard et al., 2014)
3CJ4	Crystal structure of hepatitis C virus RNA -dependent RNA polymerase ns5b in complex with optimized small molecule fragments	SX5	Thumb	2.07	(Antony samy et al., 2008)
5QJ0	Crystal structure of the hepatitis C virus genotype 2a strain jfh1 ns5b RNA -dependent RNA polymerase in complex with 6-[ethyl(methylsulfonyl)amino]-2-(4-fluorophenyl)-n-methyl-5-(3-{[1-(pyrimidin-2-yl) cyclopropyl] carbamoyl} phenyl)-1-benzofuran-3-carboxamide	J6D	Palm	2.08	(Yeung et al., 2018)
4MK8	Hepatitis C virus polymerase ns5b genotype 1b (bk) in complex with inhibitor 4 (n-(4-{2-[3-tert-butyl-2-methoxy-5-(2-oxo-1,2-dihydropyridin-3-yl) phenyl] ethyl} phenyl) methanesulfonamide)	28Q	Palm I	2.09	(Schoenfeld et al., 2013)
2D41	X-ray crystal structure of hepatitis C virus RNA -dependent RNA polymerase in complex with non-nucleoside inhibitor	SNH	Thumb	2.1	(Biswal et al., 2006)
3H59	Hepatitis C virus polymerase ns5b with thiazine inhibitor 2	H59	Palm	2.1	(de Vicente, Hendricks, Smith, Fell, Fischer, Spencer, Stengel, Mohr, Robinson, Blake, Hilgenkamp, Yee, Zhao, et al., 2009)

2AX1	Hepatitis C virus ns5b RNA polymerase in complex with a covalent inhibitor (5ee)	5EE	Inhibitors bound covalently to Cys366 in the palm domain	2.1	(Powers et al., 2006)
4J08	Crystal structure of HCV ns5b polymerase in complex with 2-[(4-methylphenyl) sulfonyl] amino }-5-phenoxybenzoic acid	1JH	Thumb	2.1	(Stammers, Coulombe, Rancourt, et al., 2013)
3CO9	Crystal structure of HCV ns5b polymerase with a novel pyridazinone inhibitor	3MS	Palm	2.1	(Ruebsam, Webber, et al., 2008)
3CDE	Crystal structure of HCV ns5b polymerase with a novel pyridazinone inhibitor	N3H	Palm	2.1	(L. S. Li et al., 2008)
4DRU	HCV ns5b in complex with macrocyclic indole inhibitor	0LN	Thumb	2.1	(L. S. Li et al., 2008)
4KE5	HCV ns5b gt1b n316y with gsk5852	1PV	Palm 2	2.11	(Maynard et al., 2014)
3QGH	Crystal structure of the hepatitis C virus ns5b RNA-dependent RNA polymerase genotype 1a complex with n-cyclopropyl-6-[(3r)-3-{[4-(trifluoromethoxy) benzyl] carbamoyl}-4-{[4-(trifluoromethoxy) phenyl] sulfonyl} piperazin-1-yl] pyridazine-3-carboxamide	63F		2.14	(Gentles et al., 2011)
6MVQ	HCV ns5b 1b n316 bound to compound 31	K4M		2.14	(Chong et al., 2019)
2AWZ	Hepatitis C virus ns5b RNA polymerase in complex with a covalent inhibitor (5h)	5H	Inhibitors bound covalently to Cys366 in the palm domain	2.15	(Powers et al., 2006)
3GYN	Crystal structure of HCV ns5b polymerase with a novel monocyclic dihydropyridinone inhibitor	B42	Palm	2.15	(Ellis et al., 2009)

4WTM	Crystal structure of HCV ns5b genotype 2a jfh-1 isolate with s15g e86q e87q c223h v321i mutations in complex with RNA template 5'-uagg, RNA primer 5'-pcc, mn2+, and UDP	UDP		2.15	(Appleby et al., 2015)
5QJ1	Crystal structure of the hepatitis C virus genotype 2a strain jfh1 l30s ns5b RNA-dependent RNA polymerase in complex with 6-(ethylamino)-2-(4-fluorophenyl)-5-(3-[[1-(5-fluoropyrimidin-2-yl) cyclopropyl] carbamoyl]-4-methoxyphenyl)-n-methyl-1-benzofuran-3-carboxamide	J6J	Palm	2.17	(Yeung et al., 2018)
3UDL	3-heterocyclyl quinolone bound to HCV ns5b	KLI	Thumb	2.174	(Kumar et al., 2011)
3FQK	Hepatitis C virus polymerase ns5b (bk 1-570) with hcv-796 inhibitor	79Z	Palm 2	2.2	(Hang et al., 2009)
1OS5	Crystal structure of HCV ns5b RNA polymerase complexed with a novel non-competitive inhibitor.	NH1	Thumb	2.2	(Love et al., 2003)
2I1R	Novel thiazolones as HCV ns5b polymerase inhibitors: further designs, synthesis, SAR and X-ray complex structure	VXR	Thumb	2.2	(Yan, Larson, et al., 2007)
2IJN	Isothiazoles as active-site inhibitors of HCV ns5b polymerase	221	Cys 366 of the 'primer-grip'	2.2	(Yan, Appleby, Gunic, et al., 2007)
2GC8	Structure of a proline sulfonamide inhibitor bound to HCV ns5b polymerase	885	Between palm and thumb	2.2	(Yan, Appleby, Gunic, et al., 2007)
3PHE	HCV ns5b with a bound quinolone inhibitor	C9A	Thumb	2.2	(Kumar et al., 2011)
4JJS	Crystal structure of HCV ns5b polymerase in complex with compound 2	1M9	Thumb 2	2.2	(Beaulieu et al., 2013)
3G86	Hepatitis C virus polymerase ns5b (bk 1-570) with thiazine inhibitor	T18	Palm	2.2	(de Vicente, Hendricks, Smith, Fell, Fischer, Spencer, Stengel, Mohr,

					Robinson, Blake, Hilgenkamp, Yee, Adjabeng, Elworthy, Tracy, et al., 2009)
2DXS	Crystal structure of HCV ns5b RNA polymerase complexed with a tetracyclic inhibitor	JTP	Thumb	2.2	(Ikegashira et al., 2006)
3MWV	Crystal structure of HCV ns5b polymerase			2.2	(LaPlante et al., 2010)
3D5M	Crystal structure of HCV ns5b polymerase with a novel pyridazinone inhibitor	4MS	Palm	2.2	(Kim et al., 2008)
4JU7	Crystal structure of HCV ns5b polymerase in complex with compound 24	1O6	Thumb 2	2.2	(Stammers, Coulombe, Duplessis, et al., 2013)
4JU6	Crystal structure of HCV ns5b polymerase in complex with compound 24	1O6	Thumb 2	2.2	(Stammers, Coulombe, Duplessis, et al., 2013)
3I5K	Crystal structure of the ns5b polymerase from hepatitis C virus (HCV) strain JFH1	PO4		2.2	(Simister et al., 2009)
2O5D	Thiazolone-acylsulfonamides as novel HCV ns5b polymerase allosteric inhibitors: convergence of structure-based drug design and X-ray crystallographic study	VR1	Thumb	2.2	(Yan, Appleby, Larson, et al., 2007)
1YVZ	Hepatitis C virus RNA polymerase genotype 2a in complex with non-nucleoside analogue inhibitor	JPC	Thumb	2.2	(Biswal et al., 2005)
4WTJ	Crystal structure of HCV ns5b genotype 2a jfh-1 isolate with s15g e86q e87q c223h v321i mutations in complex with RNA template 5'-aucc, RNA primer 5'-pgg, mn2+, and ADP	ADP		2.2	(Appleby et al., 2015)
4WTJ	Crystal structure of HCV ns5b genotype 2a jfh-1 isolate with s15g e86q e87q c223h v321i mutations in complex with RNA template 5'-aucc, RNA primer 5'-pgg, mn2+, and ADP	B3P		2.2	(Appleby et al., 2015)

5PZK	Crystal structure of the hepatitis C virus ns5b RNA -dependent RNA polymerase in complex with 2-(4-fluorophenyl)-n-methyl-6-[(methylsulfonyl)amino]-5-(propan-2-yloxy)-1-benzofuran-3-carboxamide	23E	Thumb	2.2	(Yeung et al., 2017)
5PZK	Crystal structure of the hepatitis C virus ns5b RNA -dependent RNA polymerase in complex with 2-(4-fluorophenyl)-n-methyl-6-[(methylsulfonyl)amino]-5-(propan-2-yloxy)-1-benzofuran-3-carboxamide	2N5	Palm	2.2	(Yeung et al., 2017)
4IH6	Hepatitis C virus polymerase ns5b (bk) with fragment-based compounds	1EP	Palm 1	2.2	(Talamas et al., 2013)
4JY0	Crystal structure of HCV ns5b polymerase in complex with compound 3	1O9		2.2	
4IZ0	Crystal structure of HCV ns5b polymerase in complex with 2,4,5-trichloro-n-(5-methyl-1,2-oxazol-3-yl) benzene sulfonamide	2BI	Thumb 2	2.22	(Stammers, Coulombe, Rancourt, et al., 2013)
5PZN	Crystal structure of the hepatitis C virus ns5b RNA -dependent RNA polymerase in complex with 5-[3-(tert-butylcarbonyl) phenyl]-2-(4-fluorophenyl)-n-methyl-1-benzofuran-3-carboxamide	23E	Thumb	2.25	(Yeung et al., 2017)
5PZN	Crystal structure of the hepatitis C virus ns5b RNA -dependent RNA polymerase in complex with 5-[3-(tert-butylcarbonyl) phenyl]-2-(4-fluorophenyl)-n-methyl-1-benzofuran-3-carboxamide	8XP	Palm	2.25	(Yeung et al., 2017)
2XHU	HCV-J4 ns5b polymerase orthorhombic crystal form	SO4		2.287	(Harrus et al., 2010)
3Q0Z	Crystal structure of the hepatitis C virus ns5b RNA-dependent RNA polymerase complex with (2e)-3-(4-{{[(1-{{[(13-cyclohexyl-6-oxo-6,7-dihydro-5h-indolo[1,2-d] [1,4] benzodiazepin-10-yl) carbonyl] amino} cyclopentyl) carbonyl] amino} phenyl) prop-2-enoic acid	23E	Thumb	2.29	(Zheng et al., 2011)

2HWH	HCV ns5b allosteric inhibitor complex	RNA	Thumb	2.3	(Yan et al., 2006)
5TRI	Crystal structure of the hepatitis C virus ns5b RNA -dependent RNA polymerase in complex with 3-[(4-chlorophenyl) methoxy]-2-(1-oxo-1,3-dihydro-2h-isoindol-2-yl) benzoic acid	23E	Thumb	2.3	(Parcella et al., 2017)
5TRI	Crystal structure of the hepatitis C virus ns5b RNA -dependent RNA polymerase in complex with 3-[(4-chlorophenyl) methoxy]-2-(1-oxo-1,3-dihydro-2h-isoindol-2-yl) benzoic acid	7HM	An allosteric site located at the convergence of the palm and thumb regions. Palm 2	2.3	(Parcella et al., 2017)
4MIB	Hepatitis C virus polymerase ns5b genotype 1b (bk) in complex with compound 48 (n-({(3s)-1-[6-tert-butyl-5-methoxy-8-(2-oxo-1,2-dihydropyridin-3-yl) quinolin-3-yl] pyrrolidin-3-yl} methyl) methanesulfonamide)	28M	Palm I	2.3	(Talamas et al., 2014)
3D28	Crystal structure of HCV ns5b polymerase with a novel benzisothiazole inhibitor	B34	Palm	2.3	(Kim et al., 2008)
6MVK	HCV ns5b 1b n316 bound to compound 18	K4J		2.3	(Chong et al., 2019)
3BSA	Crystal structure of HCV ns5b polymerase with a novel pyridazinone inhibitor	1PD	Palm	2.3	(Zhou et al., 2008)
4KAI	HCV ns5b gt1b n316 with gsk5852a	1PV	Palm 2	2.3	(Maynard et al., 2014)
3BR9	Crystal structure of HCV ns5b polymerase with a novel pyridazinone inhibitor	DEY	Palm	2.3	(Zhou et al., 2008)
4IH7	Hepatitis C virus polymerase ns5b (bk) with fragment-based compounds	1ER	Palm 1	2.3	(Talamas et al., 2013)
2BRK	Crystal structure of hepatitis C virus polymerase in complex with an allosteric inhibitor (compound 1)	CMF	Thumb	2.3	(Di Marco et al., 2005)

3CVK	Crystal structure of HCV ns5b polymerase with a novel pyridazinone inhibitor	N34	Palm	2.31	(Ruebsam, Sun, et al., 2008)
3GNW	HCV ns5b polymerase in complex with 1,5 benzodiazepine inhibitor 4c	XNC	Allosteric site near the interface of the palm and thumb subdomains.	2.39	(Vandyck et al., 2009)
4J0A	Crystal structure of HCV ns5b polymerase in complex with 2-{[(4-methylphenyl) sulfonyl] amino }-4-phenoxybenzoic acid	1JL	Thumb	2.4	(Stammers, Coulombe, Rancourt, et al., 2013)
4JU4	Crystal structure of HCV ns5b polymerase in complex with compound 22	1O3	Thumb 2	2.4	(Stammers, Coulombe, Duplessis, et al., 2013)
3CWJ	Crystal structure of HCV ns5b polymerase with a novel pyridazinone inhibitor	321	Palm	2.4	(Ellis et al., 2008)
4JVQ	Crystal structure of HCV ns5b polymerase in complex with compound 9	1ML	Thumb 2	2.4	(LaPlante et al., 2014)
2BRL	Crystal structure of hepatitis C virus polymerase in complex with an allosteric inhibitor (compound 2)	POO	Thumb	2.4	(Di Marco et al., 2005)
4AEX	HCV-JFH1 ns5b polymerase structure at 2.4 angstrom in a primitive orthorhombic space group	PO4		2.41	(Scrima et al., 2012)
4KHR	HCV ns5b gt1a c316y with gsk5852	1PV	Palm 2	2.45	(Gentles et al., 2011)
3QGF	Crystal structure of the hepatitis C virus ns5b RNA-dependent RNA polymerase complex with (2e)-3-(4-{{[(1-{{[(13-cyclohexyl-6-oxo-6,7-dihydro-5h-indolo[1,2-d] [1,4] benzodiazepin-10-yl) carbonyl] amino } cyclopentyl) carbonyl] amino } phenyl) prop-2-enoic acid and (2r)-4-(6-chloropyridazin-3-yl)-n-(4-methoxybenzyl)-1-{{[4-	23E	Thumb	2.45	(Gentles et al., 2011)

	(trifluoromethoxy) phenyl] sulfonyl} piperazine-2-carboxamide				
3QGF	Crystal structure of the hepatitis C virus ns5b RNA -dependent RNA polymerase complex with (2e)-3-(4-{{[(1-{{[(13-cyclohexyl-6-oxo-6,7-dihydro-5h-indolo[1,2-d] [1,4] benzodiazepin-10-yl) carbonyl] amino } cyclopentyl) carbonyl] amino } phenyl) prop-2-enoic acid and (2r)-4-(6-chloropyridazin-3-yl)-n-(4-methoxybenzyl)-1-{{[4-(trifluoromethoxy) phenyl] sulfonyl} piperazine-2-carboxamide	46F		2.45	(Gentles et al., 2011)
3SKH	I. Novel HCV ns5b polymerase inhibitors: discovery of indole 2-carboxylic acids with c3-heterocycles	58	Active site cavity of NS5B at the palm site.	2.5	(Anilkumar et al., 2011)
1YVF	Hepatitis C virus ns5b RNA -dependent RNA polymerase complex with inhibitor pha-00729145	PH7	Primer grip site	2.5	(Pfefferkorn, Greene, et al., 2005)
4WT9	Apo crystal structure of HCV ns5b genotype 2a jfh-1 isolate with e86q e87q s15g c223h v321i and delta8 mutations	EPE		2.5	(Appleby et al., 2015)
4WTA	Apo crystal structure of HCV ns5b genotype 2a JFH-1 isolate with beta hairpin loop deletion	SO4		2.5	(Mosley et al., 2012)
4WTK	Crystal structure of HCV ns5b genotype 2a jfh-1 isolate with s15g e86q e87q c223h v321i mutations in complex with RNA template 5'-agcc, RNA primer 5'-pgg, mn2+, and CDP	CDP		2.5	(Appleby et al., 2015)
4WTK	Crystal structure of HCV ns5b genotype 2a jfh-1 isolate with s15g e86q e87q c223h v321i mutations in complex with RNA template 5'-agcc, RNA primer 5'-pgg, mn2+, and CDP	B3P		2.5	(Appleby et al., 2015)
4OBC	Crystal structure of HCV polymerase ns5b genotype 2a jfh-1 isolate with the s15g, c223h, v321i resistance mutations against the guanosine analog gs-0938 (psi-3529238)	MES		2.5	(Lam et al., 2014)

1YV2	Hepatitis C virus ns5b RNA - dependent RNA polymerase genotype 2a	SO4	Thumb	2.5	(Biswal et al., 2005)
1QUV	Crystal structure of the RNA directed RNA polymerase of hepatitis c virus			2.5	(Bressanelli et al., 1999)
4RY6	C-terminal mutant (w550a) of HCV/J4 RNA polymerase			2.52	(Cherry et al., 2015)
2XWY	Structure of mk-3281, a potent non-nucleoside finger-loop inhibitor, in complex with the hepatitis C virus ns5b polymerase	IB8	Finger-loop inhibitor	2.53	(Narjes et al., 2011)
5PZM	Crystal structure of the hepatitis C virus ns5b RNA -dependent RNA polymerase in complex with 3-[2-(4-fluorophenyl)-3-(methylcarbamoyl)-1-benzofuran-5-yl] benzoic acid	23E	Thumb	2.54	(Yeung et al., 2017)
5PZM	Crystal structure of the hepatitis C virus ns5b RNA -dependent RNA polymerase in complex with 3-[2-(4-fluorophenyl)-3-(methylcarbamoyl)-1-benzofuran-5-yl] benzoic acid	8XS	Palm	2.54	(Yeung et al., 2017)
5TRJ	Crystal structure of the hepatitis C virus ns5b RNA -dependent RNA polymerase in complex with 2-{[2-(carboxymethoxy) benzene-1-carbonyl] amino }-3-[(4-chlorophenyl) methoxy] benzoic acid	23E	Thumb	2.57	(Parcella et al., 2017)
5TRJ	Crystal structure of the hepatitis C virus ns5b RNA -dependent RNA polymerase in complex with 2-{[2-(carboxymethoxy) benzene-1-carbonyl] amino }-3-[(4-chlorophenyl) methoxy] benzoic acid	7HO	An allosteric site located at the convergence of the palm and thumb regions.	2.57	(Parcella et al., 2017)
4OOW	HCV ns5b polymerase with a fragment of quercetagenin	CAQ		2.57	(Ahmed-Belkacem et al., 2014)
4RY4	C-terminal mutant (y448f) of HCV/J4 RNA polymerase			2.59	(Cherry et al., 2015)

2QE5	Structure of HCV ns5b bound to an anthranilic acid inhibitor	617	A site on NS5B between the thumb and palm regions adjacent to the active site.	2.6	(Nittoli et al., 2007)
3QGD	Crystal structure of the hepatitis C virus ns5b RNA -dependent RNA polymerase complex with (2e)-3-(4-{{[(1-{{[(13-cyclohexyl-6-oxo-6,7-dihydro-5h-indolo[1,2-d] [1,4] benzodiazepin-10-yl) carbonyl] amino } cyclopentyl) carbonyl] amino } phenyl) prop-2-enoic acid and (2r)-4-(2,6-dimethoxypyrimidin-4-yl)-1-[(4-ethylphenyl) sulfonyl]-n-(4-methoxybenzyl) piperazine-2-carboxamide	23E	Thumb	2.6	(Gentles et al., 2011)
3QGD	Crystal structure of the hepatitis C virus ns5b RNA -dependent RNA polymerase complex with (2e)-3-(4-{{[(1-{{[(13-cyclohexyl-6-oxo-6,7-dihydro-5h-indolo[1,2-d] [1,4] benzodiazepin-10-yl) carbonyl] amino } cyclopentyl) carbonyl] amino } phenyl) prop-2-enoic acid and (2r)-4-(2,6-dimethoxypyrimidin-4-yl)-1-[(4-ethylphenyl) sulfonyl]-n-(4-methoxybenzyl) piperazine-2-carboxamide	26S	Palm	2.6	(Gentles et al., 2011)
3IGV	Crystal structure of HCV ns5b polymerase with a novel monocyclic dihydro-pyridinone inhibitor	B80	Palm	2.6	(Ellis et al., 2009)
4JTY	Crystal structure of HCV ns5b polymerase with compound 2	1NV	Thumb 2	2.6	(Hucke et al., 2014)
4JY1	Crystal structure of HCV ns5b polymerase in complex with compound 5	NN3		2.6	
3BSC	Crystal structure of HCV ns5b polymerase with a novel pyridazinone inhibitor	2PD	Palm	2.65	(Zhou et al., 2008)

4WTF	Crystal structure of HCV ns5b genotype 2a jfh-1 isolate with s15g e86q e87q c223h v321i mutations and delta8 beta hairpin loop deletion in complex with gs-639475, mn2+ and symmetrical primer template 5'-caaaaauuu	5GS		2.65	(Appleby et al., 2015)
2XHW	HCV-J4 ns5b polymerase trigonal crystal form			2.66	(Harrus et al., 2010)
5TRH	Crystal structure of the hepatitis C virus ns5b RNA-dependent RNA polymerase in complex with 2-[(benzenecarbonyl)amino]-3-[(4-chlorophenyl) methoxy] benzoic acid	23E	Thumb	2.7	(Parcella et al., 2017)
5TRH	Crystal structure of the hepatitis C virus ns5b RNA -dependent RNA polymerase in complex with 2-[(benzenecarbonyl)amino]-3-[(4-chlorophenyl) methoxy] benzoic acid	7HL	Palm 2. An allosteric site located at the convergence of the palm and thumb regions.	2.7	(Parcella et al., 2017)
4GMC	Crystal structure of HCV ns5b polymerase in complex with a thumb inhibitor	1BI	Thumb I	2.7	10.1139/cjc-2012-0319
4JU2	Crystal structure of HCV ns5b polymerase in complex with compound 12	1O0	Thumb 2	2.7	(Hucke et al., 2014)
4WTD	Crystal structure of HCV ns5b genotype 2a jfh-1 isolate with s15g e86q e87q c223h v321i mutations and delta8 beta hairpin loop deletion in complex with ADP, mn2+ and symmetrical primer template 5'-auaaaauuu	ADP		2.7	(Appleby et al., 2015)
4TN2	Ns5b in complex with lactam-thiophene carboxylic acids	33J	Thumb 2	2.7	(Barnes-Seeman et al., 2014)
3CSO	HCV polymerase in complex with a 1,5-benzodiazepine inhibitor	XNI		2.71	(Nyanguile et al., 2008)
4RY5	C-terminal mutant (w550n) of HCV/J4 RNA polymerase	MN		2.71	(Cherry et al., 2015)

4NLD	Crystal structure of the hepatitis C virus ns5b RNA-dependent RNA polymerase complex with bms-791325 also known as (1ar,12bs)-8-cyclohexyl-n-(dimethylsulfamoyl)-11-methoxy-1a-[[[(1r,5s)-3-methyl-3,8-diazabicyclo [3.2.1] oct-8-yl] carbonyl}-1,1a,2,12b-tetrahydrocyclopropa[d]indolo[2,1-a][2] benzazepine-5-carboxamide and 2-(4-fluorophenyl)-n-methyl-6-[(methylsulfonyl)amino]-5-(propan-2-yloxy)-1-benzofuran-3-carboxamide	2N7	Thumb 1	2.75	(Gentles et al., 2014)
4NLD	Crystal structure of the hepatitis C virus ns5b RNA -dependent RNA polymerase complex with bms-791325 also known as (1ar,12bs)-8-cyclohexyl-n-(dimethylsulfamoyl)-11-methoxy-1a-[[[(1r,5s)-3-methyl-3,8-diazabicyclo [3.2.1] oct-8-yl] carbonyl}-1,1a,2,12b-tetrahydrocyclopropa[d]indolo[2,1-a][2] benzazepine-5-carboxamide and 2-(4-fluorophenyl)-n-methyl-6-[(methylsulfonyl)amino]-5-(propan-2-yloxy)-1-benzofuran-3-carboxamide	2N5	Thumb 1	2.75	(Gentles et al., 2014)
3GNV	HCV ns5b polymerase in complex with 1,5 benzodiazepine inhibitor 1b	XNZ	Allosteric site near the interface of the palm and thumb subdomains.	2.75	(Vandyck et al., 2009)
4WTC	Crystal structure of HCV ns5b genotype 2a jfh-1 isolate with s15g e86q e87q c223h v321i mutations and delta8 beta hairpin loop deletion in complex with CDP, mn2+ and symmetrical primer template 5'-agaaauuu	CDP		2.75	(Appleby et al., 2015)
4MK7	Hepatitis C virus polymerase ns5b genotype 1b (bk) in complex with inhibitor 2 (3-(3-tert-butyl-4-methoxyphenyl) pyridin-2(1h)-one)	28O	Palm I	2.8	(Schoenfeld et al., 2013)

4MIA	Hepatitis C virus polymerase ns5b genotype 1b (bk) in complex with rg7109 (n-{4-[6-tert-butyl-5-methoxy-8-(6-methoxy-2-oxo-2,5-dihydropyridin-3-yl) quinolin-3-yl] phenyl} methanesulfonamide)	28L	Palm I	2.8	(Talamas et al., 2014)
1Z4U	Hepatitis C virus ns5b RNA - dependent RNA polymerase complex with inhibitor pha-00799585	PH9	Primer grip site	2.8	(Pfefferkorn, Nugent, et al., 2005)
3MWW	Crystal structure of HCV ns5b polymerase	BIW	Thumb 1	2.8	(LaPlante et al., 2010)
4JTZ	Crystal structure of HCV ns5b polymerase in complex with compound 4	1NW	Thumb 2	2.8	(Hucke et al., 2014)
4WTI	Crystal structure of HCV ns5b genotype 2a jfh-1 isolate with s15g e86q e87q c223h v321i mutations in complex with RNA template 5'-acgg, RNA primer 5'-pcc, mn2+, and GDP	GDP		2.8	(Appleby et al., 2015)
4WTI	Crystal structure of HCV ns5b genotype 2a jfh-1 isolate with s15g e86q e87q c223h v321i mutations in complex with RNA template 5'-acgg, RNA primer 5'-pcc, mn2+, and GDP	B3P		2.8	(Appleby et al., 2015)
4WTA	Crystal structure of HCV ns5b genotype 2a JFH-1 isolate with s15g e86q e87q c223h v321i mutations and delta8 beta hairpin loop deletion in complex with UDP, mn2+ and symmetrical primer template 5'-caaaaauu	UDP		2.8	(Appleby et al., 2015)
5PZO	Crystal structure of the hepatitis C virus ns5b RNA-dependent RNA polymerase c316n in complex with 2-(4-fluorophenyl)-n-methyl-5-[3-({2-methyl-1-oxo-1-[(1,3,4-thiadiazol-2-yl) amino] propan-2-yl} carbamoyl) phenyl]-1-benzofuran-3-carboxamide	23E	Thumb	2.8	(Yeung et al., 2017)
5PZO	Crystal structure of the hepatitis C virus ns5b RNA -dependent RNA polymerase c316n in complex with 2-(4-fluorophenyl)-n-methyl-5-[3-({2-methyl-1-oxo-1-[(1,3,4-thiadiazol-2-yl) amino] propan-2-yl} carbamoyl) phenyl]-1-benzofuran-3-carboxamide	8XM	Palm	2.8	(Yeung et al., 2017)

1CSJ	Crystal structure of the RNA - dependent RNA polymerase of hepatitis c virus			2.8	(Bressanelli et al., 1999)
5W2E	HCV ns5b RNA -dependent RNA polymerase in complex with non-nucleoside inhibitor mk-8876	9VY	Palm 2	2.8	(McComas et al., 2017)
3GOL	HCV ns5b polymerase in complex with 1,5 benzodiazepine inhibitor (r)-11d	XND		2.85	(McGowan et al., 2009)
1NHV	Hepatitis C virus RNA polymerase in complex with non-nucleoside analogue inhibitor	154	Thumb about 35 Å from the active site.	2.9	(M. Wang et al., 2003)
2QE2	Structure of HCV ns5b bound to an anthranilic acid inhibitor	452	A site on NS5B between the thumb and palm regions adjacent to the active site.	2.9	(Nittoli et al., 2007)
4JU1	Crystal structure of HCV ns5b polymerase in complex with compound 6	1NZ	Thumb 2	2.9	(Hucke et al., 2014)
4E78	Crystal structure of a product state assembly of HCV ns5b genotype 2a JFH-1 isolate with beta hairpin loop deletion bound to primer-template RNA with 3'-dg			2.9	(Mosley et al., 2012)
4WTE	Crystal structure of HCV ns5b genotype 2a jfh-1 isolate with s15g e86q e87q c223h v321i mutations and delta8 beta hairpin loop deletion in complex with GDP, mn2+ and symmetrical primer template 5'-acaaauuu	GDP		2.9	(Appleby et al., 2015)
4WTG	Crystal structure of HCV ns5b genotype 2a jfh-1 isolate with s15g e86q e87q c223h v321i mutations and delta8 beta hairpin loop deletion in complex with sofosbuvir diphosphate gs-607596, mn2+ and symmetrical primer template 5'-caaaauuu	6GS		2.9	(Appleby et al., 2015)

5UJ2	Crystal structure of HCV ns5b genotype 2a jfh-1 isolate with s15g e86q e87q c223h v321i mutations and delta8 neta hairpoin loop deletion in complex with gs-639476 (diphsohate version of gs-9813), mn2+ and symmetrical primer template 5'-auaaaauuu	8B4		2.9	(Kirschberg et al., 2017)
5PZP	Crystal structure of the hepatitis C virus ns5b RNA-dependent RNA polymerase in complex with 4-fluoro-2-(4-fluorophenyl)-n-methyl-5-(2-methyl-5-[[1-(pyrimidin-2-yl) cyclopropyl] carbamoyl] phenyl)-1-benzofuran-3-carboxamide (bms-929075)	23E	Thumb	2.95	(Yeung et al., 2017)
5PZP	Crystal structure of the hepatitis C virus ns5b RNA -dependent RNA polymerase in complex with 4-fluoro-2-(4-fluorophenyl)-n-methyl-5-(2-methyl-5- [[1-(pyrimidin-2 yl) cyclopropyl] carbamoyl] phenyl)-1-benzofuran-3-carboxamide (bms-929075)	8XJ	Palm	2.95	(Yeung et al., 2017)
3QGE	Crystal structure of the hepatitis C virus ns5b RNA -dependent RNA polymerase complex with (2e)-3-(4-[[[(1-[[[(13-cyclohexyl-6-oxo-6,7-dihydro-5h-indolo[1,2-d] [1,4] benzodiazepin-10-yl) carbonyl] amino} cyclopentyl) carbonyl] amino} phenyl) prop-2-enoic acid and (2r)-4-(2,6-dimethoxypyrimidin-4-yl)-n-(4-methoxybenzyl)-1-{[4-(trifluoromethoxy) phenyl] sulfonyl} piperazine-2-carboxamide	23E	Thumb	3	(Gentles et al., 2011)
3QGE	Crystal structure of the hepatitis C virus ns5b RNA -dependent RNA polymerase complex with (2e)-3-(4-[[[(1-[[[(13-cyclohexyl-6-oxo-6,7-dihydro-5h-indolo[1,2-d] [1,4] benzodiazepin-10-yl) carbonyl] amino} cyclopentyl) carbonyl] amino} phenyl) prop-2-enoic acid and (2r)-4-(2,6-dimethoxypyrimidin-4-yl)-n-(4-methoxybenzyl)-1-{[4-	26F	Palm	3	(Gentles et al., 2011)

	(trifluoromethoxy) phenyl] sulfonyl} piperazine-2-carboxamide				
4JTW	Crystal structure of HCV ns5b polymerase in complex with COUPOND 1	1NU	Thumb 2	3	(Hucke et al., 2014)
4E7A	Crystal structure of a product state assembly of HCV ns5b genotype 2a jfh-1 isolate with beta hairpin deletion bound to primer-template RNA with a 2',3'-ddc			3	(Mosley et al., 2012)
4RY7	C-terminal mutant (d559e) of HCV/J4 RNA polymerase			3	(Cherry et al., 2015)
5TWN	Crystal structure of the hepatitis C virus ns5b RNA - dependent RNA polymerase in complex with 5-[3-(tert-butylcarbamoyl) phenyl]-6-(ethylamino)-2-(4-fluorophenyl)-n-methylfuro[2,3-b] pyridine-3-carboxamide	23E	Thumb	3.04	(Eastman et al., 2017)
5TWN	Crystal structure of the hepatitis C virus ns5b RNA - dependent RNA polymerase in complex with 5-[3-(tert-butylcarbamoyl) phenyl]-6-(ethylamino)-2-(4-fluorophenyl)-n-methylfuro[2,3-b] pyridine-3-carboxamide	7NG	Primer grip site	3.04	(Eastman et al., 2017)
6GP9	Structural studies of hepatitis C virus non-structural protein-5b of genotype 4a			3.1	
3QGG	Crystal structure of the hepatitis C virus ns5b RNA -dependent RNA polymerase complex with (2e)-3-(4-[[[(1-[[[(13-cyclohexyl-6-oxo-6,7-dihydro-5h-indolo[1,2-d] [1,4] benzodiazepin-10-yl) carbonyl] amino } cyclopentyl) carbonyl] amino } phenyl) prop-2-enoic acid and n-cyclopropyl-6-[(3r)-3-{[4-(trifluoromethoxy) benzyl] carbamoyl]-4-{[4-(trifluoromethoxy) phenyl] sulfonyl} piperazin-1-yl] pyridazine-3-carboxamide	23E	Thumb	3.22	(Gentles et al., 2011)

3QGG	Crystal structure of the hepatitis C virus ns5b RNA -dependent RNA polymerase complex with (2e)-3-(4- {[(1- {[(13-cyclohexyl-6-oxo-6,7-dihydro-5h-indolo[1,2-d] [1,4] benzodiazepin-10-yl) carbonyl] amino } cyclopentyl) carbonyl] amino } phenyl) prop-2-enoic acid and n-cyclopropyl-6-[(3r)-3-{[4-(trifluoromethoxy) benzyl] carbamoyl}-4-{[4-(trifluoromethoxy) phenyl] sulfonyl} piperazin-1-yl] pyridazine-3-carboxamide	63F		3.22	(Gentles et al., 2011)
2N1P	Structure of the c-terminal membrane domain of HCV ns5b protein				